Winter 2-14-2014

# The West Tidewater Earthflow, Northern Oregon Coast Range

Barry A. Sanford
*Portland State University*

THESIS APPROVAL

The abstract and thesis of Barry A. Sanford for the Master of Science in Geology were presented March 1, 2002 and accepted by the thesis committee and the department.

COMMITTEE APPROVALS:

[redacted]

Kenneth M. Cruikshank

[redacted]

Christina L. Hulbe

[redacted]

Trevor D. Smith
Representative of the Office of Graduate Studies

DEPARTMENT APPROVAL:

[redacted]

Michael L. Cummings, Chair
Department of Geology

# ABSTRACT

An abstract of the thesis of Barry A. Sanford for the Master of Science in Geology presented March 1, 2002

Title: The West Tidewater Earthflow, Northern Oregon Coast Range.

The West Tidewater earthflow, one of the largest in Oregon's history, occurred in December of 1994. The earthflow is located approximately 15 km north of Jewel, Oregon near the summit of the Northern Oregon Coast Range Mountains. The earthflow is 900 m long and 250 m wide, giving it a surface area of 9 ha, or 22 acres. Volume is 3.5 million $m^3$. The earthflow occurred in low strength, well-bedded, tuffaceous, carbonaceous, micaceous, clay-rich mudstone, and very fine-grained, feldspathic, clay-rich siltstone of the lower Miocene age Northrup Creek Formation. The soil clay fractions contain up to 90% smectite with indications of halloysite. This earthflow is a reactivation of a 650-year-old landslide (C-14 dating of uncovered buried trees). The failure mode is examined using a Janbu slope analysis and includes double wedge failure near the headscarp. High soil pore water pressure is one of the major causes of this slope failure. Rainfall levels for October, November, and December of 1994 were twice the previous five-year average. Present day groundwater level within the basin is less than one meter below ground surface. The earthflow is partially controlled by two faults of regional extent that dissect the basin

near the headscarp in NW-SE and NE-SW directions. The Inceptisol soils in the basin remain moist below 20 cm year around. Soil in the basin may have been further weakened due to loss of root strength following timber harvest on the site in 1991. Soil liquid limits range from 42% to 95%, with PI values ranging from 2% to 77%. Soil clay content ranges between 18% and 30%. Direct shear tests on the mudstone and siltstone bedrock in both drained and undrained conditions produced internal friction angles of 14-18°, with cohesion values of 4 - 8 kPa. Back calculation of study area soil strength using the modified Bishop method results in a residual friction angle of 20.7°. The failure mode of the earthflow is from the headscarp downward and is modeled using Janbu methods. The study includes a detailed topographic map and a failure analysis of the earthflow basin.

# THE WEST TIDEWATER EARTHFLOW,

# NORTHERN OREGON COAST RANGE

by

BARRY A. SANFORD

A thesis submitted in partial fulfillment of the
requirements for the degree of

MASTER OF SCIENCE
in
GEOLOGY

Portland State University
2004

ACKNOWLEDGEMENTS

Many thanks to Associate Professor Ken Cruikshank and the students of his Landslide Anatomy class of 1996 at Portland State University for their assistance in mapping the West Tidewater earthflow. Jared May provided extensive field assistance for the surveying, mapping, and soil investigation. Dave Michael and the Oregon Department of Forestry office in Forest Grove, Oregon provided access to their aerial photo library. Dr. Trevor Smith and the Civil Engineering Department of Portland State University allowed me to use their soils laboratory and test equipment. Dr. Christina Hulbe helped me organize my thoughts and edit my writing. Special thanks to Dr. Scott Burns, for his role as advisor, and his never-ending enthusiasm, encouragement, and dedication to education.

TABLE OF CONTENTS

LIST OF TABLES

LIST OF FIGURES

# LIST OF PLATES

# CHAPTER 1

# INTRODUCTION

Landslide is the general term for various modes of catastrophic mass wasting including mudflow, earthflow, debris flow, and rock fall (Chassie and Goughnour, 1976). Although landslides occur naturally, human impacts can substantially increase their frequency and scope.

The West Tidewater earthflow was remobilized in December of 1994. This was one of the largest landslides to occur in the Oregon Coast Range and one of the largest in Oregon's modern history. The duration of the actual movement has been estimated at between four and 24 hours (personal communication, Dave Michael, Oregon Department of Forestry, 1995). Small, one to two meter soil blocks have continued to separate from the main scarp sporadically since the remobilization. These smaller failures were observed in late winter, spring, and summer of 1996.

The goals of this project are to determine what happened to the soils of the Tidewater Summit region of the Oregon Coast Range Mountains to cause them to fail and to discover how they failed. A 1 : 3000 scale map of the earthflow describes the geometry and topography of the slide. The chemical and physical properties of the soils are examined using Atterberg limits, particle size gradations, and a clay mineralogy determination. The soil cohesion and internal friction angles were quantified by direct shear testing on drained and undrained samples. Other workers

have examined the regional geology, structure, and formation relations through previously published material. The groundwater characteristics in the basin were examined using several monitoring wells installed during the course of this project. The data gathered by the above mentioned methods were used to perform a stability analysis of the earthflow basin. The purpose of this earthflow characterization and study is to map the earthflow, to examine engineering properties of the soils, to investigate soil behavior during a large earthflow event, and to perform a stability analysis of the slopes in order to determine the overall failure mode.

# CHAPTER 2

# STUDY AREA

## LOCATION

The Tidewater earthflow is located in Clatsop County, Oregon approximately 15 km northwest of Jewel, Oregon on State Highway 202, milepost 22 (Figure 1). This part of the crest of the Coast Range is known as the Tidewater Summit. Map coordinates of the earthflow study area are; SE 1/4, NE 1/4, Section 18, Township 6 North, Range 7 West, Wickiup Mountain, Oregon, U.S.G.S. 7.5 minute quadrangle, or 46° 00' 42" north latitude, 123° 35' 50" west longitude.

## DESCRIPTION

The drainage basin that contains the West Tidewater earthflow has been subject to at least one, and possibly several historic failures. Aerial photos suggest older earthflow events in nearly the same location as the current failure (Figure 2). Lighter colored new growth vegetation can be seen extending down the drainage basin to the south and west. The standing timber within most of the study area and slide margins was harvested by clear-cut logging methods in 1991 (personal communication, Dave Michael, Oregon Department of Forestry, 1995). The east-west timber cut boundary, also visible in Figure 2, roughly parallels and lies just

north of the apex of the structural ridge that forms the headscarp and northern study area margin.

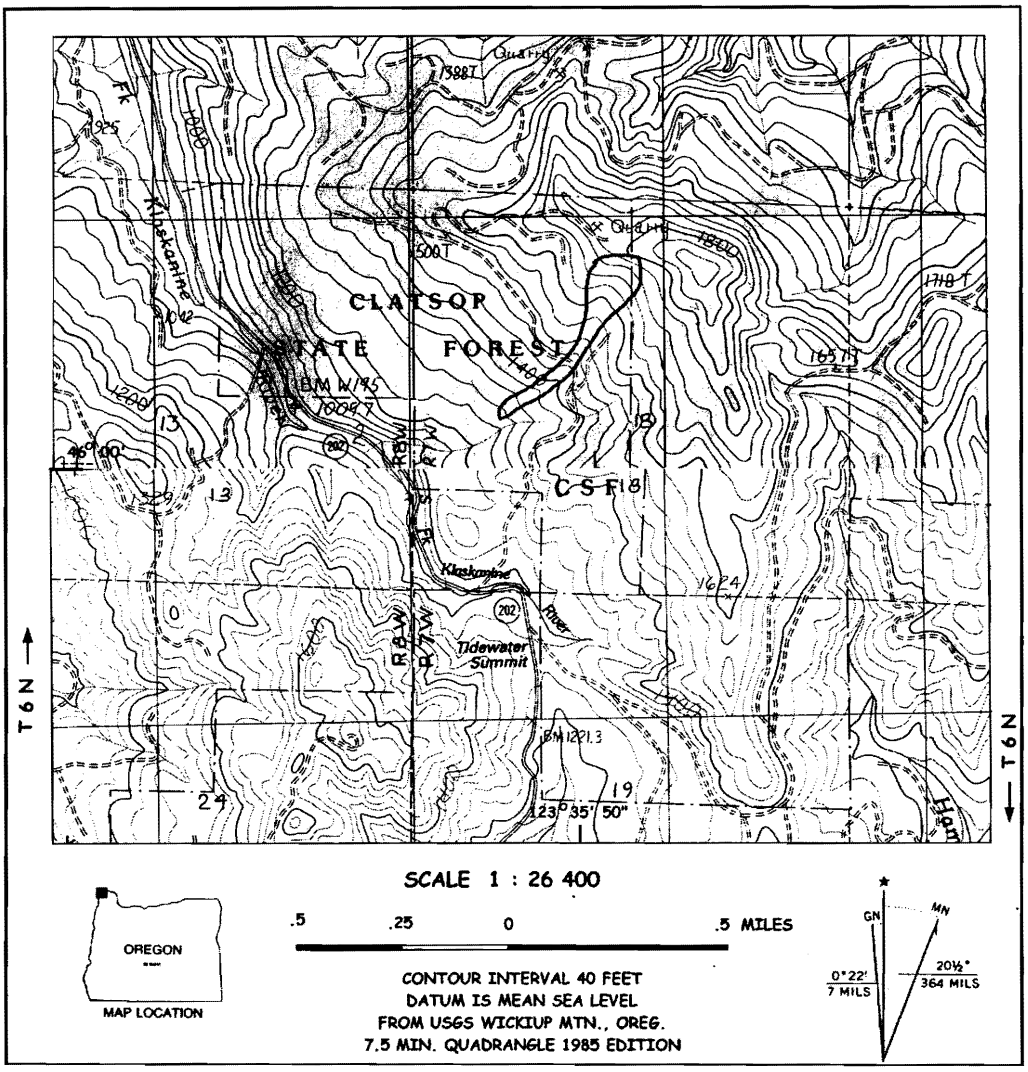


**Figure 1. Tidewater earthflow location map. The earthflow basin and study area is outlined at the figure center.**

The earthflow is approximately 250 m at the widest point and 900 m long, with a calculated surface area of 8.7 ha (Figure 3). About 100 meters of logging road

embankment drained with a single corrugated steel culvert was destroyed by the earthflow event. Remnants of this road can be seen on the map (Figure 3), along contour 447 m on both lateral margins of the earthflow. A small pond has formed just downslope, south, from where the road previously crossed the earthflow basin. The orphaned portion of this road continues northward, upslope, beyond the western margin of the slide, passing an abandoned basalt rock crushing quarry along the ridge just above the head scarp along contour 580 m. A stream consolidates towards the distal toe of the slide basin near contour 430 m. It is fed by numerous seeps and springs exposed in the major and minor scarps on the earthflow. This zero-order stream drains the earthflow basin and joins the headwaters of the Klaskanine River as it crosses Oregon Highway 202 about 500 m downstream of the toe area. The colluvial soils are being deeply and rapidly eroded as base level of this stream is re-established.

Appendix A contains aerial photographs dating from the 1960's to the most current photos available. The photos in this series suggest a previous landslide in the study area. The photos also serve as a visual vegetative and human impact history of timber harvest, road building, and plant succession in the Tidewater Summit region of the Oregon Coast Range. Regional structural and geologic features are also visible in these photographs and are discussed in the course of this study.


**Figure 2. Aerial photo of the Tidewater earthflow study area. Black lines indicate current earthflow features, access roads, and rock quarry. The area of new growth suggests a previous slope failure in the basin. The east west timber cut boundary (AB) parallels the ridge that is the northern margin of the study area. Photo is courtesy of the Oregon Department of Forestry, I.D. # NOW-CLATS-08, 20-30, 04-27-1980.**

Trees that appear to have been buried at some time in the past are evidence of a previous slope failure in this basin. Two of these trees are now protruding from a 3-4 m high soil thrust front about 1 m north of well 4 near contour 465 m (Plate 1). Samples of these trees have been C-14 dated to 700 +/- 50 BP (Beta-132479) and are explained in the Results section.

## SIMILAR EARTHFLOWS IN OREGON

Landslide investigations in other parts of Oregon have identified earth movements with failure histories of hundreds and even thousands of years (Swanston and Swanson, 1976). Slope failures are classified using criteria set forth and published by a number of workers in engineering geology such as Varnes (1996). These criteria are as specific as possible but classification of landslides still remains somewhat subjective. Landslides are classified in terms of the type of earth materials involved, the rates of movement, water content, topography, vegetative content, and time. The West Tidewater failure is classified as an earthflow due to the predominance of fine-grained soil materials, areas of well defined lateral boundaries, and the presence of a discreet shearing surface (Easterbrook, 1993). The term "earth flow" (Varnes, 1978) is the most appropriate formal classification (Figure 4B) for this event.

Landslides and small earth movements are relatively common to the Oregon Coast Range. Even so, relatively little work has been published concerning earthflows in the region. One of the largest earthflows in the Oregon Coast Range was the Drift Creek slide that occurred in 1975. This failure was a deep-seated, fast moving earthflow within a timber harvest boundary that began moving while logging operations were in progress (Thrall et al., 1980). There had been a previous failure at that site, and rainfall for the week prior to the event was reported as very heavy. The geology at the site is described as thinly bedded, slightly dipping, low shear strength

siltstone of the Tyee Formation. Thrall et al. (1980) state that even though this particular failure may have occurred without the timber harvest activity, it is very likely that road building and disruption of the natural drainage and soil conditions accelerated the processes leading to the failure event.

A

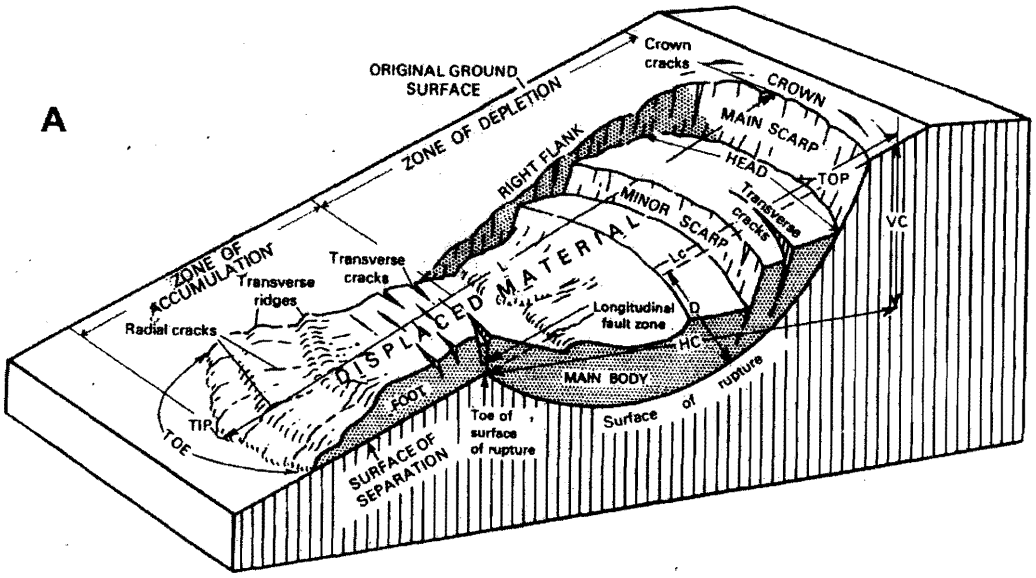


B

| TYPE OF MOVEMENT | | | TYPE OF MATERIAL | | |
|---|---|---|---|---|---|
| | | | BEDROCK | ENGINEERING SOILS | |
| | | | | Predominantly coarse | Predominantly fine |
| FALLS | | | Rock fall | Debris fall | Earth fall |
| TOPPLES | | | Rock topple | Debris topple | Earth topple |
| SLIDES | ROTATIONAL | FEW UNITS | Rock slump | Debris slump | Earth slump |
| | TRANSLATIONAL | MANY UNITS | Rock block slide<br>Rock slide | Debris block slide<br>Debris slide | Earth block slide<br>Earth slide |
| LATERAL SPREADS | | | Rock spread | Debris spread | Earth spread |
| FLOWS | | | Rock flow (deep creep) | Debris flow (soil creep) | Earth flow |
| COMPLEX | | | Combination of two or more principal types of movement | | |

**Figure 4. (A) Drawing of an earthflow with typical features labeled (Schuster and Kristed, 1978). (B) Landslide classifications based on soil material type and movements (Varnes, 1958).**

Another substantial Cascade landslide is the Lookout Creek earthflow, (Pyles et al., 1987). Lookout Creek is located in the H. J. Andrews Experimental Forest about 70 km east of Eugene, Oregon. This failure is part of a relatively large earthflow complex covering approximately 4 $km^2$ . This slide often remobilizes during the winter months when normal winter-time precipitation causes pore water pressure within the shear zone to reduce effective stress and thereby reduce soil strength. The regional groundwater regime at this site is reported to be very complex and poorly understood (Pyles et al., 1987).

The Lookout Creek flow is similar to the West Tidewater earthflow in several respects. It moves on a discrete shear zone and the materials involved are in a fine-grained matrix. Lookout Creek has an arcuate, slumping headscarp form and sits against a basalt intrusive body just as the West Tidewater earthflow. Both study areas have a history of timber harvest and previous failure, contain numerous springs and seeps, have a road embankment distal to the failure scarp within the slide boundary, and both failed during the high-rainfall winter months.

## GEOLOGY

The West Tidewater earthflow lies within the Northrup Creek Formation (Niem and Niem, 1985). The formation is a lower Miocene sedimentary unit consisting of about 500 m of well-bedded, carbonaceous and micaceous, laminated, medium to dark gray mudstone, with subordinate thin, fine-grained to very fine-

grained feldspathic, minor tuffaceous, yellow-gray siltstone. The Northrup Creek Formation is currently classified as an informal sub-unit of the Astoria Formation (Cooper, 1981). The Astoria Formation as originally described by Howe (1926), included a large portion of northwestern Oregon and the northern Oregon Coast Range. The Coast Range has been consistently described by many workers as extensively faulted and intruded, as can be seen in a recent map (Figure 5) by Niem and Niem (1985). Local structure and regional tectonics can play an important role in the mobilization of landslides, and as we will see, the Tidewater region is no exception. A right-lateral fault traverses the basin in a NW-SE direction. Since Howe's original work in 1926, other workers have further refined the formation descriptions (Lowry and Baldwin, 1952) and rock associations (Pease and Hoover, 1957; Dodds, 1963; Rau, 1967; Snavely et al., 1969) in the Astoria basin (Figure 6).

The surficial geology of the earthflow site consists of approximately 1.5 m of poorly developed soil material resting on about 4 m of pebbly to bouldery colluvium derived from siltstone and mudstone bedrock. A ridge-forming basalt intrusion that was being quarried until the time of failure is exposed on the northwest face of the headscarp. The structural ridge forms the northern boundary of the study section and bears NW-SE. Many of these basalt intrusives in the Astoria basin have a chemical composition very similar to the Miocene age Grand Ronde flood basalts (Niem and Niem, 1985), found in the Columbia Gorge. Most of the basalt dikes and sills seen

in outcrop in the Northern Oregon Coast Range have been reclassified as invasive basalt flows by Beeson et al. (1979) and Wells (1989).

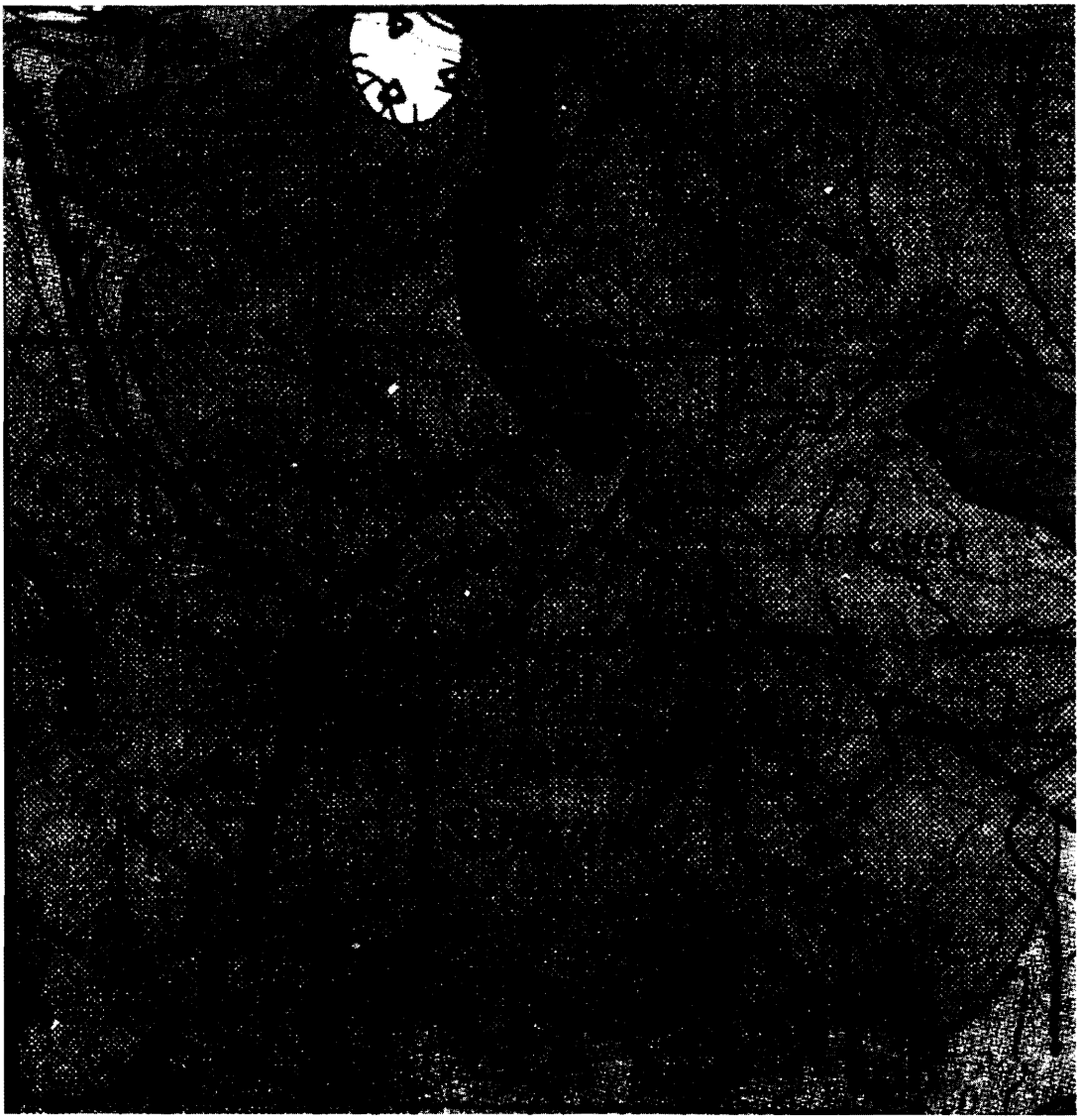

**Figure 5. Geologic map of the Tidewater Summit area. The study area including the earthflow is outlined in black. Highway 202 runs north and south at figure left, (Niem and Niem, 1985). Figure scale is approximately 1 : 30 000**

EXPLANATION

Faults – bar and ball on downthrown side,
dashed where inferred,
dashed where concealed.

Tn Northrup Creek Formation
Tpb Pittsburg Bluff Formation
Tgri Intrusive Grand Ronde Basalt

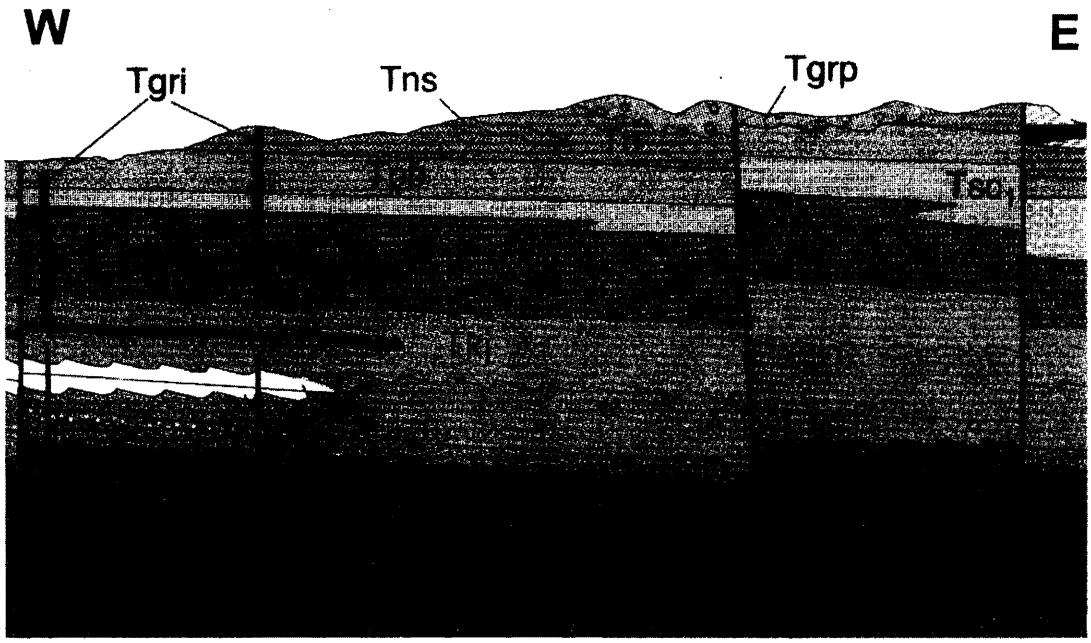


**Figure 6. Cross-section diagram showing stratigraphic relationships of a portion of the Northern Oregon Coast Range. The section shown lies about 3 km NE of the study area. The Tidewater study lies within the Northrup Creek Formation. (Niem and Niem, 1985). Scale is approximate.**

EXPLANATION

Tgri Intrusive Grand Ronde Basalt (middle Miocene)
Tgrp Grand Ronde Basalt pillow palagonite (middle Miocene)
Tn Northrup Creek Formation (lower Miocene)
Tpb Pittsburg Bluff Formation (Oligocene)
Tsc Sager Creek Formation (upper Eocene)
Tkj Kesey Formation (upper Eocene)
Tc Cowlitz Formation (upper Eocene)

## HYDROLOGY

The groundwater investigation for the project is limited to the immediate drainage basin containing the earthflow. The regional hydrology of the Tidewater Summit area was not characterized. Most of the local seeps and springs emerge near the eastern margin of the study area. These outflows form numerous marshy bogs ranging from 2 - 20 $m^2$ on the earthflow colluvial surface. The majority of the springs were observed to flow year-round with some seasonal variation. Outflow disappears and resurfaces randomly along most of the length of the earthflow. The study area groundwater regime appears to flow from northeast to southwest, feeding the zero-order gaining stream that drains the basin. One groundwater source appears to be perched on the ridge of invasive basalt (Beeson et al., 1979) that extends to the east across the northern margin of the study area. A horizontal line of springs flows from the soil block face on the eastern margin approximately 10-15 m from the ground surface (Figure 7). A significant amount of groundwater flows from the colluvial slopes on the eastern flank of the study basin near contour 495 m forming a small stream. A single, ephemeral seep emerges near the northwest margin, originating near the basalt to siltstone contact exposed on the headscarp face.

## STUDY AREA SOILS

Many of the local soils are residual Inceptisols, immature poorly developed soils lacking distinct B horizons or accumulation zones (Birkeland, 1984). The soil in the earthflow basin is thin, immature, poorly developed and originates from the

weathered surface of Northrup Creek siltstone. The taxonomy of the soil in the study area is determined to be a fine-loamy mixed, isomesic Andic Humitropept of the Skipanon series (Smith, and Shipman, 1988). Exposures of the Northrup Creek mudstones and siltstones commonly display a 'popcorn' textured subaerial weathering surface throughout the study area. A detailed description of the local soil type is excerpted from the Soil Conservation Service soil survey (Smith and Shipman, 1988) and can be found in Appendix B.

**Figure 7. View of the earthflow looking north from instrument station one(Plate 1). Areas of spring outflow are indicated by ⬋ symbols. X's indicate piezometers. The ridge at figure right is a groundwater source area. The distance to the headscarp is 400 m.**

In this portion of the Coast Range the soils are poorly developed due to constant overturning. The soils here rarely lie undisturbed long enough for distinct accumulation horizons to develop. The steep slopes, strong winds, and abundant rainfall contribute to frequent timber blow down in this densely forested environment. The resulting pit-and-mound surface morphology, sometimes mistaken for earth movements, demonstrates the thin soils and shallow tree root systems that are common throughout the coastal forests of Oregon (personal communication, Dr. Scott Burns, Portland State University, 1995).

Field soil-trench observations within the study area are sited on the east side of the study area access road, approximately one half mile north of the milepost 22 junction with Highway 202. The excavation reveals a thin, dark brown surface zone, an umbric epipedon, with an 'O' organic horizon, less than one centimeter thick. The uppermost 'A' horizon ranges from 3 - 5 cm and has medium brown Munsell color of 5YR 2.5/1, with indistinct upper and lower boundaries. The next lower 'AB' layer ranges from 40 - 50 cm thick, has medium brown Munsell color of 2.5 YR 2.5/2, and contains an abundance of yellow to gray subangular rock fragments ranging from 1 – 15 mm in diameter. No definable accumulation horizons are observed within the soil study pit. With increasing depth, the rock fragments increase in size and frequency and gradually consolidate into a highly oxidized and fragmented upper bedrock zone of yellow-gray siltstone. This markedly altered contact zone is designated the 'Cox' or oxidation horizon. It contains gravel and

cobbles that are predominately subangular to sub round with diameters to 40 cm, and Munsell colors ranging from 10 YR 4/4 in the matrix, to 2.5 YR 6/3 in the pebbles and cobbles (Table 1).

**Table 1. Soil horizons observed in the study area test pit.**

| SOIL HORIZON | HORIZON THICKNESS | MUNSELL COLOR | SOIL DESCRIPTION |
|---|---|---|---|
| | | | |
| O | 0 - 3 cm | NA | black to dark brown, sandy, crumbly, 50% pine needles and wood chips |
| A | 3 - 5 cm | 5YR 2.5/1 | dark brown, moist, sandy, wavy lower boundary, abundant plant roots |
| AB | 40 - 50 cm | 2.5YR 2.5/2 | light brown, sandy, silty, 1-13 mm yellow-brown pebbles, some plant roots, indistinct lower boundary |
| Cox | 40+ cm | 10YR 4/2 | mixed light and dark brown, gray to yellow orange to red, 1 mm - 40 cm subangular rock fragments with overall Munsell color 2.5YR 6/3. |

(These are surface horizons and do not represent the probable slide plane)

# CHAPTER 3

# METHODS

The West Tidewater earthflow site was mapped during the fall and winter of 1996. The study basin was surveyed using a Sokkia Total Station with the absolute elevations determined using GPS. Ground features and topography were mapped using control stations established during the survey. The numbered control stations were organized using Excel© and plotted on D-size plotter paper using the Surfer© software application. The plots were taken to the study area, where the topography and earthflow features were drawn. A final map was drafted from the field version (Figure 3).

Soil samples for laboratory testing were collected at locations and depths determined to be representative of the site in general and below the surface weathering zone. Sample locations are indicated on the project map (Figure 3). A Shelby tube sample of carbonaceous mudstone bedrock was collected for shear-strength testing. The Shelby tube was driven into a previously undisturbed and unremolded bed of mudstone by hand using a sledge hammer and block of wood. Mudstone and siltstone samples were collected for bulk density and natural water content determinations. Samples were selected for laboratory testing based on their suitability for cross testing.

Four monitoring wells were installed in order to determine the phreatic surface and flow regime of the study area (Figure 3). Three of these piezometers

were constructed of threaded sections of 02.5 cm O.D. steel pipe. Holes were drilled in the lower sections of the pipes to allow water to infiltrate and collect in the pipes. Pointed metal ends were fabricated to allow the pipes to be driven into the ground. The drive-probe capped piezometers were installed at selected locations using a Forest Service-approved slide hammer (Hall et al., 1994). Blow counts were recorded during the installations to detect the presence and determine the depth of a subsurface shearing zone (Table 7). Well 3, located about 10 m beyond the eastern earthflow boundary, was installed with a hand-held gasoline- powered auger. A 10 cm diameter auger hole was excavated to a depth of about 4 m, lined with PVC tubing and backfilled. The fieldwork taught us that the steel pipe drive-probe type monitoring well installation was the superior method for a small scale, low budget field investigation (Hall et al., 1994).

Soil testing conducted in the Portland State University Geology Department includes Atterberg limits (Casagrande, 1948) and gradation analyses by sieve and pipette (Galehouse, 1971). Clay mineralogy of the earthflow soil materials was determined by x-ray diffraction analysis (Chen, 1977; Moore, and Reynolds, 1989). Direct shear testing was performed in the Portland State University Civil Engineering Department Laboratory (Das, 1985) in accordance with ASTM standards (ASTM, 1988).

# CHAPTER 4

# RESULTS

## ATTERBERG LIMITS

The Atterberg test results are shown in Table 2. Soil samples for all testing methods were collected at depths greater than 25 cm from the sites indicated on the project base map (Figure 3). The liquid limits of the carbonaceous mudstone samples are somewhat higher than the liquid limits of the siltstone samples. The plasticity indices follow the same general trend. Laboratory data for Atterberg tests can be found in Appendix C.

**Table 2. Atterberg limits test results in percent moisture.**

| SOIL TYPE | MUDSTONE | MUDSTONE | SILTSTONE | SILTSTONE |
|---|---|---|---|---|
| SAMPLE I.D. | STA-1 | A - 2 | A - 3 | A - 5 |
| IN SITU WATER CONTENT | 28 % | 30 % | NA | NA |
| LIQUID LIMIT | 53 % | 95 % | 46 % | 43 % |
| PLASTIC LIMIT | 25 % | 18 % | 34 % | 41 % |
| PLASTICITY INDEX | 28 % | 77 % | 12 % | 2 % |

PENETRATION TEST

Blow counts were recorded during the groundwater monitoring well installation using drive probes and are reported in Table 3. The blow count is the number of blows per foot required to advance the drive probe into the soil.

**Table 3. Drive Probe Penetration Test Data**

| Well #1 Scarp well | | Well #2 Upper slide | | Well #3 Lower slide | |
|---|---|---|---|---|---|
| Depth, ft | Blows | Depth, ft | Blows | Depth, ft | Blows |
| 0 | | 0 | | 0 | |
| 1 | 15 | 1 | 8 | 1 | 8 |
| 2 | 22 | 2 | 7 | 2 | 7 |
| 3 | 44 | 3 | 10 | 3 | 9 |
| 4 | 55 | 4 | 3 | 4 | 8 |
| 5 | 85 | 5 | 7 | 5 | 12 |
| 6 | 75 | 6 | 15 | 6 | 22 |
| 7 | 123 | 7 | 19 | 7 | 26 |
| 8 | 107 | 8 | 18 | 8 | 31 |
| 9 | 134 | 9 | 33 | 9 | 31 |
| 10 | 147 | 10 | 51 | 10 | 51 |
| 11 | 250 | 11 | 57 | 11 | 60 |
| | | 12 | 48 | 12 | 65 |
| | | 13 | 48 | 13 | 98 |
| | | 14 | 79 | 14 | 132 |
| | | 15 | 150 | 15 | 88 |
| | | | | 16 | 120 |
| | | | | 17 | 95 |
| | | | | 18 | 135 |
| | | | | 19 | 200 |
| | | | | 20 | 210 |

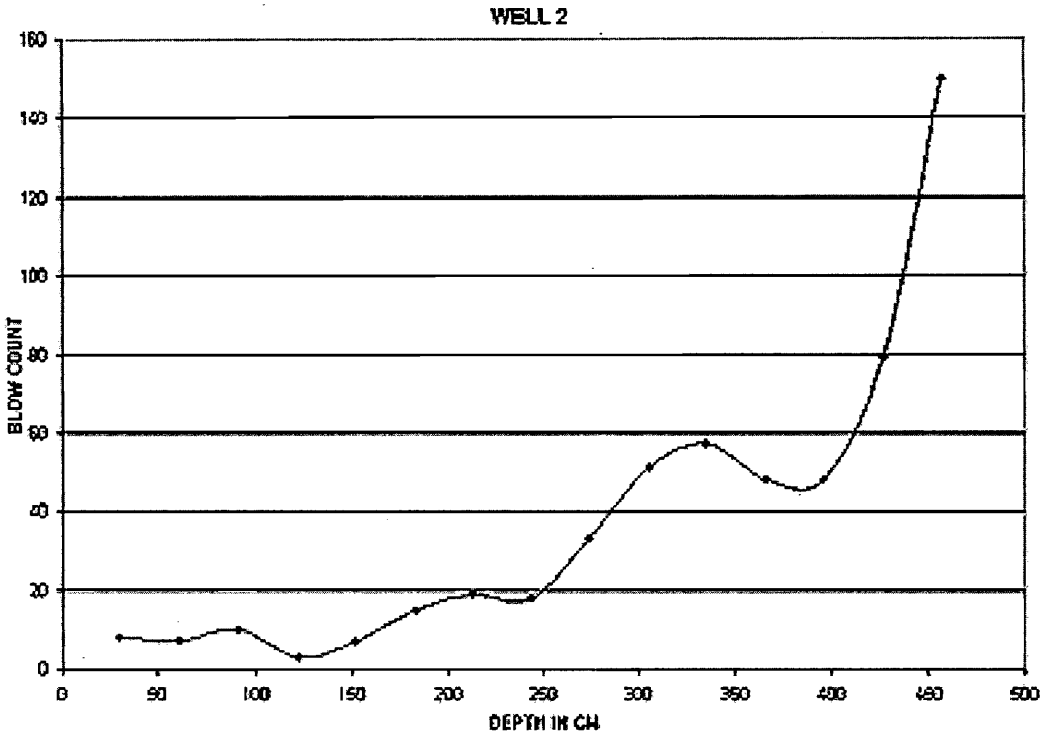


**Figure 8. Graph of drive probe penetration test data for Well 2. Top of mudstone appears at 220 cm (7 ft) depth. Zone of weakness appears at 340 cm (11 ft) depth.**

Zones of weakness are indicated by a decrease in the number of blows required to advance the probe. Three such decreases can be seen in Figure 8. The greatest decrease in blow count appears at a depth of 3 - 4 m below the present ground surface. This zone of weakness is interpreted as the shearing plane of the earthflow. From the surface morphology of the earthflow it appears that from 35-45 m of soil has been displaced from the surface of the basin where the penetration test of well 2 was performed. The failure surface is interpreted to be at a depth ranging from 40 - 50 m below the pre-failure ground surface in this location (personal communication, Arvid M. Johnson, Purdue University, 1996).

## PARTICLE SIZE ANALYSIS

The soil samples used for the particle size gradation analysis have variable gross characteristics. Particle size analysis for three samples thought to be representative of the study area soils are shown in Figures 9, 10 and 11. Particle analysis developed from sample STA-1, undisturbed dark gray mudstone collected at a depth of 1m below the bedding surface using a Shelby tube is shown in Figure 9. This mudstone sample is cohesive, uniformly very fine grained, has a very slight gritty, silty component, slightly friable, markedly sticky, and fragments can be fractured by hand. Pebble to boulder sized, competent, subangular mudstone fragments were excavatable using a shovel or rock hammer.

Particle size analysis developed from yellow-gray siltstone samples collected from two locations within the study area (Figure 3) are shown in Figures 10 and 11. Sample A-3 (Figure 10) was collected from one of several colluvial wedges exposed on the headscarp face. Sample A-5 (Figure 11) is from a colluvial deposit near contour 475 m. The siltstone samples are slightly friable, brittle, have yellow-gray color and sandy, silty texture with moderate to marked stickiness when moist. Gravel to boulder sized fragments were excavated using hand tools.

Surface colluvium in the study area appears to be in a weathered state and ranges in size from sand to cobbles. Popcorn texture is common to both mudstone and siltstone when exposed. Pebble and gravel sized siltstone material displays a range of colors from yellow to orange to red to brown. The mudstone remains dark

gray upon exposure. The variable textural characteristics apply equally to materials examined on the earthflow surface as well as the samples collected from the subsurface.

The majority of the surface colluvium deposits on the earthflow surface consist of the yellow to yellow-gray, gravelly, sandy siltstone derived material, with very minor amounts of the gray mudstone. Appreciable quantities of dark-colored, presumably mudstone-derived colluvium occur only in the down slope portions of the earthflow below the failed road embankment near contour 440 m and near the tree raft and soil mound areas.

Initial particle-size analysis using a hydrometer appeared to be flawed, with a large step in the gradation curve at 65 μm. The pipette method (after Galehouse, 1971), resulted in a more continuous gradation curve. Laboratory data for the gradation analysis are reported in Appendix D.

## DIRECT SHEAR TESTING

Direct shear tests were performed on samples collected in undisturbed, 10 cm blocks. Sample A-3 is from a colluvial wedge exposure in the headscarp. Sample A-5 is colluvium consisting predominantly of yellow-gray siltstone. Sample STA-1 is dark-gray mudstone bedrock, collected in a Shelby tube (Table 4). Direct shear test methods conform to ASTM D3080-72 standards (ASTM, 1988).

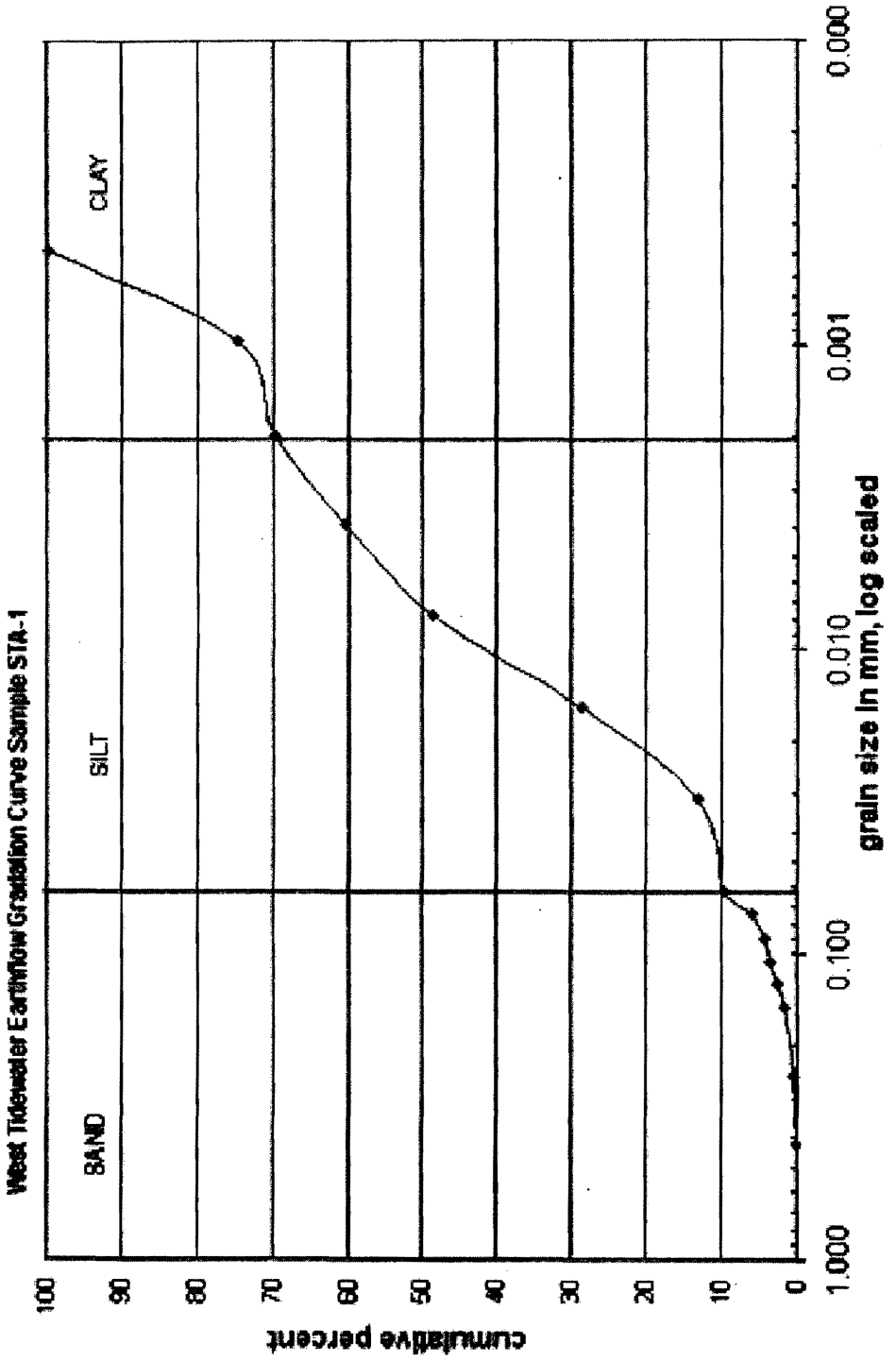


**Figure 9. Gradation curve of sample STA-1, dark-gray mudstone. Composition is 10% sand, 60% silt, and 30% clay.**

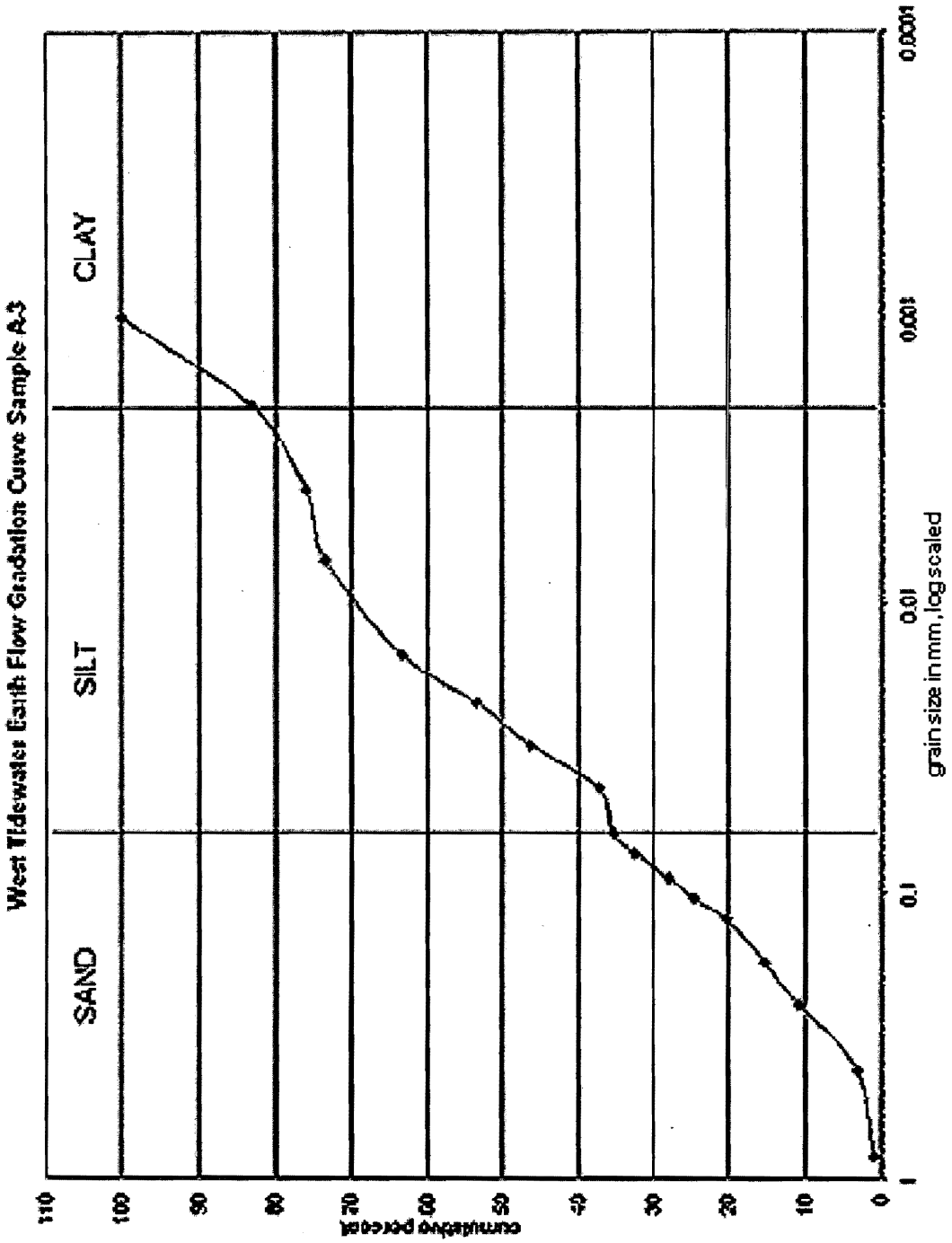


**Figure 10. Gradation curve of sample A-3, yellow-gray siltstone. Composition is 35% sand, 50% silt, and 15% clay.**

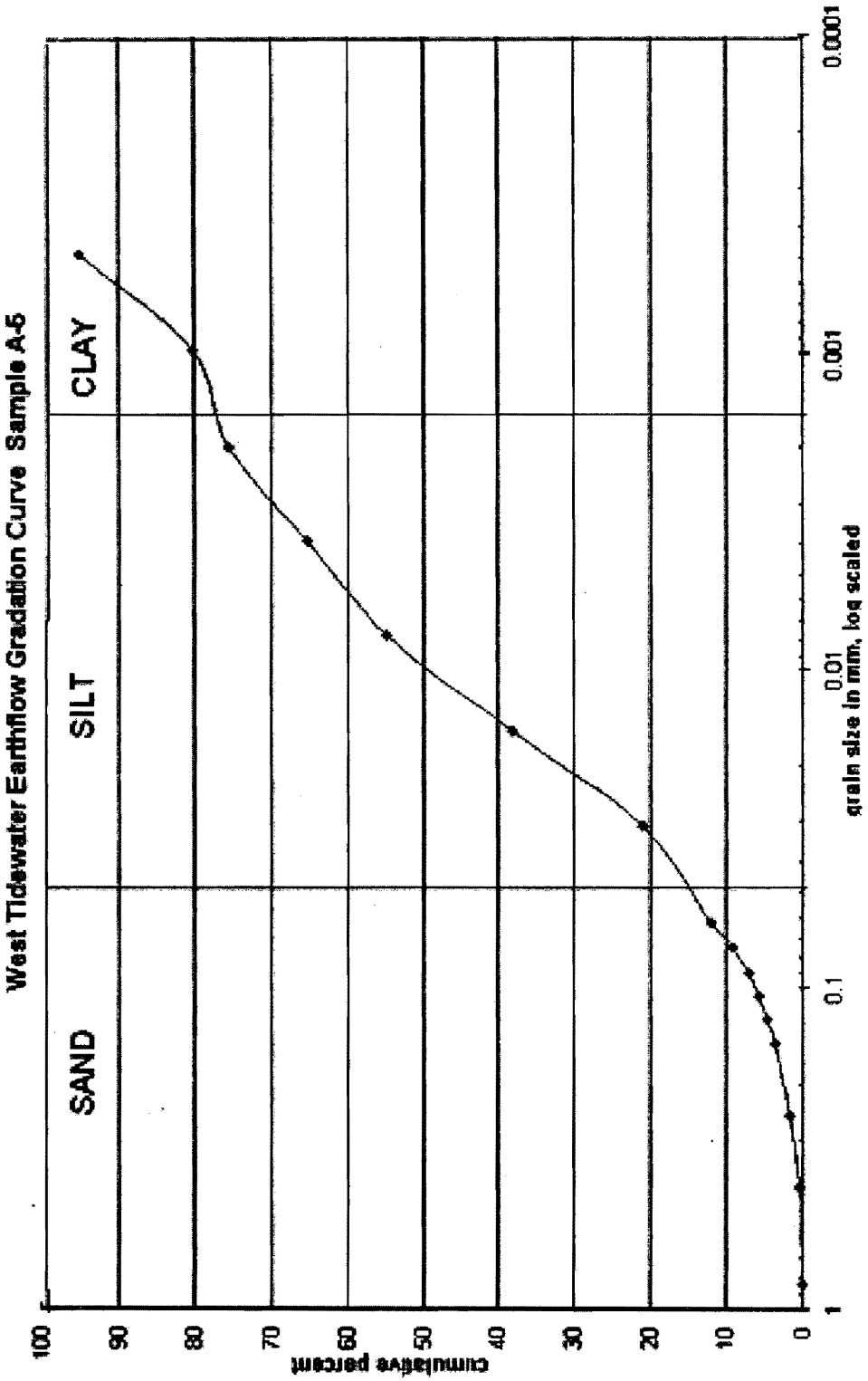


**Figure 11. Gradation curve of sample A-5, yellow-gray colluvium. Composition of sample is 15% sand, 62% silt, and 23 % clay.**

Laboratory techniques as described by Das (1985), MacIver and Hale (1970), and Dr. Trevor Smith, (personal communication, Department of Civil Engineering, Portland State University, 1997) were used in the determination of residual cohesion and residual internal friction values. Shear tests were performed on five different samples using a Soiltest direct shear apparatus in the Portland State University Civil Engineering soil-testing laboratory. The procedures were carried out in a strain-controlled method in which shearing strain is applied to the samples at a constant rate. The advantage of strain-controlled tests is that both peak and residual soil strengths can be measured. Stress-controlled tests allow only the determination of peak strengths (Skempton, 1985). Soil samples were consolidated for a minimum of 24 hours in a drained condition prior to same-state shear tests. The consolidated-drained tests are designed to reproduce the strain conditions occurring within the earthflow shear zone prior to failure. It is assumed that by shearing samples at a constant, slow rate in a drained condition and a constant volume, negligible levels of pore water pressures are generated during the tests. The test stresses are therefore taken to be effective stresses and reflect the frictional strength of the soil skeleton unsupported by water pressure. Because the West Tidewater failure is a reactivation of a previous landslide, and soil block and colluvium displacements are considered to be large, the relevant measurement of soil strength is ultimate, or residual friction (Skempton, 1985). Samples were therefore repeatedly sheared, reversed, and sheared again until it was apparent that a residual condition had been reached.

Some samples were tested in an undrained state in order to examine soil conditions during shear failure. If the soil movement along the shear plane lasted for more than just a few seconds, the remolding and associated volume changes would put the earthflow soils into and undrained state.

**Table 4. Results of direct shear tests.**

| Sample and Description | | | Residual Cohesion | Residual Friction |
|---|---|---|---|---|
| STA-1 | mudstone | CD | 4 kPa | 17° |
| A3 | siltstone | CD | 8 kPa | 18° |
| A5 | siltstone | CD | 5 kPa | 14° |
| A5 | siltstone | CU | 4 kPa | 17° |

CD : consolidated drained CU : consolidated undrained

The drained samples show effective cohesions ranging from 4 to 8 kPa. The drained effective residual friction angles range from 17° in the clay-rich mudstone to 14-18° in the sandy siltstone. The undrained siltstone sample shows a residual friction angle of 17° and residual cohesion of 4 kPa. The Mohr-Coulomb failure envelope developed from direct shear tests on mudstone sample STA-1 is shown in Figure 12A. The relationship between the size of the clay fraction versus the empirically-derived residual friction value is shown in Figure 12B as a check for reasonable values. The West Tidewater earthflow samples are indicated by labeled stars.

A

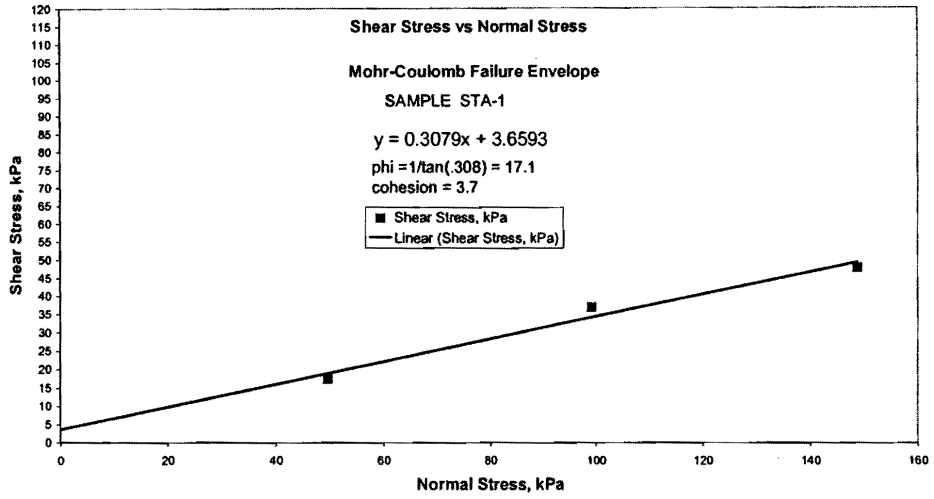


B

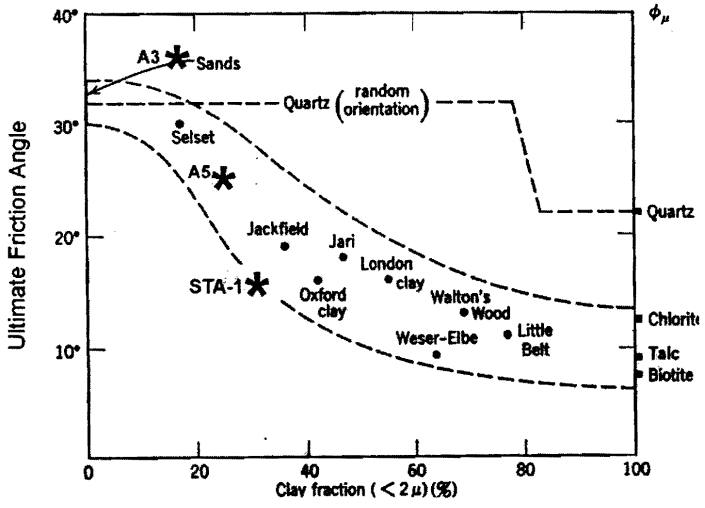


**Figure 12. 12A shows the Mohr-Coulomb failure envelope from direct shear tests on sample STA-1. Residual friction angle is 17°, residual cohesion is 3.7 kPa. 12B from Skempton (1964) compares values of ultimate or residual friction angle and the sizes of clay fractions.**

Laboratory data and stress/strain curves for direct shear tests can be found in Appendix G.

BULK DENSITY

The dry bulk density, or unit weight, of two samples of mudstone from the study area ranges between 1.25 g/cm$^3$ and 1.34 g/ cm$^3$ (Table 5).

**Table 5. Results of dry bulk density analysis of dark gray mudstone.**

| | Sample A | Sample B |
|---|---|---|
| volume | 115.5 cc | 115.5 cc |
| moist weight | 204.4 g | 216.2 g |
| dry weight | 144.70 g | 154.80 g |
| water weight | 59.70 g | 61.40 g |
| water % | 41.3 % | 39.7 % |
| Dry Bulk Density | 1.25 g/cm3 | 1.34 g/cm3 |
| Dry Unit Weight | 12.3 kN/m$^3$ | 13.1 kN/m$^3$ |
| Moist Unit Weight | 17.4 kN/m$^3$ | 18.4 kN/m$^3$ |

CLAY MINERALOGY

X-ray diffraction analysis of samples of siltstone and mudstone indicates major amounts of smectite with minor amounts of illite and kaolinite clays (Table 6).

The clay analysis was performed using laboratory methods specified by Moore and Reynolds (1989) and diffraction patterns determined by Chen (1977). An example diffraction analysis trace is shown in Figure 13. Laboratory data and graphs for the entire X-ray diffraction workup can be found in Appendix G.

**Table 6. Clay species and percent of total clays.**

| Clay Species | mudstone Sample STA-1 | siltstone Sample A-5 |
|---|---|---|
| Smectite | 90% | 80% |
| Illite | 5% | 15% |
| Kaolinite | 5% | 5% |

The interlayer spacing of a clay, or *d*-spacing, governs its ability to deform by shear. Expected results for hydrated smectites typically range from 15 to 17Å (Velde, 1992). Smectites in the West Tidewater samples show a *d*-spacing of 20.5Å. Smectite interlayer spacings of up to 50Å are possible. Expanded interlayer distances attenuate the electrical forces that hold clays in their typical layered habits, thus weakening the fine-grained portion of a clay soil. One possible explanation for increased *d* spacing is interlayer absorption of organic carbon compounds. Smectite and other clay species may swell as a result of the formation of cation-organic molecule complexing (Velde, 1992). Carbon-based compounds have the ability to bond to the oxygen in the interlayer spaces of clays (Figure 14A). These organic compounds bond in several different orientations depending on the quantity

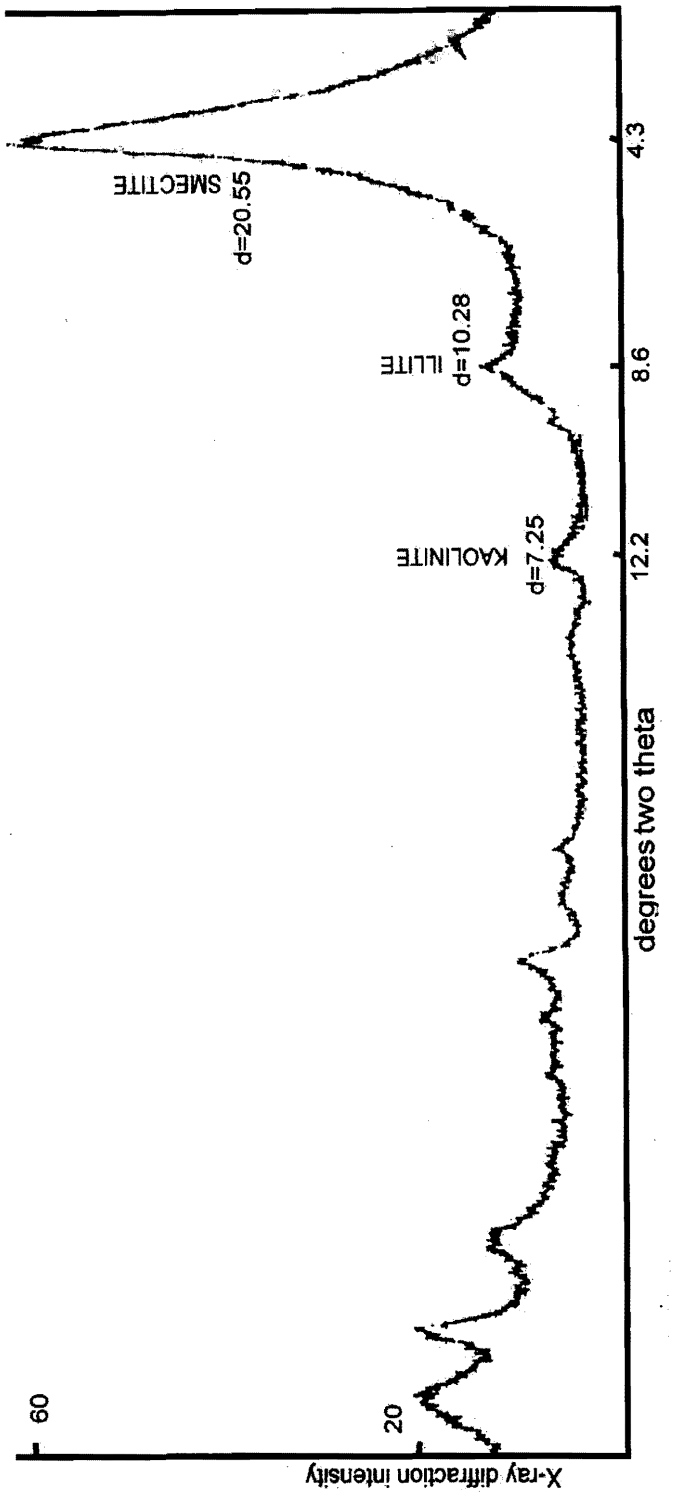


**Figure 13. X-ray diffraction pattern of the sample A-5 clay fraction. The smectite peak shows a d-space of 20.5 angstroms.**

of cation substitutions within the clay species host (Velde, 1992), (Figure 14B). An attendant reduction in soil strength due to oriented organic carbon compounds within the clay interlayers is therefore possible. If organic carbon is present in the local mudstone, it could be the cause of the expanded interlayer spacing and the dark gray coloration.

## GROUNDWATER

The initial water table depth readings were taken in August of 1996 after the monitoring wells had been allowed to equilibrate for approximately 30 days following their installation. A Fisher battery-powered well measurement e-tape was used for water level data collection. Table 7 contains the groundwater data collected during the study. The data demonstrate the seasonal variability of the water table within the study area **(http://www.ocs.orst.edu/pub_ftp/climate_data/pcp).** The water table surface in well 3 rose from 51 cm to within 18 cm of the ground surface between October of 1996 and February of 1997. The data give an indication of the groundwater regime within the study area. Sediments buried well 2 installed in the alluvial-colluvial depositional area of the upper slide shortly after the first rains in the fall of 1996. During the course of soil sampling and installing monitoring wells, it was noted that the soils and colluvium in all the areas that were examined were moist to very moist below depths of 20 cm from ground surface. This observation

A

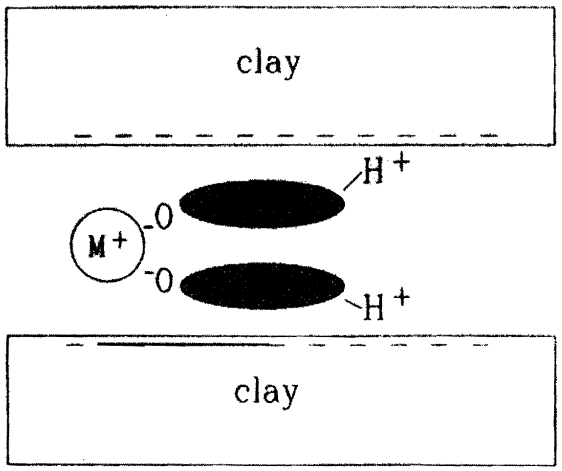


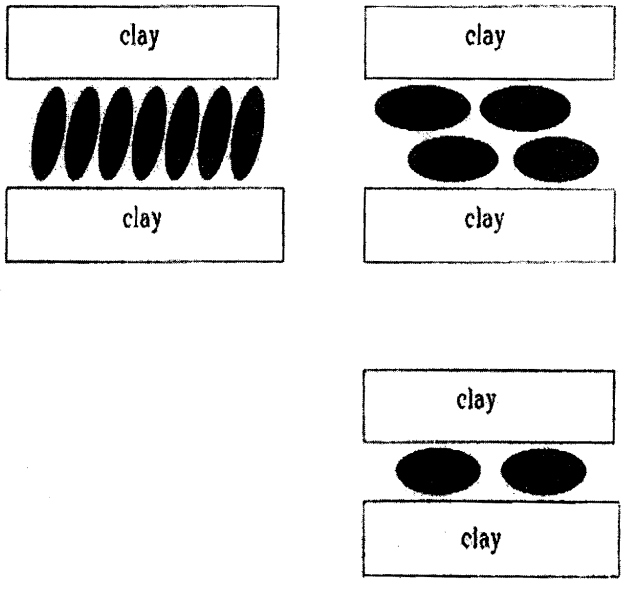


B

**Figure 14. Drawing of carbon compounds (A) bonding to cations in clay interlayers and (B) showing different possible orientations, (Velde, 1992).**

continued to be true throughout the summer months right up to the beginning of winter rain season. The study area soils apparently never completely dry out below a depth of 20 cm despite the absence of any appreciable precipitation during the summer months (**http://www.ocs.orst.edu/pub_ftp/climate_data/pcp**).

The springs and seeps along the eastern slide margin continued to flow but at a diminished level during the summer and fall of 1996. Many small stream channels are being cut into the earthflow surface as a combined result of winter rainfall and groundwater flowing up onto the colluvial surface (Figure 3).

**Table 7. Water table depths in cm from ground surface.**

| DATE | SCARP | WELL #1 | WELL #2 | WELL #3 |
|---|---|---|---|---|
| 10/11/96 | 302.0 | 83.0 | 51.0 | NA |
| 2/9/97 | 292.1 | BURIED | NA | NA |
| 2/28/97 | 305.1 | BURIED | 17.5 | 30.2 |
| 3/8/97 | 304.8 | BURIED | 14.6 | NA |
| 3/15/97 | 305.4 | BURIED | 16.5 | 48.9 |

The only groundwater source observed on the western side of the earthflow emerges from the head scarp near the basalt to sandstone contact approximately 10 m below the rim. This seep flowed until about mid-July of 1996. There is a stream drainage and marsh area approximately 20 m east of the eastern earthflow margin

just below well 3, crossing contour 495 m. The runoff from this spring and wetland flows into a stream channel that defines a 200 m-long section of the eastern margin of the earthflow. This larger outflow joins numerous minor outflows to become the principle drainage of this basin. Cut banks up to 4 m, lying at roughly 30° from vertical, have developed in many areas of the mid and lower slide. Stream waters are heavily clouded with sediment for several days after rainstorms. Colluvial materials are being redeposited in depressions on the upper and middle surfaces of the earthflow (Figures 16, 17). Colluvial gravel is also being deposited beyond the distal toe of the earthflow creating stretches of stream braiding and small gravel bars below contour 390 m.

## PRECIPTATION

The Oregon coastal mountains receive most of their yearly precipitation during winter months from October to March. The yearly precipitation in the Coast Range averages over 250 cm. The monthly rainfall levels (http://www.ocs.orst.edu/pub_ftp/climate_data/pcp) recorded at the Astoria airport weather station approximately 15 km west of the West Tidewater study area are shown in Table 8 and Figure 15. The December rainfall for the five years previous to 1994 averages 18 cm. In December of 1994 when this earthflow occurred, Table 8 shows that rainfall for the month was 38 cm, more than twice the five-year average.

Rainfall for the two months previous to the earthflow event increased by 100% in October, and 40% in November over their respective five-year monthly averages.

Rainfall intensity and duration have a significant influence on the stability of soils on slopes and embankments (Bishop et al., 1964). When the rate and quantity of rainfall exceeds the natural drainage capacity of a soil, some of the water runs off as overland flow. The water that infiltrates results in increased pore pressure that will significantly reduce the strength of a soil and reduce effective stress (Casagrande, 1948). The greater than average 1994 rainfall must therefore one of the critical factors in the West Tidewater failure.

**Table 8. Rainfall recorded at the Astoria, Oregon airport in cm.**

| YEAR | JAN | FE | MAR | APR | MAY | JUN | JUL | AUG | SEP | OC | NOV | DEC |
|---|---|---|---|---|---|---|---|---|---|---|---|---|
| 1989 | 21 | 17 | 26 | 6 | 10 | 7 | 4 | 2 | 1 | 13 | 17 | 19 |
| 1990 | 41 | 30 | 13 | 11 | 8 | 9 | 1 | 4 | 2 | 21 | 29 | 13 |
| 1991 | 17 | 22 | 14 | 24 | 10 | 5 | 1 | 6 | 0 | 6 | 27 | 17 |
| 1992 | 24 | 14 | 30 | 19 | 6 | 2 | 0.5 | 2 | 7 | 10 | 26 | 15 |
| 1993 | 16 | 4 | NA | NA | 1 | 9 | 5 | 2 | 0 | 6 | 17 | 24 |
| 5 YR AVG | 24 | 17 | 21 | 15 | 7 | 6 | 2 | 3 | 2 | 11 | 23 | 18 |
| 1994 | 17 | 29 | 17 | 11 | NA | 6 | 2 | 4 | 7 | 24 | 32 | 38 |

Human impacts on the water budget are also a factor in slope failures. Soil water loss through evapotranspiration in coniferous forests decreases by as much as 66% in summer and 50% in winter after timber clear cutting (Waring et al., 1981).

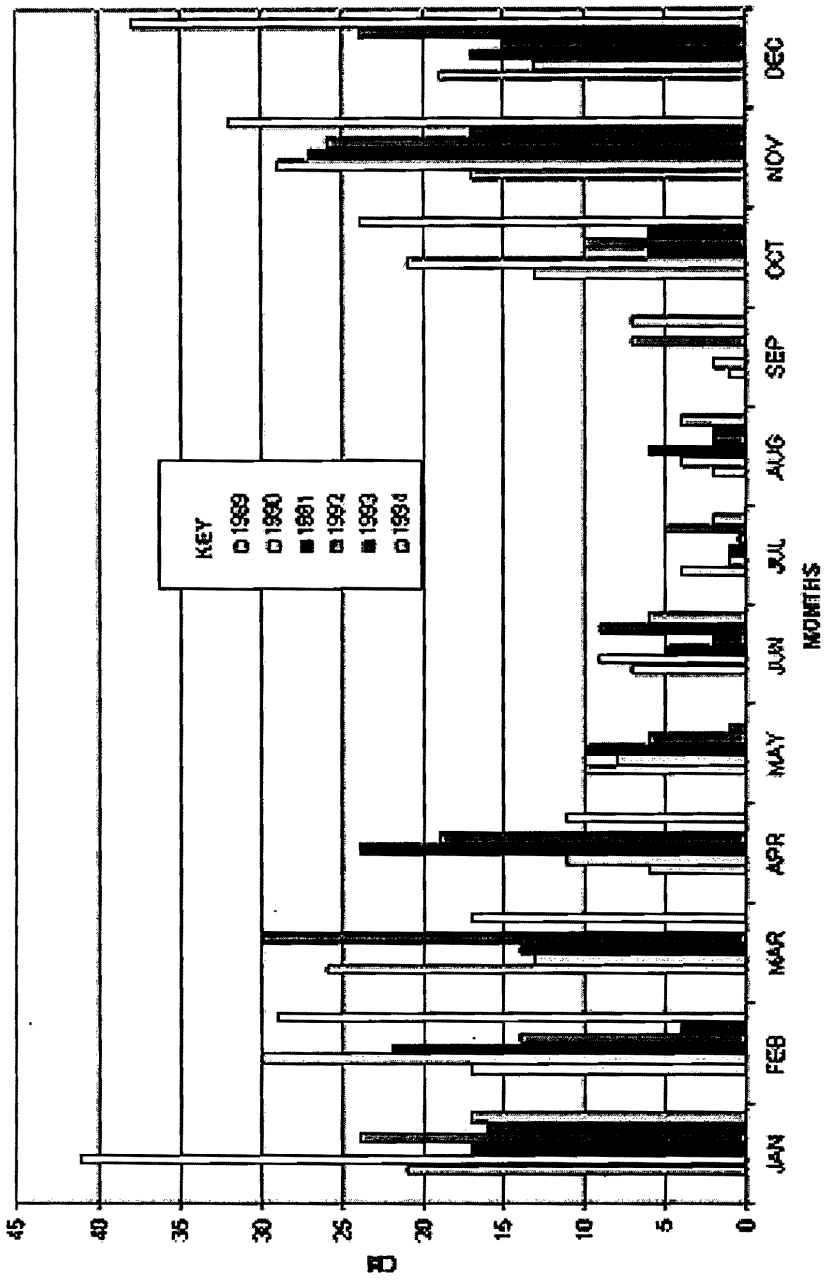


**Figure 15. Bar chart of rainfall in NW Oregon Coast Range Mountains. The rainfall totals for October, November, and December of 1994 are the bars on the far right of each group. Data was collected by Oregon State University Climate Data Center (http://www.ocs.orst.edu/pub_ftp/climate_data/pcp).**

Research in New Zealand has shown that transpiration of water by forest cover effectively reduces monthly rainfall by as much as than 30 mm in winter and 90 mm in summer (Pearce et al., 1987). Rainfall interception by the forest canopy has been shown to effectively reduce the total yearly rainfall by an average of 35 % (Marden et al., 1992). The studies just cited indicate that the combined effects of reduced vegetative transpiration and interception could effectively increase in situ soil water content, and thus could decrease overall slope stability.

## BASE MAP & EARTHFLOW FEATURES

The major earthflow features and the topography of the study area are shown on the project base map (Figure 3). Noteworthy features include several areas of alluvial deposition (Figures 16, 17), the major headscarp (Figure 18), soil blocks (Figure 19), lateral ridging on portions of both margins, several soil thrust fronts and minor scarps (Figure 20), sag ponds (Figure 21), a tree raft and soil mound area, and numerous seeps and springs.

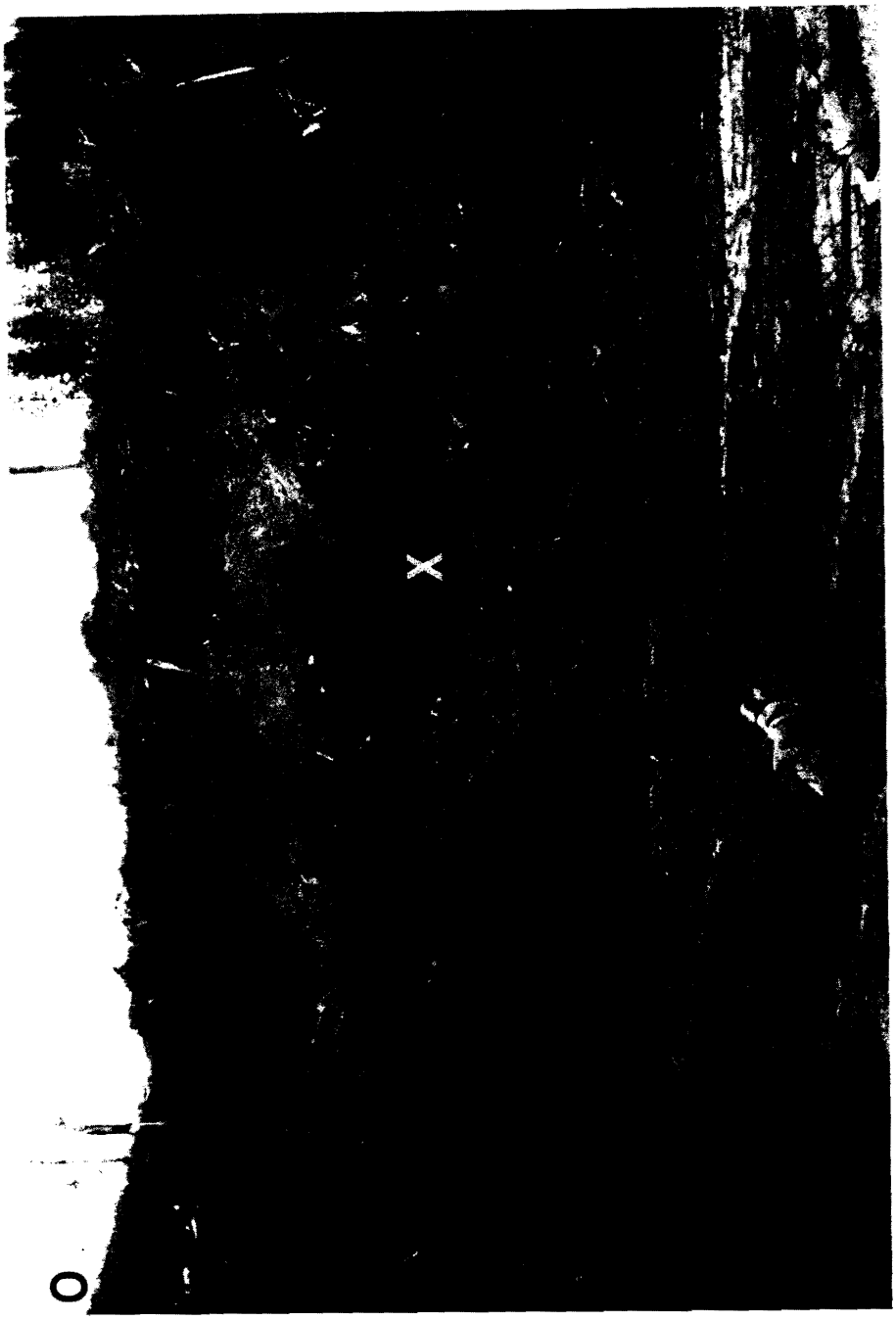


**Figure 16. Colluvium being deposited on the earthflow surface. X is the collection site for dark gray mudstone STA-1. O is Piezometer well #3.**


**Figure 17. Colluvium being fluvially deposited (lower figure) on the upper earthflow surface near contour 500 m. The black arrow indicates a fractured area of alteration that indicates a fault zone (fault trace, plate 1). The white X at the bottom is the location of well #2.**

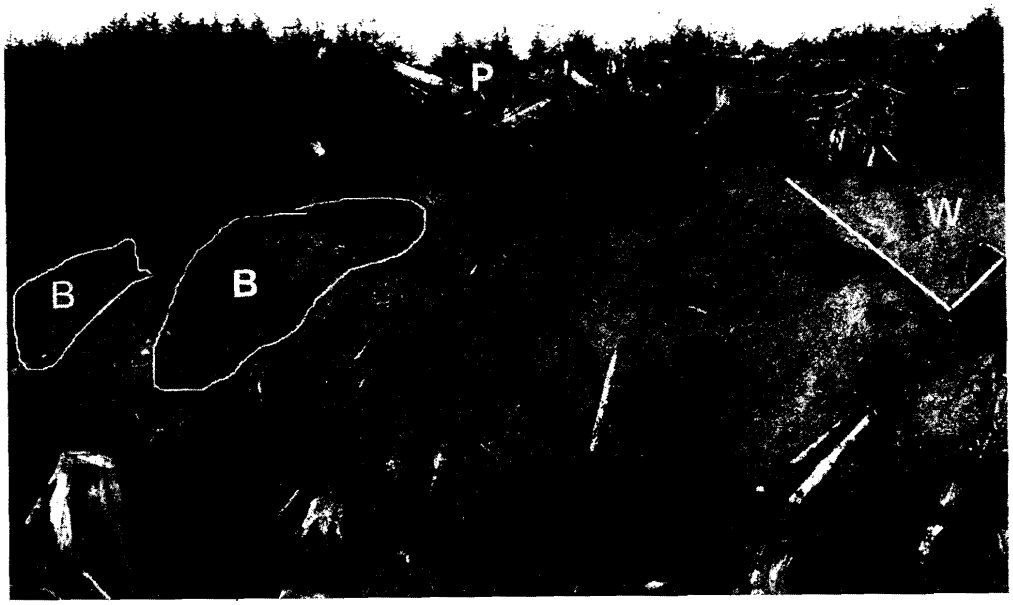


**Figure 18. View of the headscarp looking north. Areas labeled 'B' are exposures of ridge forming invasive basalt. Area labeled 'W' is a colluvial wedge. The 'P' indicates the location of Piezometer well 1.**

**Figure 19. A view looking northwest showing one of the upper soil blocks surfaces along contour 545 m, and the NW margin of the earthflow. The headscarp extends to the figure right.**

**Figure 20. Structural feature located along contour 495 m near the western margin of the earthflow about 40 m downslope from well 2 (Figure 3). The 2 - 3 m height exposes yellow-gray siltstone and colluvium.**

The earthflow has total vertical relief of about 175 m and covers a horizontal distance of about 900 m, resulting in an average surface slope angle of 10°. The adjacent, undisturbed slopes exhibit an overall slope angle of 11 - 12°. The surface terrain of the flow is very hummocky and irregular with extensive ground cracking, soil mounds, dense clear-cut slash, steep stream cutbanks, thick brush, denuded soils, and thrust toes. Fieldwork and foot travel within the slide boundary is both difficult and hazardous.

**Figure 21. Sag pond along contour 530 m near the eastern earthflow margin. Also visible is the surface of one of the upper soil blocks with a cover of new growth hemlock.**

The 15 - 20 m headscarp exposes the massive, yellow-gray siltstone and portions of the ridge forming invasive basalt. The scarp also exposes two colluvial wedges ranging from 3 - 6 m wide at the rim, with depths ranging from 3 - 4 m. The

margins of the wedges are well-defined and form sharp downward apexes. The wedges are composed of siltstone and basalt boulders and gravels in a yellow-gray, sand and silt matrix. The boulders and gravels comprise roughly 30% of the total wedge volumes.

The ridge-forming basalt had been quarried and crushed into gravel about 40 m northwest of the headscarp until the lower portion of the haul road was destroyed by the earthflow (Figure 22). This basalt body strikes N 75° W, 5°E. Extensive jointing in the quarry exposure is oriented at N 75° W, 75° S. This bedding trend reflects the overall tectonic regime of the Astoria basin and most of northwestern Oregon (Niem and Niem, 1985). This orientation also closely matches the bearing of the suspected fault shown on the Niem and Niem (1985) map that dissects the upper earthflow at contour 540 m (Figure 3). The contacts between the basalt and siltstone exposed in the quarry are indistinct, irregular, range from subvertical to subhorizontal, and show extensive alteration. There are zones of weathering along the basalt to siltstone contact with alteration colors that vary from yellow to red-brown to black. The orphaned haul road parallels the ridge 5-10 m upslope from the headscarp rim. Road-fill material cracks nearly 10 m long are forming on the downslope side of the road adjacent to the abandoned quarry. One of these cracks grew from a width of 5 cm to 22 cm between February 9 and March 14, 1997. The grade crack propagation is facilitated by poor logging road construction methods and is evidence that the road prism and possibly the adjacent road cutbank are not stable.

**Figure 22. Exposure of invasive basalt that delineates the northern structural margin of the study area. The rocks are extensively weathered, fractured, and jointed. Rock was being quarried here until the earthflow removed the access road.**

Three structural soil surface features are mapped on the earthflow surface (Figure 3). They lie along contours 495 m, 475 m, and 465 m. The convex colluvial

soil surfaces alternating with concave alluvial accumulation basins and breaks in slope give the earthflow surface an undulating, stair-step longitudinal profile. The soil front with the greatest relief is in the central slide area above the old haul road near contour 450 m. This thrust contains the exposure of historically buried trees adjacent to well #4. Two of these trees are nearly a meter in diameter and lie with their long dimension subparallel to the flow direction. Portions of the outer surfaces of the two buried trees display a two or three cm weathering rind. Other surfaces of the same trees appear fresh and are barely discolored, with minimal alteration. Most of the wood in the two trees appears to be well preserved. In order to obtain a piece of fresh wood, a sample was taken about 50 growth rings inward from the bark. Carbon-14 dating shows that the tree died 700 +/- 50 years BP (Beta 132479). Subtracting 50 years from the C-14 date yields an approximate age of 650 years.

No buried soil horizons were found anywhere in the study area. Such surfaces could help confirm or rule out a burial event or establish age

TREE RAFT

A 'tree raft' (Swanston and Swanson, 1976) approximately 150 m long and 25 m wide sits near the middle of the earthflow between contours 490 m and 470 m. The most likely source for the raft is from the northwest margin of the slide, near the trace of the transverse fault (Figure 3). This portion of the study area contains similar 10-20 cm diameter trees and was not subject to clear cutting during the

timber harvest in 1991. The root systems of the unharvested trees and brush on the surface of the raft have held the upper 1 - 2 m of soil nearly intact. Most of the vegetation on the raft is relatively undisturbed with the exception of the toppling of a few of the taller trees (Figure 23). The surface relief of the tree raft area varies by 1 - 2 m. The intact raft demonstrates the substantial tensile strength that root systems contribute to soils (Ziemer, 1981; Riestenberg et al., 1983).

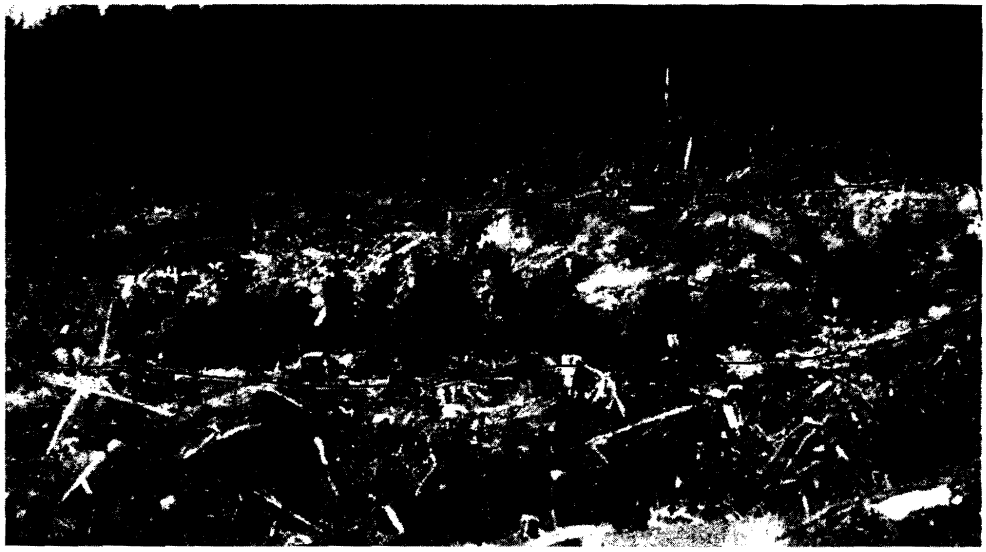

**Figure 23. A portion of a tree raft, outlined in black, resting on the earthflow surface near the western margin. Distance to the raft is about 150 m.**

SOIL MOUNDS

A number of features described as "soil mounds" are located on and around the tree raft surface and for some 25 m upslope of the upper end of the raft. These mounds are rounded, serpentine, and range from 1-10 m long, 1-2 m in width, and

from 20 cm to over 1 m in height. The mounds are composed primarily of yellow-gray colluvium, with minor amounts of dark-gray mudstone pebbles (Figure 24). Most of these mounds are arranged in a multicurved or sinusoid form. The long axes of some mounds are roughly parallel to others, but most lie at random angles to one another with no discernable orientation to the rest of the earthflow. The soil mound

**Figure 24. A 6 - 8 m long, 1 m high soil mound on the surface of the earthflow. Note the multicurved, sinusoid configuration. The ground in this area is marshy with sedges and grasses emerging from the colluvial surface.**

colluvium is indistinguishable from the colluvium on the rest of the earthflow. In the same general area, 10-15 cm diameter cobbles are found balanced on the tops of 0.5

m tall by 1 m wide cone-shaped mounds. The capstone cobbles are yellow siltstone or dark gray mudstone. The capstones are weathering in place, slaking down to popcorn textured pebbles that lie on the surface of the cones and mounds. This is one of the few areas of the earthflow where dark gray mudstone is exposed in any quantity or form other than a few centimeter-sized chips.

The origin of the soil mounds and cones is unclear. In an attempt to determine the origin of the mounds, a 1 m wide by 2 m long trench was excavated across the axis of one of the mounds near contour 485 m. About a meter of the yellow-gray colluvium and about 30-cm of underlying, dark gray mudstone were removed from the trench. No evidence of vertical cracking, loading, or soil extrusion was seen in either layer. The colluvium to mudstone contact was an indistinct 10 cm zone, wavy and slightly intermixed. The underlying mudstone showed a random pattern of arcuate; submillimeter-sized hairline cracks with a spacing of about 5 mm and no observable orientation. The moisture content of the dry surface colluvium increased steadily with depth until it became viscous yellow fluid at the mudstone contact. At the base of the colluvium, a steady flow of groundwater seeped from the contact zone at the top of the mudstone. Water began to flow freely from a 5 by 5 cm conduit as the excavation cut 10-20 cm into the underlying mudstone layer. The exact orientation of this water conduit through the mudstone was indeterminate due to the random nature of the mudstone cracks. The saturated mudstone around the water conduit was weaker and easier to excavate than the surrounding mudstone. A

drainage channel was dug on the downslope side to drain the trench in hopes of further excavations. The outflow was observed to continue at a steady rate for more than one hour. Further exploration of this trench was abandoned due to the muddy conditions and continued flow of groundwater.

# CHAPTER 5

# STABILITY ANALYSIS

The fundamental indicator of slope stability is the factor of safety. The factor of safety (FS) can be defined as: "that factor by which the shear strength parameters may be reduced in order to bring the slope into a state of limiting equilibrium along a given slip surface" (Turner and Schuster, 1996). Simply stated, the factor of safety is the ratio of the average sum of resisting forces to the average sum of driving forces. A factor of safety of unity indicates critical stability and incipient slope failure, while greater than one indicates stability and less than one indicates model or property instability.

The concept used to describe the effect of water pressure on soil strength was termed effective stress by Terzaghi (1924). The total vertical stress exerted by a given volume of soil is the product of the unit weight of the soil and the given thickness or depth. The pressure exerted by the pore space water in a given soil volume is the product of the height of the water table surface above a given subsurface point and the unit weight of water. Effective stress is taken to be the force exerted by the friction of the soil grains against each other, minus the buoyant force exerted by the water in the pore spaces (Lambe and Whitman, 1969). To determine the stress acting on a soil, water and soil are assumed to be incompressible, and the volume of the system must remain constant. The values for

cohesion and internal friction are derived from laboratory test results using Mohr-Coulomb theory and methods. The effective stress concept is then used to determine soil shear strength in terms of effective stress.

The models used to simulate the West Tidewater slope failure rely on the effective stress concept. The assumed semi-circular shape of the upper failure surface of the Tidewater earthflow is modeled by the friction circle method of slices first presented by Fellenius (1936). Janbu (1973) modified Fellenius' method of slices in subsequent work. The Janbu method is used in this study to determine the factor of safety, to examine the failure mode, and to quantify the forces acting on the earthflow shear surfaces. Inputs for the computer model include values of residual internal friction, cohesion, water table depth, depth to the failure surface, and soil moist unit weight determined from laboratory studies.

## PRE-FAILURE MODEL & ANALYSIS

A pre-failure stability analysis was performed using an infinite slope model and the soil and study area characteristics derived from laboratory and field work. The fundamentals of an infinite slope model are shown in Figure 25. This type of model is not as accurate as some other methods, but is used here to check for reasonableness. The critical thickness, $t_c$, of the soils in the study area is also determined using this method. Critical thickness is the calculated thickness of the soil body above which a slope will fail. Based on the penetration data and observed

geometry of the basin, a failure surface depth, t, of 50 m is assumed. Submerged soil conditions are also assumed due to the known high rainfall levels in the study area in October,

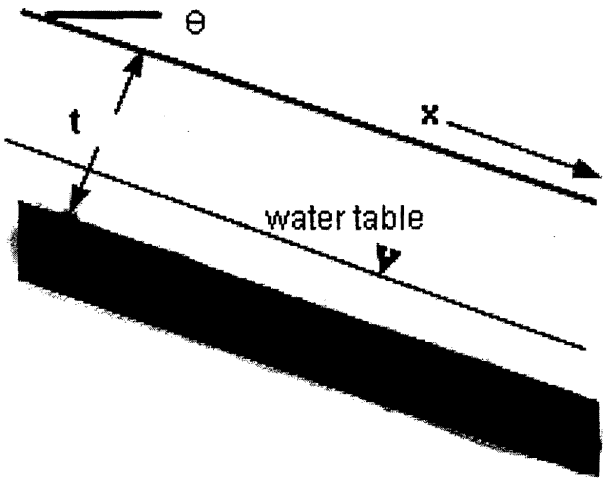


t – distance from surface to shear plane
θ - slope angle
x –distance along slope.

**Figure 25. Simplified drawing of an infinite slope model.**

November and December of 1994. The pre-failure FS is calculated using a procedure from Lambe and Whitman, (1969) and Dr. Ken Cruikshank, (Portland State University, personal communication, 1996).

$$FS = \frac{\bar{c} + t\,(\gamma_t - \gamma_w)\cos(\theta)\tan(\phi)}{t\,(\gamma_t - \gamma_w)\sin(\theta)}$$

Given:

| | |
|---|---|
| $t$ = depth to shear plane | 50 m |
| $\bar{c}$ = cohesion | 4,000 $Nm^{-2}$ |
| $\gamma_t$ = unit weight of soil | 17,400 $Nm^{-2}$ |
| $\gamma_w$ = unit weight of water | 9810 $Nm^{-2}$ |
| $\theta$ = slope angle | 10° |
| $\phi$= residual friction angle | 17° |

The calculated infinite slope pre-failure factor of safety is **1.79.**

Critical thickness is calculated in a similar manner using the same assumptions and values as above:

$$t_c = \frac{\bar{c}}{(\gamma_t - \gamma_w) \cos(\theta) \{\tan(\theta) - \tan(\phi)\}}$$

The pre-failure critical thickness, $t_c$, is calculated to be **8.3 m.**

These infinite slope calculations indicate that a submerged 10° slope in the Tidewater study area with a soil layer 8.3 m thick would be stable with a FS of 1.79.

A residual friction angle of Tidewater mudstone can also be "back calculated" using the modified Bishop (1955) method of slices where

$$\tan(\Phi) = \frac{\Sigma W_i \sin(\theta i)}{\Sigma Ni}$$ in which

$$Ni = Wi\cos(\theta i) - \frac{(ui)(b)(\delta x)}{\cos(di)}$$

This calculation results in a residual friction angle of **20.7°** (Table 9).

A Janbu (1973) circular slip surface model of the pre-failure study basin using software for the method of slices (personal communication, Dr. Ken Cruikshank,

Portland State University, 1996), is shown in Table 10. Figure 26 is the assumed slip circle profile for the earthflow, and Figure 27 is the force parameters graph.

The Janbu model of the Tidewater study area calculates a pre-failure factor of safety of **0.85,** indicating unstable slope conditions.

**Table 9. Back Calculations of Residual Friction Angle.**

| INPUTS | Units | SLICE 1 | SLICE 2 | SLICE 3 | SLICE 4 | SLICE 5 | SLICE 6 | SLICE 7 |
|---|---|---|---|---|---|---|---|---|
| C | kPa | 4 | 4 | 4 | 4 | 4 | 4 | 4 |
| gamma | kN/m3 | 17.4 | 17.4 | 17.4 | 17.4 | 17.4 | 17.4 | 17.4 |
| Dxi | m | 100 | 100 | 50 | 50 | 100 | 95 | 5 |
| Wisin(di) | kN | 14485 | 52505 | 23762 | -11772 | 57046 | -40489 | -865 |
| ui | kN | -16765 | -208825 | -27538 | 36188 | 43840 | -27959 | -1112 |
| tan di | deg | -4 | 8 | 15 | 26 | 44 | 54 | 90 |
| Ni | kN | 7297 | 201186 | 9487 | -43804 | 13197 | 61536 | 1499 |

| **sum Wi** | **sum Ni** | **Wi / Ni** | **Tangent Wi/Ni** | **degrees** |
|---|---|---|---|---|
| 94672 | 250398 | 0.38 | **20.71** | |

(slices are from the Janbu model in Table 10)

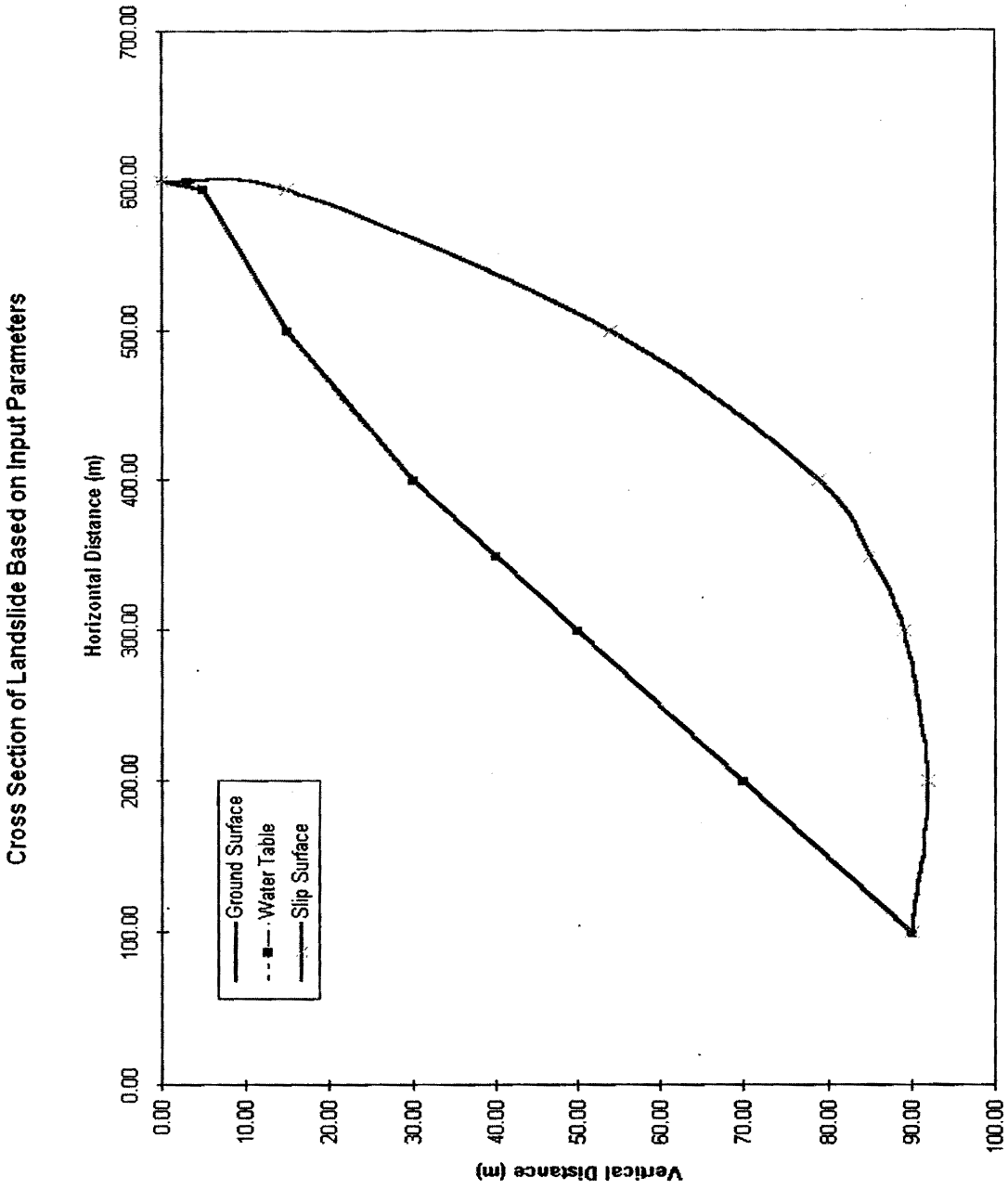


**Figure 26. Assumed slip circle profile of the earthflow using Janbu methods and Excel© inputs. The water table is set at ground surface.**

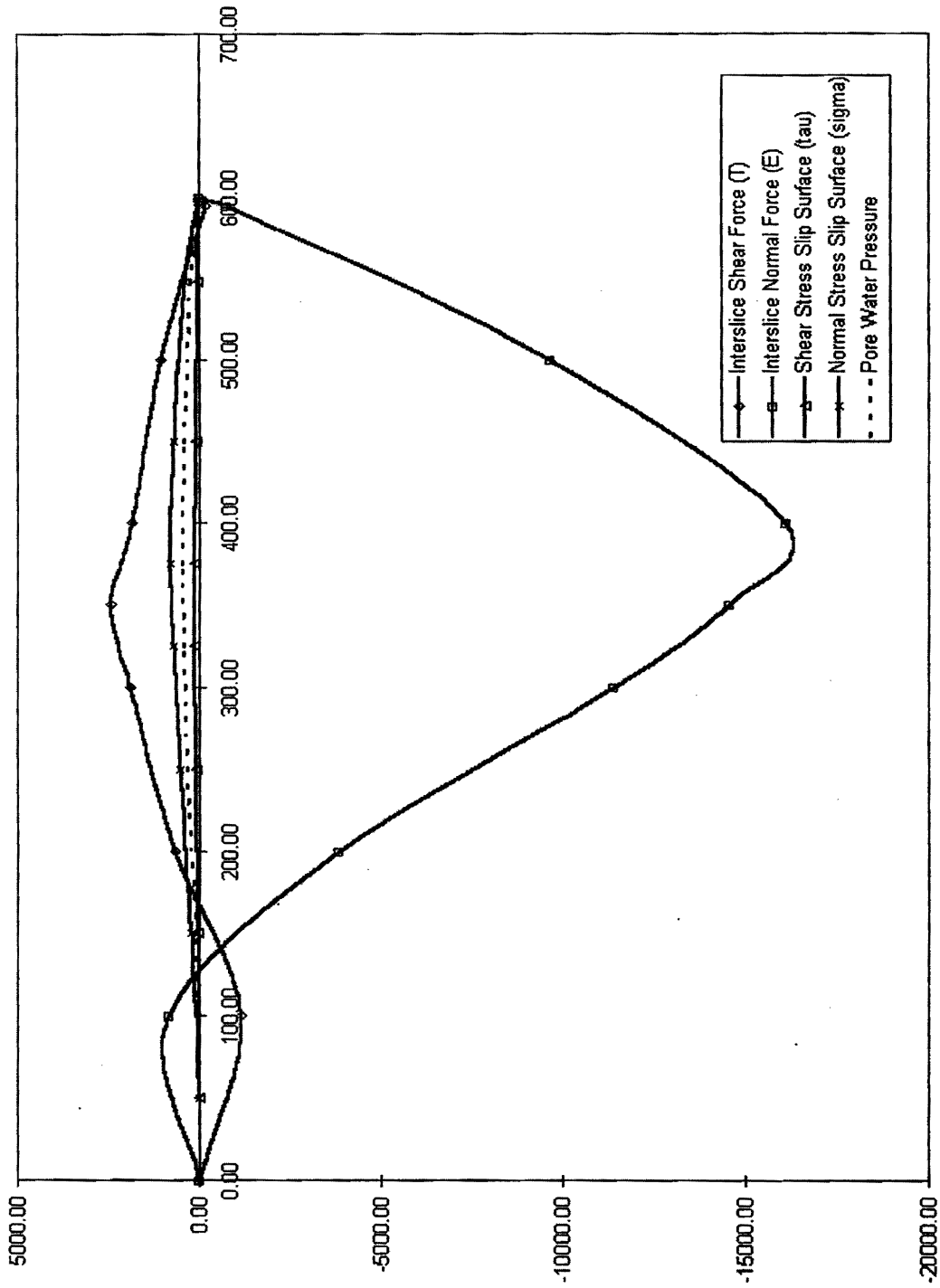


**Figure 27. Force parameter diagram of the pre-failure earthflow basin using Janbu methods and Excel© inputs.**

# CHAPTER 6

# DISCUSSION

## PHYSICAL STRENGTH OF SOIL

The most important quantitative property in slope failure analysis is the physical strength of the soil materials involved (Lambe and Whitman, 1969). Currently, the most widely accepted measure of soil strength or resistance to deformation is internal friction angle and cohesion. In landslide analysis, large spatial displacements dictate the use of the ultimate, or residual soil frictional strength to accurately assess failure potentials. Peak soil strength is only relevant to first-time failure events and to engineering design constraints in the construction of embankments and foundations.

A series of drained tests on consolidated specimens is required to accurately measure effective residual soil strength (personal communication, Trevor Smith, Civil Engineering Department, Portland State University, 1996). The soil samples in the West Tidewater study were consolidated and repeatedly sheared in both drained and undrained conditions using a series of increasing test loads until an ultimate, or residual condition was reached. The value for cohesion is also empirically determined from the same series of shear tests. In nature, soil cohesion may be influenced by capillary force within soil samples, and negative effective stresses are sometimes induced by partial saturation of the soils above the phreatic surface. There is therefore some question as to the validity of including residual

cohesion in total strength computations for remolded soil materials. Soil suction force created by adsorption of pore space water into smectite clay interlayers can also be a factor in determining and interpreting the strength of clay soils (Warkentin and Yong, 1962). Stresses due to the swelling soil pressure may increase effective shear strength by creating negative pore pressure within the soil matrix when the soil volume remains constant. It is conceivable that the absorption of water into smectite clay interlayers will actually increase soil strength by creating negative pressure within the pore spaces. In a subsurface shear zone with substantial overburden pressure, volumes may or may not remain constant.

The primary cause of earthflow is the attenuation of grain-to-grain contact of the fine-grained fraction of the soil material due to excess soil water content (Turner and Schuster, 1996). Elevated pore water pressure reduces the soil frictional strength as well as the interparticle cohesion. Additional factors affecting soil mobility are: clay content; clay mineralogy; slope angle; particle size and gradation; vegetative root strength; soil layer thickness; colloidal contents; consolidation pressure; void ratio; groundwater level and subsurface flow; and any previous movement of the soil mass in question (Taylor, 1948). When the combined effect of the many combinations of these individual stability factors approaches a critical level, the FS reduces to unity, and slope failure occurs. It is important to note that equilibrium conditions at one point on a hillside may be very different from stable conditions elsewhere on the same hillside. The interdependence of factors that modify soil

behavior and control mobility must be kept in mind when dealing with earth movement problems.

## EARTHFLOW MODELS

The infinite-slope earthflow model calculations indicate a pre-failure FS of 1.79 when the shearing surface is at a depth of 8.3 m or less. As the shearing surface is determined to be 40-50 m deep, this model indicates slope failure with the given soil conditions in the study area in December of 1994.

The pre-failure Janbu model (Table10, Figures 26, 27) represents the circular slip surface of the upper 500 m of the earthflow. The water table is set at the ground surface to simulate the saturated soil conditions present during October, November and December of 1994. Under these conditions, the Janbu model calculates a FS of 0.85, also indicating unstable conditions in the upper 500 m of the study area slope. This result suggests that the lower portion of the earthflow basin had an overall stabilizing effect on the hillside by anchoring the toe area of the earthflow basin. The second Janbu model (Table 11, Figures 28, 29) represents a toe failure at the logging road crossing. The FS for this model is 0.80. Although the decreased FS indicates a more unstable overall condition for the slip circle, the forces diagram in Figure 29 indicates increased resisting forces in the toe area of the model. These two model results suggest that toe failure mode is unlikely with the given conditions in the study area.

The third Janbu model (Table 12, Figures 30, 31) represents the slip circle in a dry or undrained state. The FS of this model is 1.89, indicating very stable slope conditions. This result points out the destabilizing effect of increased pore water pressure, in this case due to the very heavy rainfall during the winter months of 1994. Figure 32 illustrates the forces acting upon the individual slices or assumed soil block margins in the Janbu force diagrams.

## CLAY MINERALOGY

The presence of smectite clay in the West Tidewater soil samples is consistent with work by Istok and Harward (1982) correlating clay species with failure modes. In their study of slope instability in the Oregon Coast Range, smectite was the clay species most often found in soil samples from large, rotational slumps in mudstones. Their study also found halloysite clay and amorphous gel material consistently present in earthflow soils. Halloysite is not specifically identified in the West Tidewater samples, but dehydrated halloysite and kaolinite cannot be differentiated by XRD methods, so the species cannot be ruled out. Additionally, the presence of halloysite or gels is strongly suspected in light of the observation that the West Tidewater soils generally do not dry out below a 20-cm depth. Soil water retention is not only precursor to the formation of smectites, amorphous gels, and both hydrated and dehydrated forms of halloysite, it is also an indicator of their presence.

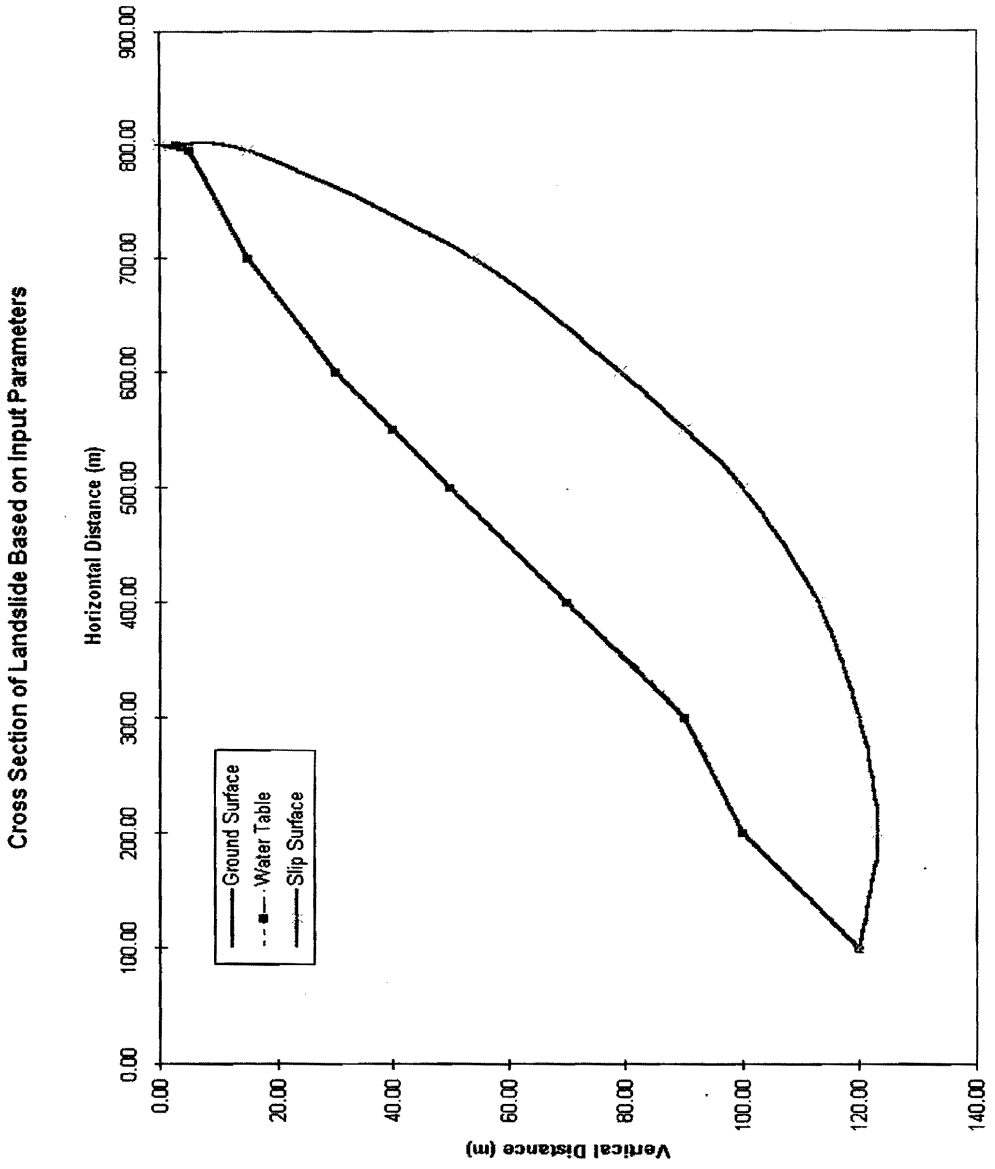


**Figure 28. Slip surface profile of the Janbu model with the toe down slope of the logging road crossing . Toe failure model.**

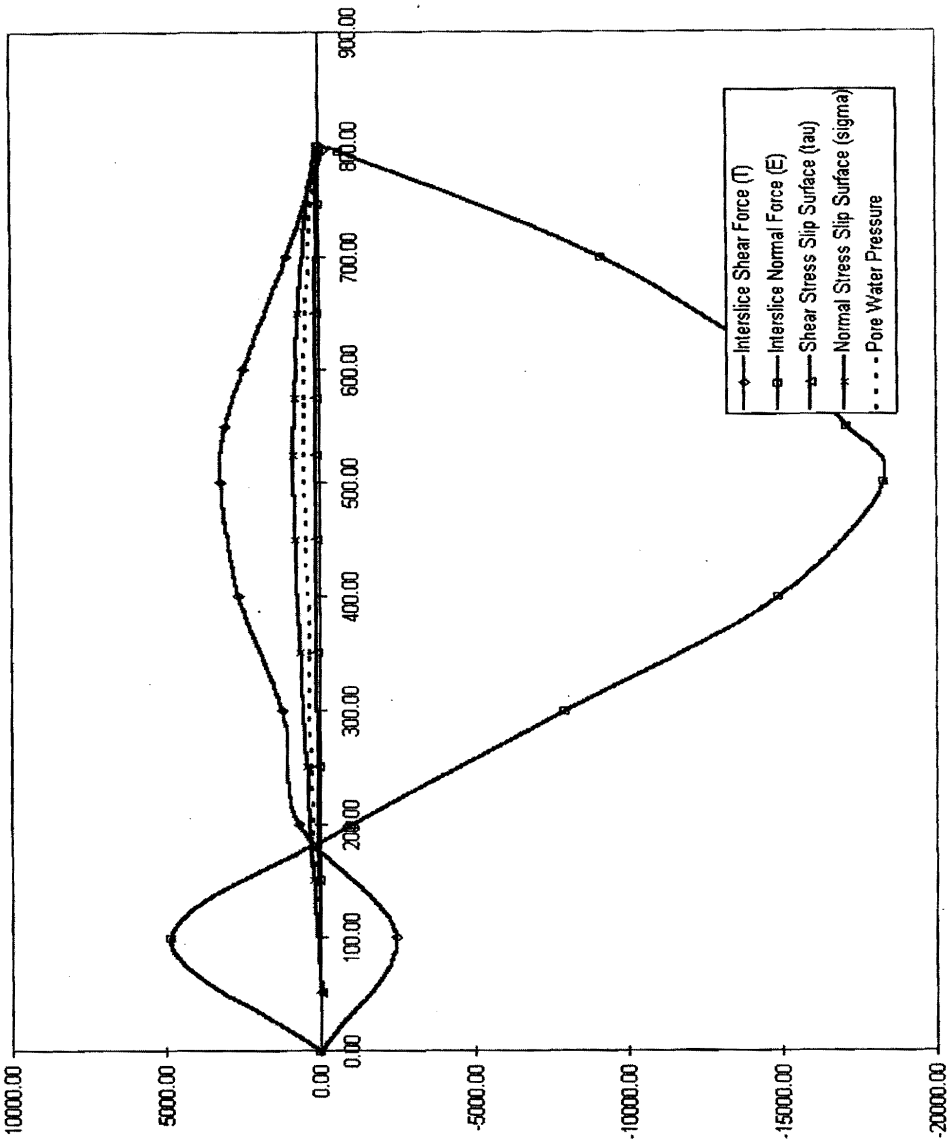


**Figure 29. Force parameter diagram based on Janbu Excel© inputs. This model simulates toe failure at the road crossing.**

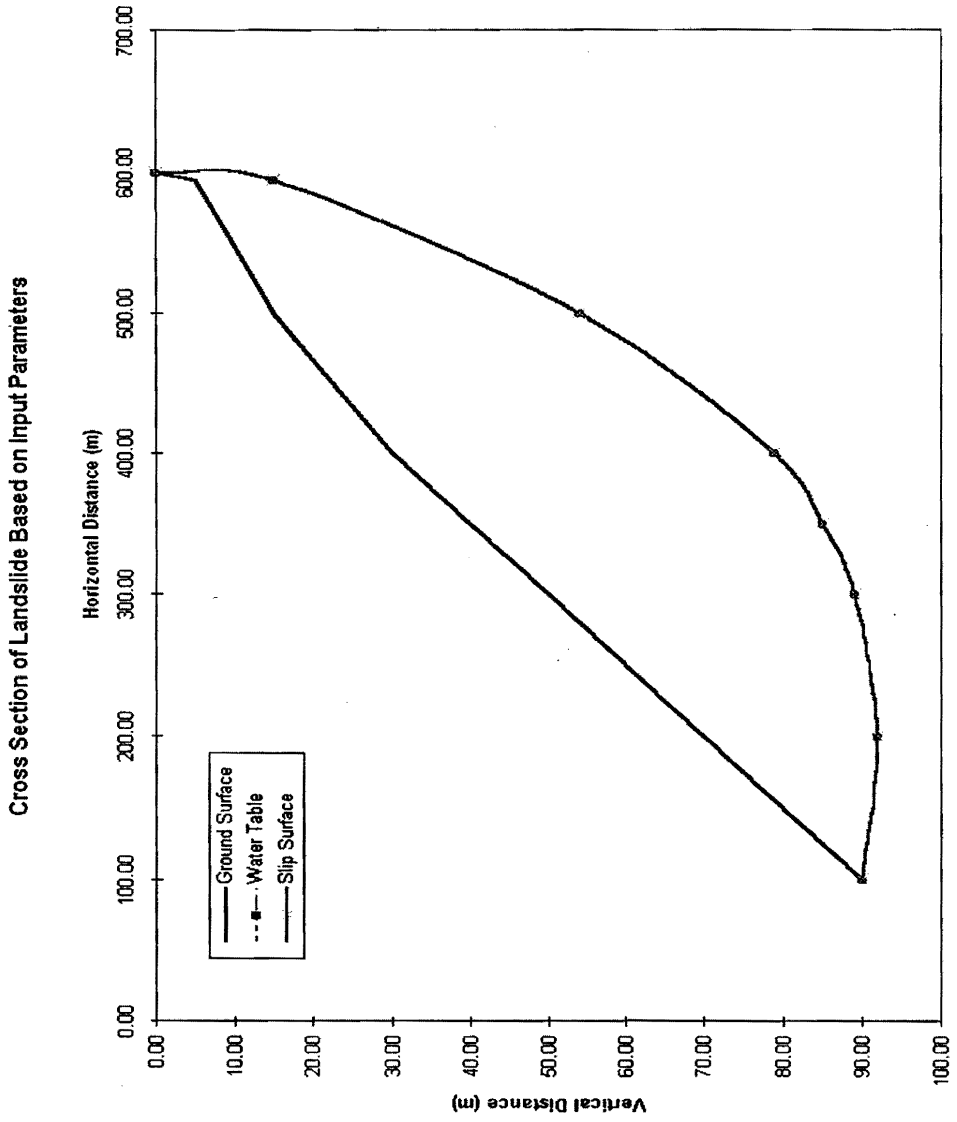


**Figure 30. Profile of the undrained Janbu earthflow model with the water table set at the slip surface.**

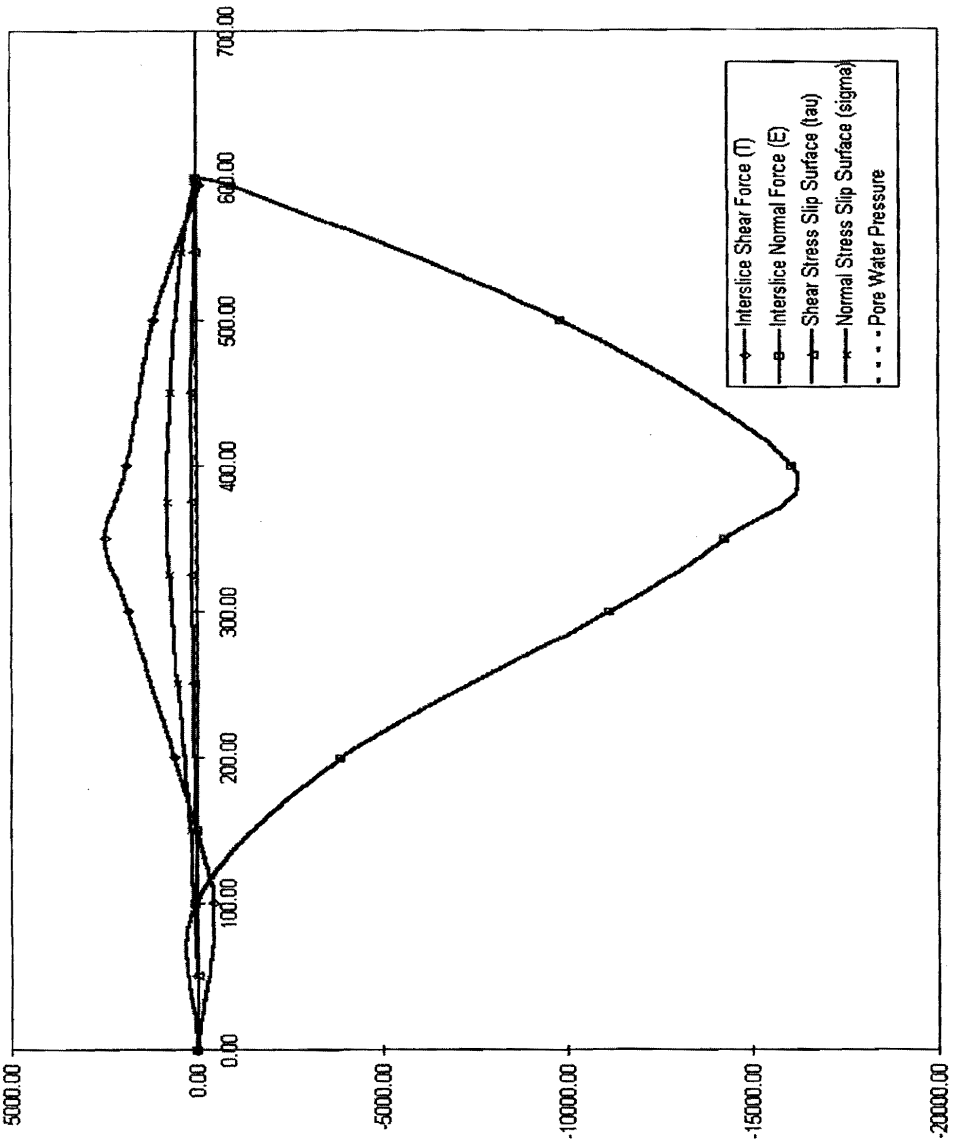


**Figure 31. Force diagram of the undrained Janbu model with the water table set at the slip surface.**

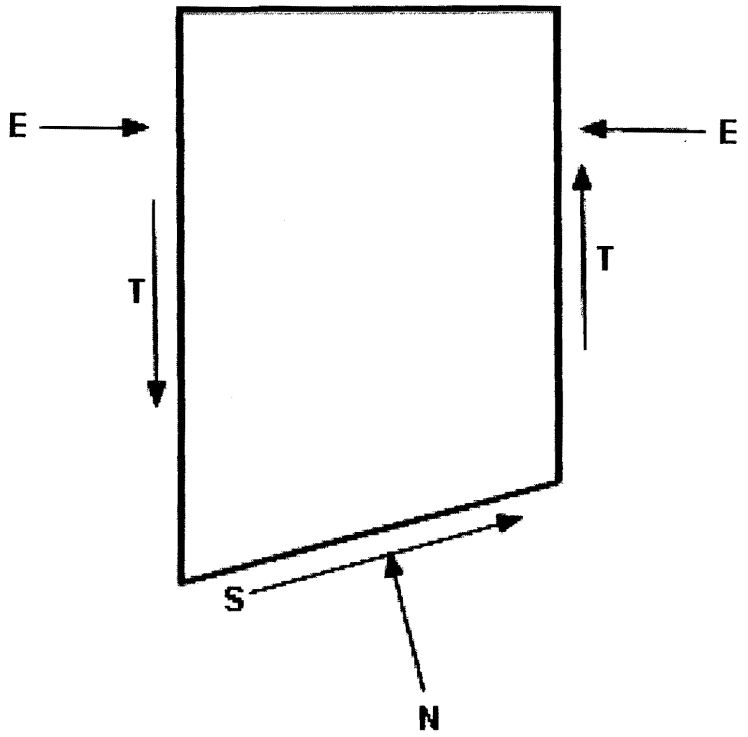


Explanation:
T – Interslice Shear Force
E – Interslice Normal Force
S – Shear Stress Slip Surface (tau)
N – Normal Stress Slip Surface (sigma)

**Figure 32. Diagram of forces acting on a slice in the Janbu computer model of the earthflow. Forces correspond to the diagrams in Figures 27, 30 and 33.**

An alternate or additional explanation for the soil moisture retention in the Tidewater soils may be related to smectite shrinkage. As a soil containing smectite loses water, the associated reduction in volume partially preserves the volume ratio of water to soil. Consequently, the soil appears to maintain fairly constant moisture content. The rate of soil shrinkage is so slow as to be perceptible only by precise methods of laboratory measurement that are beyond the scope of this project.

## CLAY CONTENT

Clay mineralogy and content are important and sometimes controlling elements of soil strength. Soils with clay contents of 25 % or less exhibit very low cohesion values and generally have friction angles similar to sands or silts (Skempton, 1985). In soils with clay contents greater than 50 %, strength is controlled predominately by the friction angle of the clay mineral species present. In soils with total clay percentages between 25 and 50 %, which includes West Tidewater earthflow soils, soil strength is a combined function of clay content, mineralogy, and the physical characteristics of the soil matrix. Soil strengths in this latter case are understandably variable. Friction angles for common clay minerals have been experimentally determined to be approximately 15° for kaolinite, 10° for illite and mica, and 5° for smectite (Warkentin and Yong, 1962). Because smectite clay is the dominant clay species in the earthflow soil samples, lowered friction angles are to be expected in the West Tidewater samples.

The orientation and dilatency of soil materials controls their strength. In laboratory shear tests and field studies of failure events, the clay minerals within shear zones have been shown to reorient themselves parallel to the direction of shearing forces (Skempton 1985). The shear force required to reorient clay and soil particles is reflected in laboratory tests as the peak strength value. Once the soil particles are in a more parallel configuration (Figure 33), strength falls to the residual level. Laboratory tests show that displacements of as little as 4 - 10 mm will reduce internal friction in a clay soil to the residual level (Skempton 1985). There is also evidence that shearing of clay soils induces a natural increase in water content that further reduces shear strength (Lambe and Whitman, 1969).

The large number of variables affecting soil strength makes characterizing slope failures difficult. The choice of methods and the precision of laboratory techniques can be the limiting factors and significant sources of error during testing and subsequent analysis.

## GEOMETRY OF THE EARTHFLOW

The depth and geometry of the Tidewater earthflow headscarp slump and shear plane are interpreted from field study. The vertical offsets of the uppermost soil block surface ranges from 15 to 20 m. There is no exposure of dark-gray

mudstone on the headscarp face. The vertical displacement of the upper 500 m of the earthflow containing the assumed semi-circular failure surface is approximately 70 m.

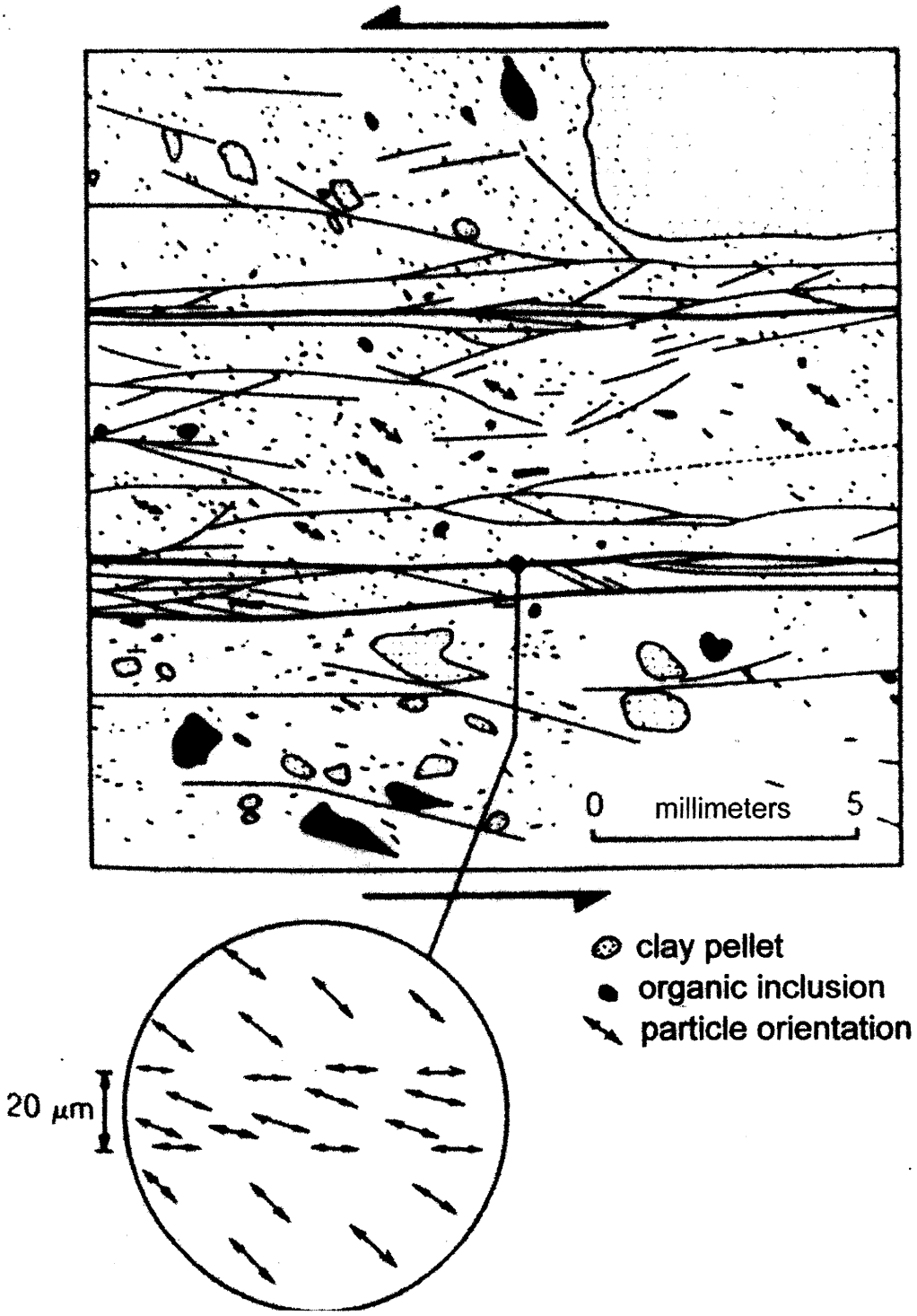


**Figure 33. Drawing of particle reorientation during shear. Peak and residual strengths are affected by spacial alteration during soil movement, from Skempton (1985).**

A penetration test was performed during the monitoring well 2 installation, located between map contour 500 and 505 m, at a horizontal displacement of 290 m from the apex of the main scarp. The penetration data indicate a zone of weakness 3-4 m below the present ground surface. With the topography and the assumption that the penetration test data are the expression of the primary shearing surface, failure arc geometry and depth are interpreted and used to model the earthflow (personal communication, A.M Johnson, Purdue University, 1996).

The lower third of the earthflow starting about 600 m from the scarp apex, bounded above by contour 455 m, has different characteristics from the upper portion. There is a significant increase in slope angle and a pronounced narrowing of the earthflow lateral boundaries. There is also a greater proportion of tree and plant material mixed into, and resting on top of, the colluvium of the lower slide. The tree and plant material is not just clearcut slash as in the upper portion, but includes dozens of live trees up to 30 m tall with diameters of up to 1 m. It appears that as the earthflow toppled live trees, the uprooted trees knocked down additional trees as they were carried down hill. The evidence is in the number of partially uprooted trees leaning downslope with recently uprooted trees lying against them on the upslope side. Despite these differences, the lower portion is still defined as earthflow because the material involved is predominantly fine-grained soil (Varnes, 1996).

## WOODY DEBRIS FACTOR

Discussion of the stability of forested slopes should include the role of woody vegetation and root strength on overall stability. Plant roots enhance the resistance to movement of soils and slopes by virtue of their substantial tensile strength. Tree roots lose the bulk of their strength within three years of the death of the tree (Riestenberg and Sovonick-Dunford, 1983). Vertical and horizontal stability of slopes are enhanced by the vegetative mat resident in the upper two meters of soil or colluvial cover (Bishop and Stevens, 1964; Zaruba and Mencl, 1969; Nakano, 1971). Even on slopes subject to deep-seated failures, tree roots provide substantial horizontal anchoring of overburden materials across zones of weakness (Swanston and Swanson, 1977). Vegetative cover reduces the rate and quantity of water infiltration, chemical and physical soil alteration, and subsurface piping and erosion. The water control function provided by plants increases overall slope stability by attenuating the rate and magnitude of pore pressure fluctuations within underlying soils and zones of failure (Gray, 1970). It is significant that the West Tidewater earthflow occurred three years after the clear-cutting timber harvest in the basin (Figure 34).

## FAILURE MODE

Landslides can fail at the toe and propagate headward, or they may fail at the head and flow out to form a distal toe. Neither the morphology nor the structure of the West Tidewater earthflow gives strong indications of failure mode. The steep structural ridge at the headscarp apex and numerous soil thrust toes within the body of the flow suggest a downward-propagating failure mode. The multiple soil toes along contour 465 m are the obvious result of soil flowing down slope over the top of the previous ground surface. The soil forming the thrust toes had to be moving at a faster rate than the surface it now covers. The earthflow becomes more flat and open between contour 470 m and 445 m suggesting an extensional mode in this area. This level area divides the earthflow into an upper zone above 470 m and a distal earthflow below contour 445 m. Shortly before the failure, the culvert under the destroyed logging road crossing at contour 450 m was reported to be clear with stream-water freely flowing, and with no ponded water against the embankment (personal communication, Dave Michael, Oregon Department of Forestry, 1997). The slope angle of the basin increases significantly just down slope of the road along contour 445 m. The width of the basin also begins to constrict just above the road crossing. A small, 5 m wide sag pond lies along contour 445 m, suggesting slumping just below the road crossing. Extensional features such as minor scarps, cracks, or slumps are absent from the earthflow below contour 445 m. The logging road prism

resting on the narrowing stream basin with an increasing slope angle makes this the most likely area for a possible toe failure to occur. These observations are reflected in the Janbu model for toe failure (Table 11).

Soil cracks and secondary slumps are found within the large 20 to 30 m wide soil blocks at the head of the flow above contour 500 m. A reverse scarp along contour 545 m suggests possible retrograde failure near the headscarp. The soil thrust feature along contour 495 m, seen in Figure 19 has a low potential of being an area of earthflow initiation due to its limited size and width.

The Janbu models indicate initial headscarp failure and downslope propagation of the Tidewater earthflow. The toe failure model in Table 11 has a lower average FS, but the forces diagram in Figure 29 shows an increase in the interslice normal force in the toe area, making toe failure mode unlikely.

## INFLUENCE OF STRUCTURAL FEATURES

Local structure is probably the secondary contributing cause of this earthflow after rainfall. At least one, and possibly two, faults of regional extent intersect within or very near to the earthflow boundaries (Figure 3, Figure 5). A fault bearing N 75° W cuts across the upper part of the slide basin about 120 m below the main scarp along contour 540 m, subparallel to the ridge, and subnormal to the outflow (Niem and Niem, 1985). The location of this fault across the earthflow basin is adjacent to a parallel line of springs emerging from the soil block faces along contour 515 m on

**Figure 34. Soil crack within one of the upper soil blocks near the main scarp along contour 530 m. This crack is about two meters wide at the surface. Root diameters range from 1 mm to about 10 cm.**

both eastern and western margins (Figure 3).

Figures 35 and 36 show locally-exposed features that indicate faulting within the upper basin. Lineaments through the study area that are interpreted as regional fault traces are visible in aerial photos (Figure 37). A major fault adjacent to a

groundwater source would allow significant seepage into the siltstone and mudstone bedrock at the base of the structural ridge and headscarp. The presence of two intersecting faults and a groundwater source adjacent to the basalt ridge strongly suggest structural control of this earthflow (Figure 38).

The morphology of the upper most soil block and headscarp suggests the possibility of a double-wedge failure or some part of a retrograde movement near the scarp. Triangular, apex downward driving blocks drop and drive lower soil blocks in double wedge failures (Figure 39). The soil block face on contour 545 m, (Figure 3) is probably too small to have controlled this entire slope failure, but does show a reverse scarp that could be the driving wedge portion of small double wedge component of the upper portion. It seems more likely that some retrograde movement occurred shortly after the largest soil blocks moved.

**Figure 35. Exposed soil block face forming part of the eastern slide margin. The arrow indicates a zone of alteration and suspected fault. The O➔ indicates groundwater outflow.**

**Figure 36. Soil block face on the western margin of the earthflow. The arrow points to the suspect fault curving toward the main scarp. The headscarp is in the background.**

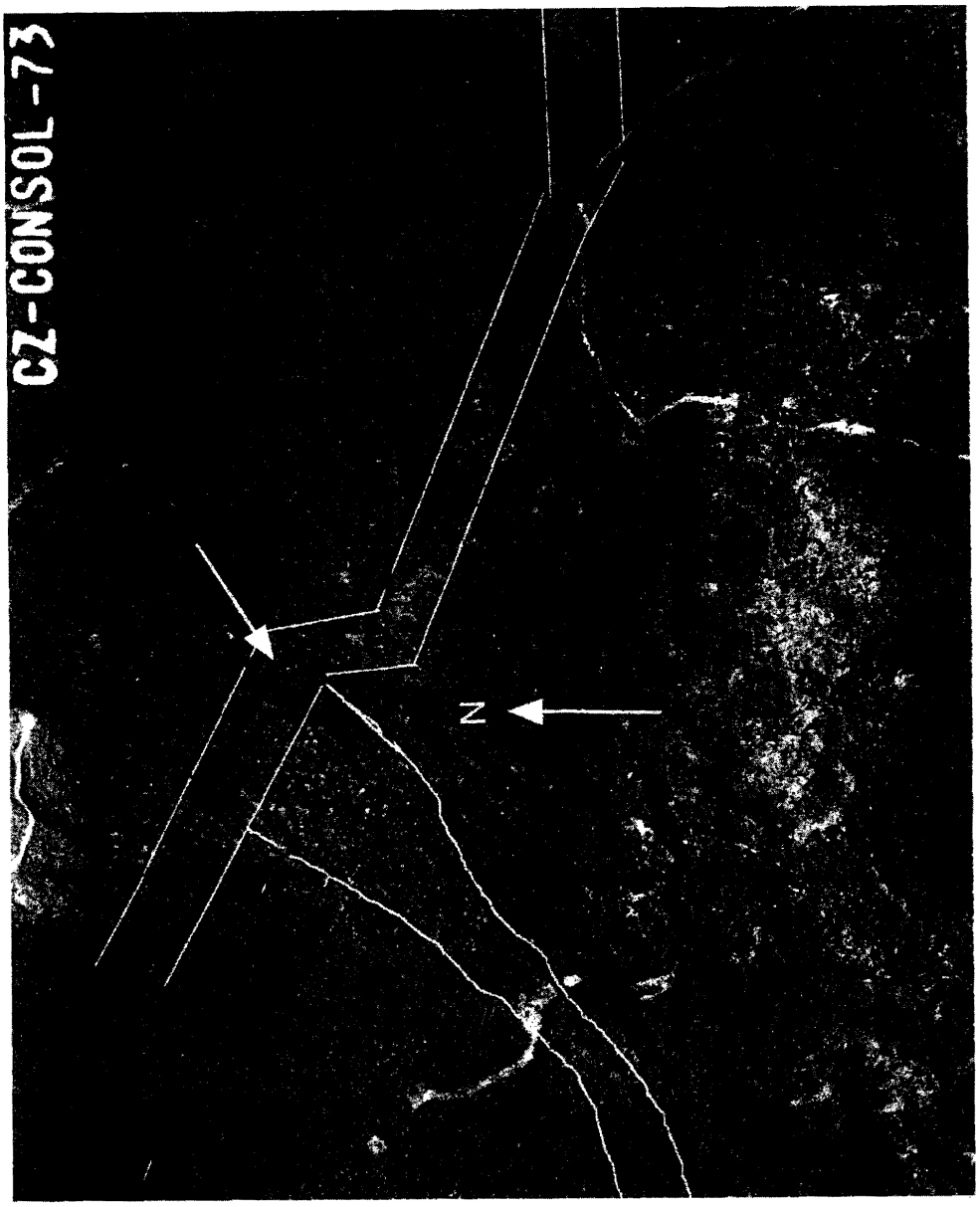


**Figure 37. Aerial photo of the study area dated 1973. Possible lineaments corresponding to the faults mapped my Niem and Niem (1985) are outlined in white. The earthflow basin is outlined at lower figure. Photo courtesy of The Oregon Department of Forestry, Astoria, Oregon.**

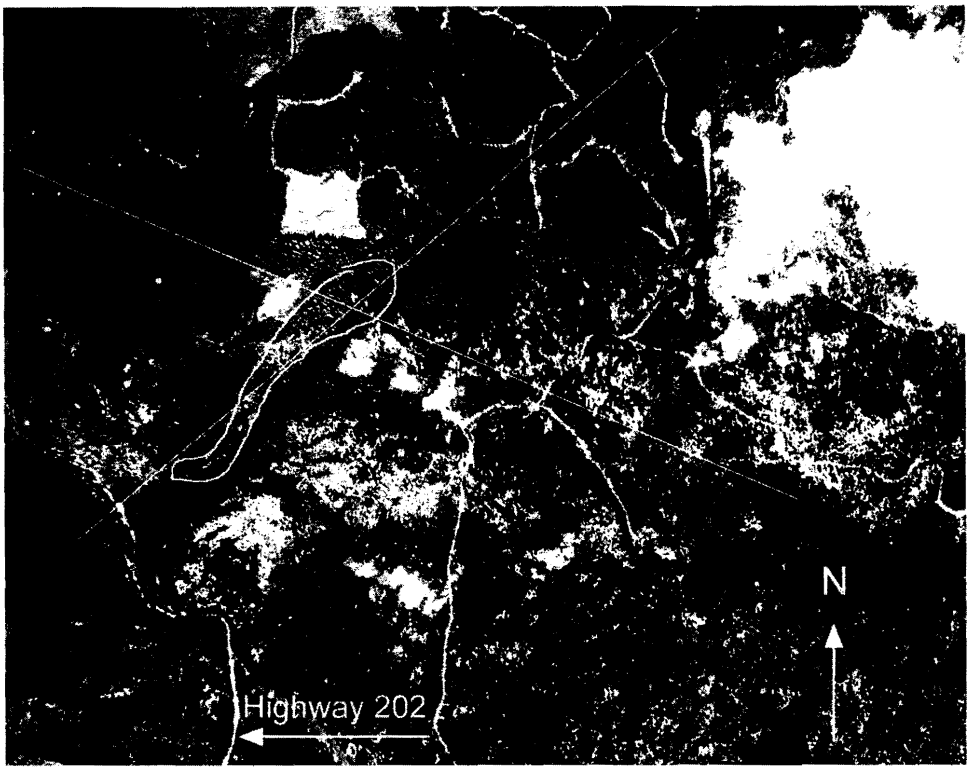


**Figure 38. The Tidewater Summit region with the earthflow circled. The faults mapped by Niem and Niem (1985) are approximated with white lines. Aerial photo dated 3-30-1970; scale is 1 cm: 250 m. Photo courtesy of The Oregon Department of Forestry, Astoria, Oregon.**

## VEGETATION REMOVAL FACTOR

Removal of the dominant vegetative cover from the study basin very likely reduced the overall slope stability. The effect of removal of vegetative cover from steep or colluvial terrains has been the subject of many studies for at least three decades (Swanston and Walkottaen, 1969). It is now widely accepted that denuded or graded slopes represent a greater risk of slope failure than undisturbed slopes

(Swanston and Swanson, 1976). Road building and clear-cut timber harvesting also have a documented detrimental effect on the stability of steep, forested slopes

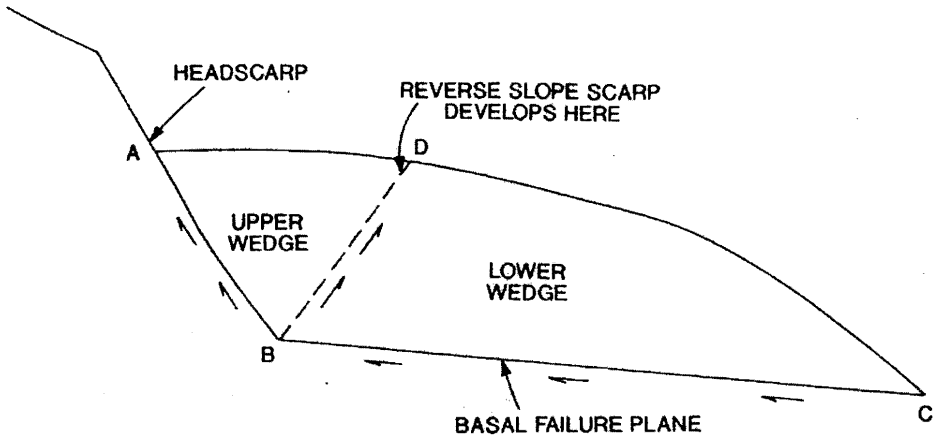


**Figure 39. Drawing of a double wedge type slope failure. The upper wedge drives the lower wedge along a nearly horizontal failure plane. Drawing is from Cornforth and Vessely (1992).**

(Swanston and Swanson, 1976). Slopes destabilized by clear-cut timber harvesting also produce lower quality timber from subsequent plantings and harvests (Jared May, MayCo, personal communication, 1994). Trees grown out of their normal vegetation succession are good for paper pulp only and are therefore of much less value. The increased sediment load in local streams induced by denuded slopes creates further negative environmental impacts on water quality and fisheries (Kelsey, 1978).

In the Tidewater Summit region and throughout the northwest, clear cutting has been the harvest method of choice since the turn of the century. The air photo

series in Appendix A documents some of the road building, vegetative succession, and timber harvest history within the region. The photos document the fact that the study area was stable from 1971, the date of the oldest photo, until the failure event of December 1994. Three years after harvesting by clear-cutting in 1991, the basin was subject to a large slope failure event.

# CHAPTER 7

# CONCLUSIONS

The West Tidewater earthflow occurred in December of 1994 in the Oregon Coast Range Mountains. It is believed to be one of the largest earthflows in the Oregon coastal mountains in modern history. Morphologic evidence of previous failures in the study area in the form of new-growth trees is documented in aerial photos dating back to the 1970's. Aerial photos show disturbed slopes in the area surrounding the project study area now covered in similar new growth.

The earthflow dimensions are approximately 250 m wide by 900 m long, giving it a surface area of about 8.7 hectares, or nearly 22 acres. Taking into account the depth of the failure surface, the height of the headscarp, and the final position of the largest soil toe, the volume of earth materials involved in the initial failure is about 3.5 million $m^3$.

The materials involved in this earthflow are low-strength micaceous siltstone and clay-rich carbonaceous mudstone of the Northrup Creek Formation. The clay content of both rock types ranges from 18 - 30 %, 90 % of which are smectite. There are indications that halloysite and colloidal gels are present in these soils as well. The liquid limits of the soils vary from 42 - 95 %, with accompanying plasticity indexes ranging from 2 - 77 %. The laboratory-determined internal friction angles range from 14° in the clay rich samples to 18° in the siltstone samples. Soil cohesion values were determined to vary from 4 - 8 kPa.

The slope failure reactivation time as determined from C-14 dating of previously buried trees is 600 +/- 50 years. New vegetative growth in the study basin suggests a shorter reactivation time. The overall mode of the current failure is most likely from the headscarp propagating downward to the toe area. There are minor indications of either retrograde or double wedge failure on one of the upper soil blocks. The contrasting morphology of the upper and lower portions of the earthflow does not in itself suggest a dominant failure mode. A number of factors contributed to the reactivation of this earthflow. Greater than normal precipitation is a primary factor. Rainfall levels during October, November, and December of 1994 were twice the previous five year average.

The earthflow has some degree of structural control. The headscarp sits against an invasive basalt ridge. The steep slope angle here would create a significant amount of shear stress on the soils. There is strong evidence that a NW - SE trending fault crosses the earthflow basin subparallel to the structural ridge. The fault would be a natural vertical slip surface and would allow water infiltration, thereby promoting weakening of the siltstone and mudstone bedrock and elevated soil pore water pressures. There is evidence of a second NE - SW trending intersecting fault (Niem and Niem, 1984) within the basin, subnormal to the traversing fault. The second fault may be part of the eastern earthflow lateral margin above contour 490 m. The intersection of these two faults appears on the Niem and Niem (1984) map to be within the earthflow basin.

Computer generated models of the earthflow slip surface calculate an average FS of 0.84 at the time of failure. The Janbu models also suggest that upper 500 m of the earthflow was the most unstable portion of the original basin surface. The force diagrams of the models indicate that the portion of the basin around the destroyed logging road crossing was more stable than the upper basin and headscarp.

Human impacts in the form of road building and timber harvesting may also have had a role in this earthflow. The timber in the earthflow basin was harvested approximately three years prior to the failure. The loss of the vegetative canopy and ground mat must have reduced evapotranspiration and allowed increased amounts of water to infiltrate the underlying soils, thereby decreasing the effective strength of the soil in the basin. The loss of living plant and tree roots diminished the anchoring effect that vegetative cover affords. Road building within the study area may have had an adverse effect on the overall stability of the basin. The oversteepened road cut bank above the headscarp and the road through the middle of the basin surely contributed to the deterioration of the natural slope equilibrium by increasing water runoff velocity and accelerating erosion in some areas.

A third major cause of the earthflow is parent material that is weak and prone to landslides. The soils in the basin are clay-rich with smectite clay as the dominant species. The earthflow that occurred in 1994 is a reactivation of at least one, and possibly several, previous slope failure events.

The combination of greater than average rainfall on a previously failed slope, smectite-rich soils, multiple fault zones, timber harvesting with accompanying loss of root strength, and destabilization of the natural slopes with logging road construction, has created a recurring earthflow complex.

## FUTURE WORK

A number of issues regarding the earthflow may be worthy of additional study. Questions remain about the clay species present in the soil samples tested. The presence of halloysite and gel could be confirmed or ruled out. The provenance, depositional environments, weathering, and diagenetic histories of the mudstone and siltstone in the study area may also be productive subjects for further study. The increased interlayer distance of the smectites found in the West Tidewater soils is not fully understood. Additional work would be needed to identify and quantify the orientation of clay interlayer organic components and their effects on soil strength. The soil mound features seen on the earthflow midsection are poorly understood. Further investigative work on these mound features may include more trenching in hopes of finding conclusive evidence of loading structures or soil extrusion.

# REFERENCES


ASTM, 1988, Annual Book of ASTM Standards: Soil and Rock, Building Stones, Geotextiles, Vol. 04-08, Designation D-3080-72, pp. 371-373.

Beeson, M., Perttu, R., and Perttu, J., 1979, The origin of the Miocene basalts of coastal Oregon and Washington: an alternative hypothesis: Oregon Geology, Vol. 4, No.10, pp. 159-166.

Birkeland, P.W., 1984, Soils and Geomorphology, Oxford University Press, New York, 372 p.

Bishop, A.W., 1955, The use of the slip circle in the stability analysis of slopes. Geotechnique, Vol. 5, pp. 7-17.

Bishop, D.M., and Stevens, M.E., 1964, Landslides on Logged Areas in Southeast Alaska: U.S. Department of Agriculture Forest Service Research Paper NOR-1,18 p.

Cassagrande, A., 1948, Classification and Identification of Soils: Transactions of the American Society of Civil Engineers, Vol. 113, p. 901.

Chassie, R.G., and Goughnour, R.D., 1976, National Highway Landslide Experience: Highway Focus, Vol. 8, No. 1, pp. 1-9.

Chen, Pei-Yuan, 1977, Table of Key Lines in X-ray Powder Diffraction Patterns of Minerals in Clays and Associated Rocks: Department of Natural Resources, United States Geological Survey Occasional Paper 21, 68 p.

Cooper, D.M., 1981, Sedimentation, stratigraphy, and facies variation of the lower to middle Miocene Astoria Formation in Oregon: Corvallis, OR, Oregon State University Doctoral Dissertation, 524 p.

Cornforth, D.H., and Vessely, D.A., 1992, Pelton Landslide, An Unusual Double Wedge Failure: Stability and Performance of Slopes and Embankments, II Proceeding, Geotechnical Division, ASCE, July 1, 1992, pp. 310-324.

Das, B.M., 1985, Principles of Geotechnical Engineering:, Prindle, Weber, & Schmidt, Duxbury Press, Boston, Mass., 571 p.

Dodds, R.K., 1963, Geology of the western half of the Svenson Quadrangle, Oregon: University of Oregon master's thesis, 1963, 114 p.

Easterbrook, D.J., 1993, Surface Processes and Landforms, MacMillan Publishing Company, New York, NY, 520 p.

Fellenius, W., 1936, Calculations of the Stability of Earth Dams: Transactions of the 2nd Congress on Large Dams, Washington, D.C., Vol. 4, 445 p.

Galehouse, J.S., 1971, Procedures in sedimentary petrology: in R. S. Carver, ed., Sedimentation Analysis, University of Georgia, Athens, Georgia, John Wiley & Sons, pp. 69-90.

Gray, D.H., 1970, Effects of forest clear-cutting on the stability of natural slopes: Bulletin of the Association of Engineering Geologists, Vol. 7, pp. 45-65.

Hall, D.E., Long, M.T., Rembolt, M.D., Prellwitz, R.W., Koler, T.E., Steward, J.E., 1994, Slope Stability Reference Guide for National Forests in the United States, Volume I, United States Department of Agriculture, Forest Service Engineering Staff, Washington, D.C., Publication Number EM-7170-13, pp. 179-180.

Howe, H.V., 1926, The Pan-American Geologist, Vol. 45, No. 5, pp. 295-306.

Istok, J.D., and Harward, M.E., 1982, Clay mineralogy in relation to landscape instability in the Coast Range of Oregon: Soil Science Society of America Journal, Vol. 46, No. 6, pp. 1326-1331.

Janbu, Nils, 1973, Slope-stability computations, in Hirschfield, R.C. and Poulos, S.J., Editors, Embankment-dam Engineering, Casagrande volume: New York, John Wiley, p. 47-86.

Kelsey, H.M., 1978, Earthflows in Franciscan Melange, Van Duzen River Basin, California: Geology, Vol. 6, pp 361-364.

Kenny, T.C., 1959, Discussion: Proceedings of the American Society of Civil Engineering, Vol. 6, pp. 224-231.

Krohn, J.P., and Slosson, J.I., 1976, Landslide potential in the United States: California Geology, Vol. 29, No.10, pp. 224-231.

Lambe, T.W., and Whitman, R.V., 1969, Soil Mechanics, John Wiley & Sons, New York, NY, 553 p.

Lowry, M.D. and Baldwin, E.M., 1952, Late Cenozoic geology of the Lower Columbia River Valley, Oregon and Washington: Geologic Society of America Bulletin, Vol. 63, pp. 1-24.

MacIver, B.N., and Hale, G.P., 1970, Laboratory Soils Testing, U.S. Army Corps of Engineers, Embankment and Foundation Branch, U.S. Army Corps of Engineers Waterways Experiment Station, Appendix IX, 20 pp.

Marden, M., Phillips, C.J., Jackson, R.J., Zhang, X.B., and Ekanayake, J., 1992, A decade of earthflow research and interrelated studies in the North Island of New Zealand: Proceedings of the Chengdu Symposium, China, July,1992,IAHS Publication no. 29, 1992, pp. 263-271.

Moore, D.M., and Reynolds, R.C., 1989, X-ray Diffraction and the Identification and Analysis of Clay Minerals: New York, Oxford University Press, 332 p.

Nakano, H., 1971, Soil and Water Conservation Functions of Forest on Mountainous Land: Report on Forest Influences by Developing Governments. (Japan), Forest Experiment Station, 66 p.

Niem, A.R., and Niem, W.A., 1985, Oil and Gas Investigation of the Astoria Basin, Clatsop and Northernmost Tillamook Counties, Northwest Oregon: Department of Geology and Mineral Industries, Portland, OR, publication number OGI-14, geologic map with well logs.

Pease, M.H, Jr. and Hoover, Linn, 1957, Geology of the Doty-Minot Peak area, Washington: United States Geologic Survey Oil and Gas Investigation Map OM-188.

Pearce, A.J., O'Loughlin, C.L., Jackson, R.J., and Zhang, X.B., 1987, Reforestation: on-site effects on hydrology and erosion, eastern Raukumara Range, New Zealand. In: Forest Hydrology and Watershed Management, Proceedings of the Vancouver Symposium, Vancouver, B.C., 1987, pp. 489-497.

Pyles, M.R., Mills, K., and Saunders, G., 1987, Mechanics and stability of the Lookout Creek earth flow: Association of Engineering Geologists Bulletin, Vol. 24, No. 2, pp. 267-280.

Rau, W.W., 1967, Geology of the Wynoochee Valley Quadrangle, Grays Harbor County, Washington: Washington Division of Mines and Geology Bulletin, Vol. 56, pp. 21-28.

Riestenberg, M.M., and Sovonick-Dunford, S., 1983, The role of woody vegetation in stabilizing slopes in the Cincinnati area, Ohio: Geological Society of America Bulletin, Vol. 94, pp. 506-518.

Schuster, R.L., and Krized, R.J., 1978, Landslides, Analysis and Control; Transportation Research Board Special Report 176, National Research Council, National Academy of Sciences, Washington, D.C., 234 p.

Skempton, A.W., 1964, Long term stability of clay slopes: Geotechnique, Vol. 14, p. 77.

Skempton, A.W., 1985, Residual strength of clays in landslides, folded strata, and the laboratory: Geotechnique, Vol. 35, No. 1, pp. 3-18.

Smith, P.R and Shipman, J.A., 1988, Soil Survey of Clatsop County, Oregon, USDA, Soil Conservation Service, Washington, D.C., 272 p.

Snavely, P.D., Jr., Wagner, H.C., and MacLeod, N.S., 1969, Geology of western Oregon north of the Klamath Mountains, in Mineral and Water Resources of Oregon: Oregon Department of Geology and Mineral Industries Bulletin, Vol. 64, pp. 32-46.

Swanston, D.N., and Swanson, F.J., 1976, Timber harvesting, mass erosion, and steepland forest geomorphology in the Pacific Northwest: in Coates, D.R., ed., Geomorphology and Engineering, Stroudsberg, Pa., Dowden, Hutchinson and Ross, Inc., pp. 199-221.

Swanston, D.N., and Walkotten, W.J., 1969, The effectiveness of rooting as a factor of shear strength in the karta soil: Study Number Fs-PNW1604:26, Nov. 21, 1969 Progress Report, 16p.

Taylor, D.W., 1948, Fundamentals of Soil Mechanics: John Wiley and Sons, 700 p.

Terzaghi, K., 1924, Die Theorie der Hydrodynamischen Spannungerscheinungen und ihr Erdbautechnishces Anwendengsgebiet: International Congress on Applied Mechanics, 1st, Delft, 1924, Proceedings, pp. 288-294.

Thrall, G.F., Jack, R., Johnson, J.J., and Stanley, D.A., 1980, Failure Mechanisms of the Drift Creek Slide, [abs.], Geologic Society of America Abstracts with Programs, Vol. 12, No. 3, p. 165.

Turner, A.K., and Schuster, R.L., 1996, Landslides, Investigation and Mitigation; Transportation Research Board Special Report 247, National Research Council, National Academy of Sciences, Washington, D.C., 673 p.

Varnes, D.L., 1958, Landslide Types and Process: in E.B. Eckel, ed., Landslides and Engineering Practice, Highway Research Board Special Publication 29, Washington, D.C., pp. 20-47.

Varnes, D.L., and Cruden, D.M., 1996, Landslide types and process: in Turner, A.K., and Schuster, R.L., 1996, Landslides, Investigation and Mitigation; Transportation Research Board Special Report 247, National Research Council, National Academy of Sciences, Washington, D.C., 673 p.

Velde, B., 1992, Introduction to Clay Minerals: Chemistry, Origins, Uses and Environmental Significance: Chapman and Hall, 198 p.

Waring, R.H., Rogers, J.J., and Swank, W.T., 1981, Water relations and hydrologic cycles: in Reichle, D.E., ed., Dynamic Properties of Forest Ecosystems, Chapter 4, Cambridge University Press, Cambridge, MA, pp. 204-264.

Warkentin, B.P., and Yong, R.N., 1962, Shear strength of montmorillonite and kaolinite related to interparticle forces: Clays and Clay Minerals, Vol. 9, pp. 210-218.

Wells, R., 1989, Correlation of Miocene Flows of the Columbia River Basalt Group from the Central Columbia River Plateau to the Coast of Oregon and Washington: Geologic Society of America, Special Paper 239, pp. 113-128.

Zarbu, Q., and Menel, V., 1969, Landslides and Their Control: Elsevier, New York, 205 p.

Ziemer, A. A., 1981, Roots and the stability of forested slopes: International Symposium on Erosion Sediment Transport in Pacific Rim Steepland, Christchurch, New Zealand, 19 p.

# APPENDICES

## WEST TIDEWATER EARTHFLOW

Appendix A – Aerial Photos

Appendix B – Soil Characteristics

Appendix C– Atterberg Limits

Appendix D – Particle Size Analysis

Appendix E – Direct Shear Testing

Appendix F – X-ray Diffraction

Appendix G- Radiocarbon Dating

# Appendix A

West Tidewater Earthflow

Air Photos of the Study Area.

1966 to 1991

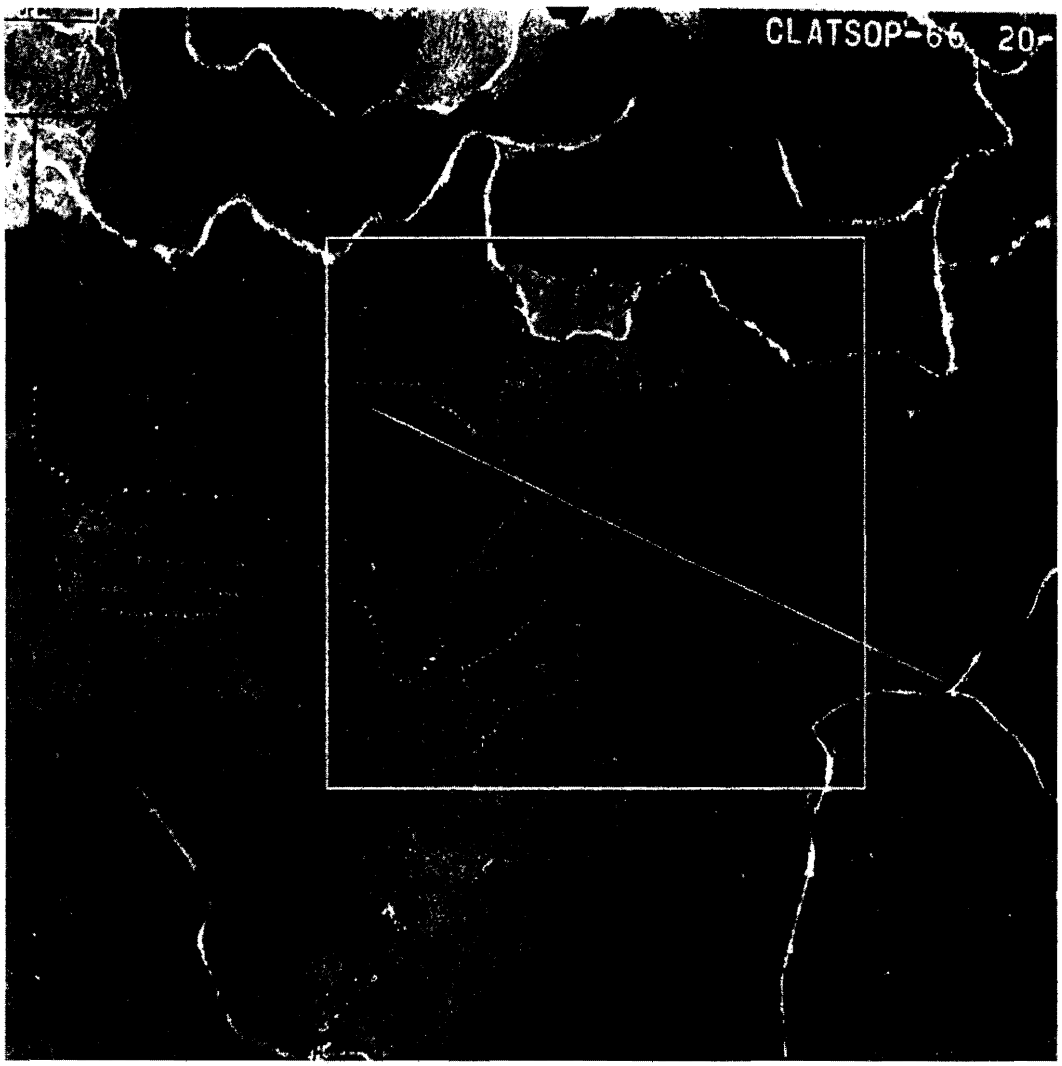


1966 Tidewater earthflow is outlined.

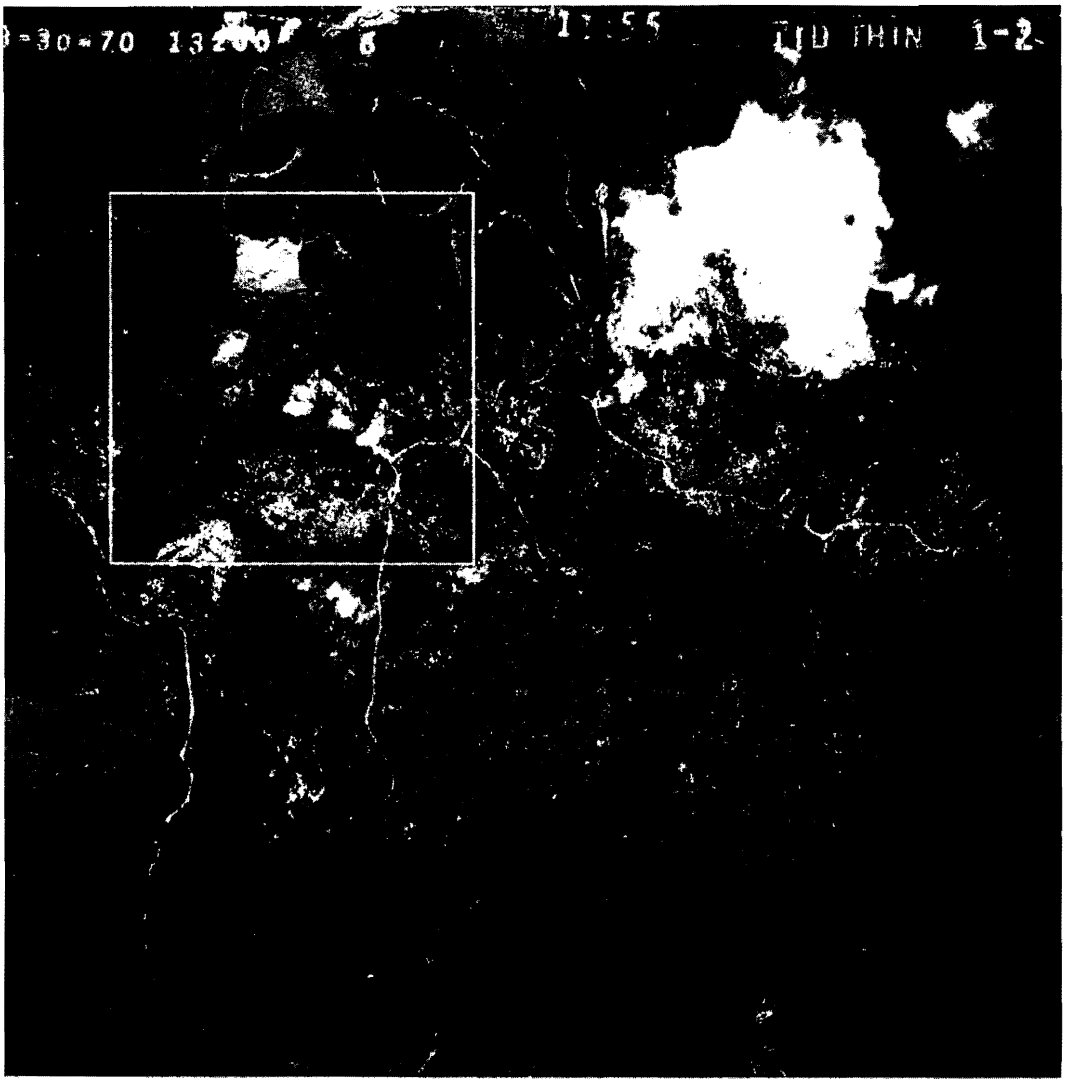

1970 Tidewater earthflow is outlined.

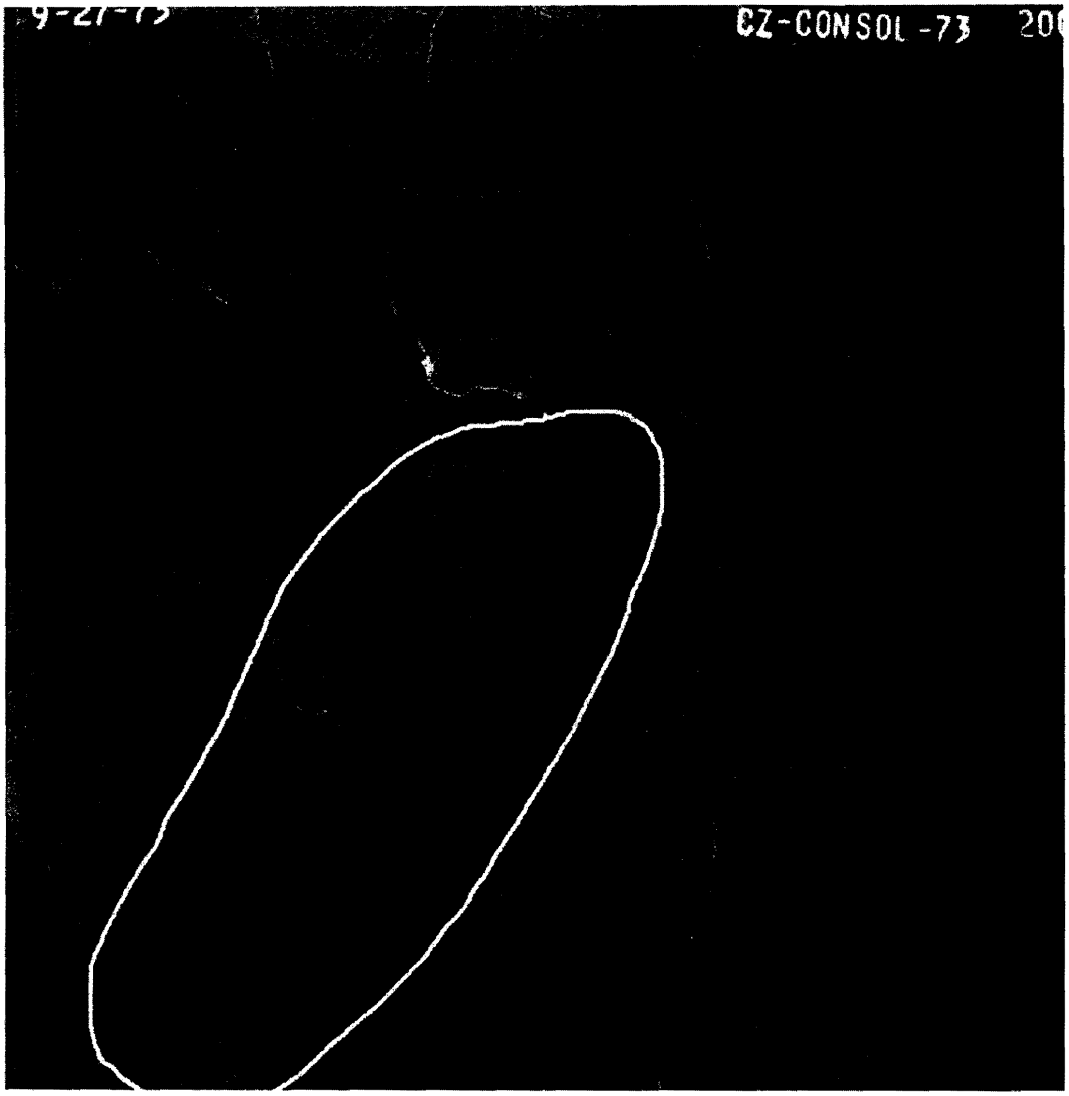


1973 Tidewater earthflow is outlined.

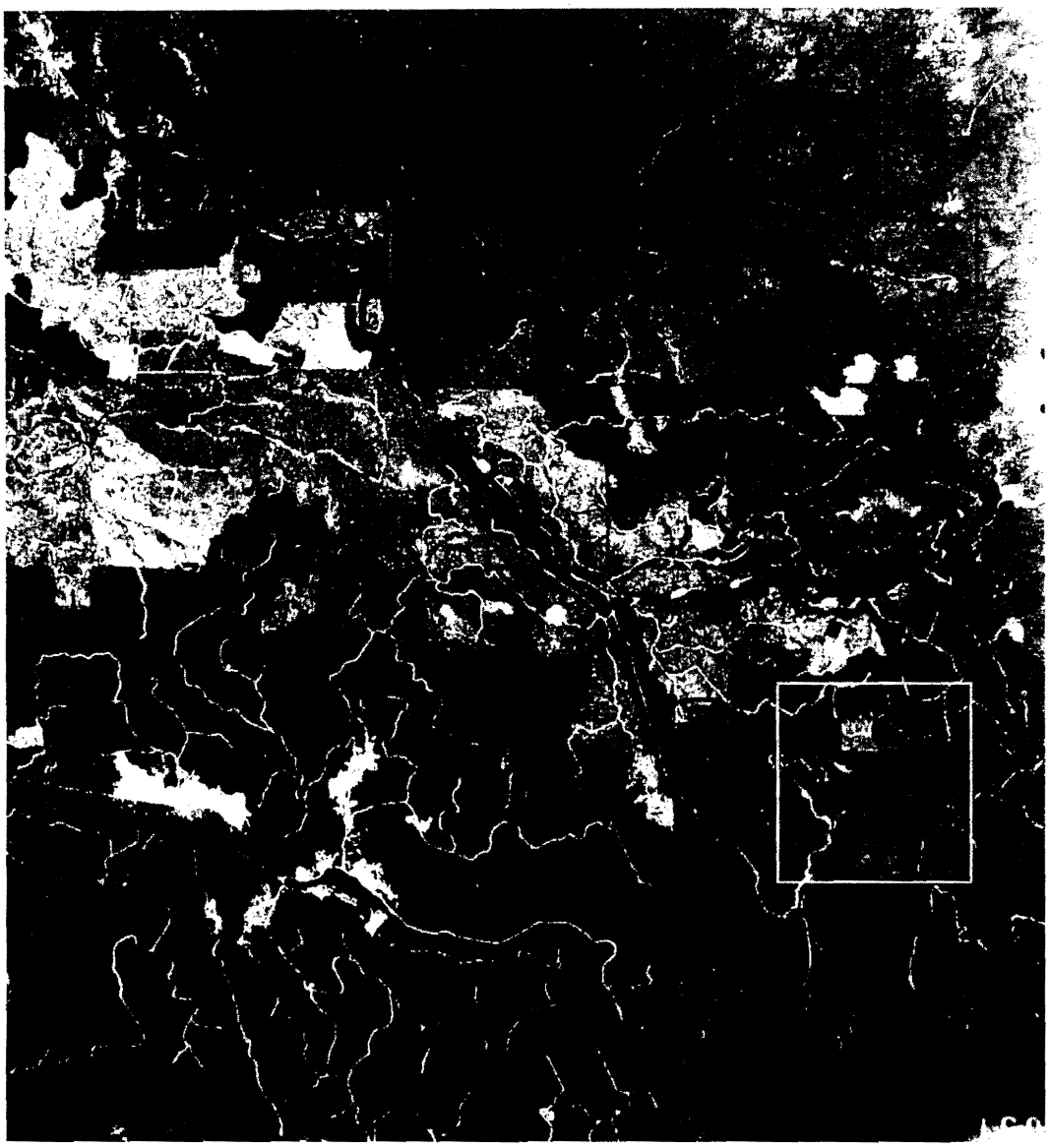

1974 Tidewater earthflow is outlined.

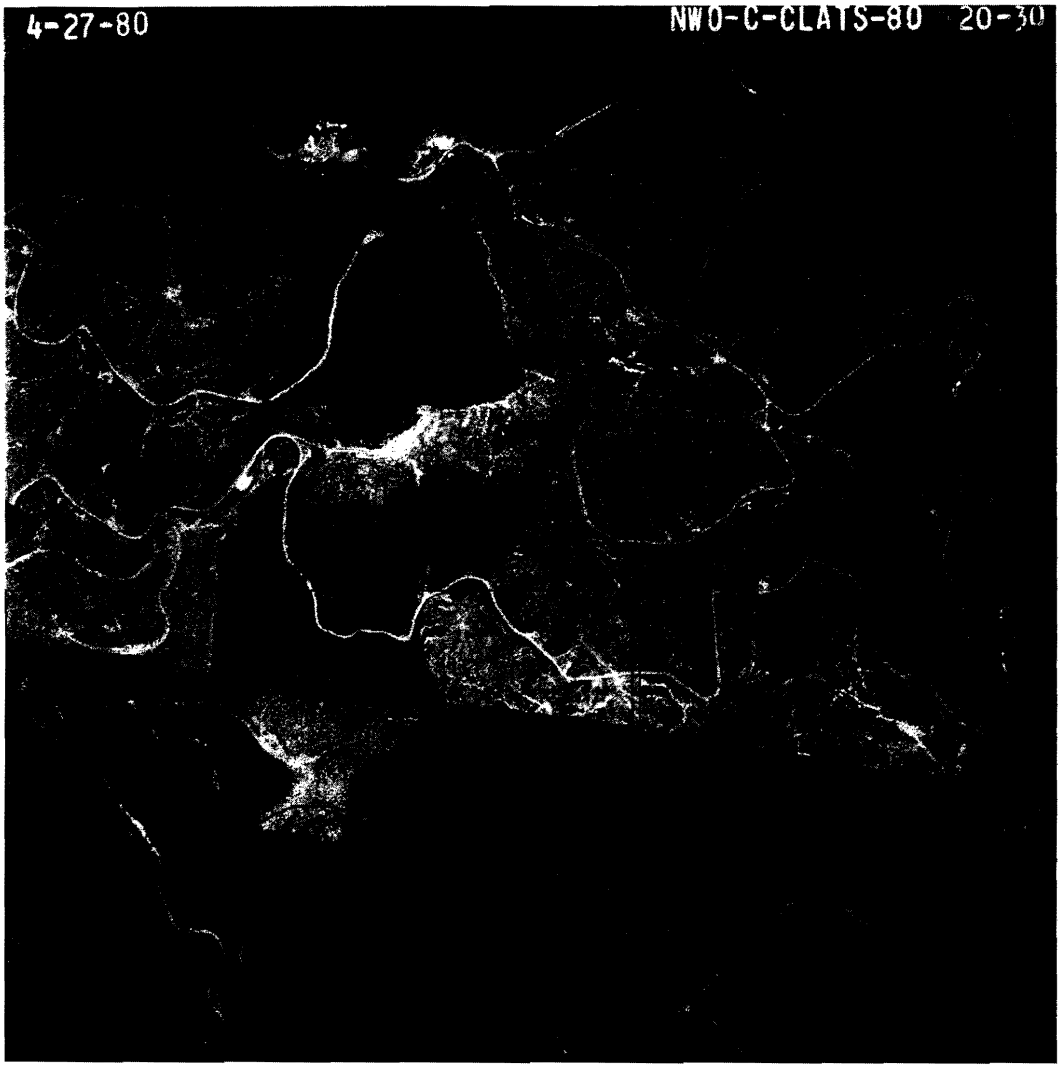


1980 Tidewater earthflow is outlined.

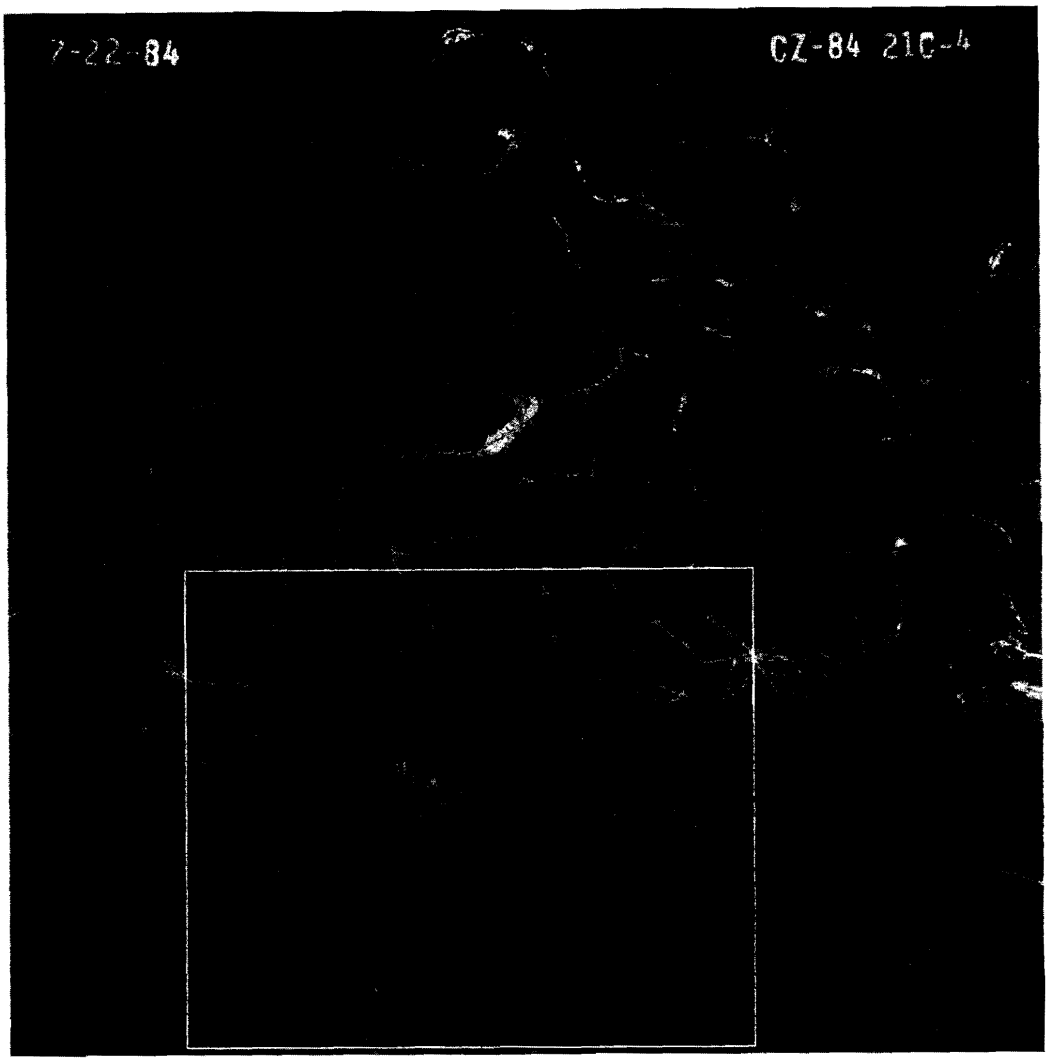


1984 Tidewater earthflow is outlined.

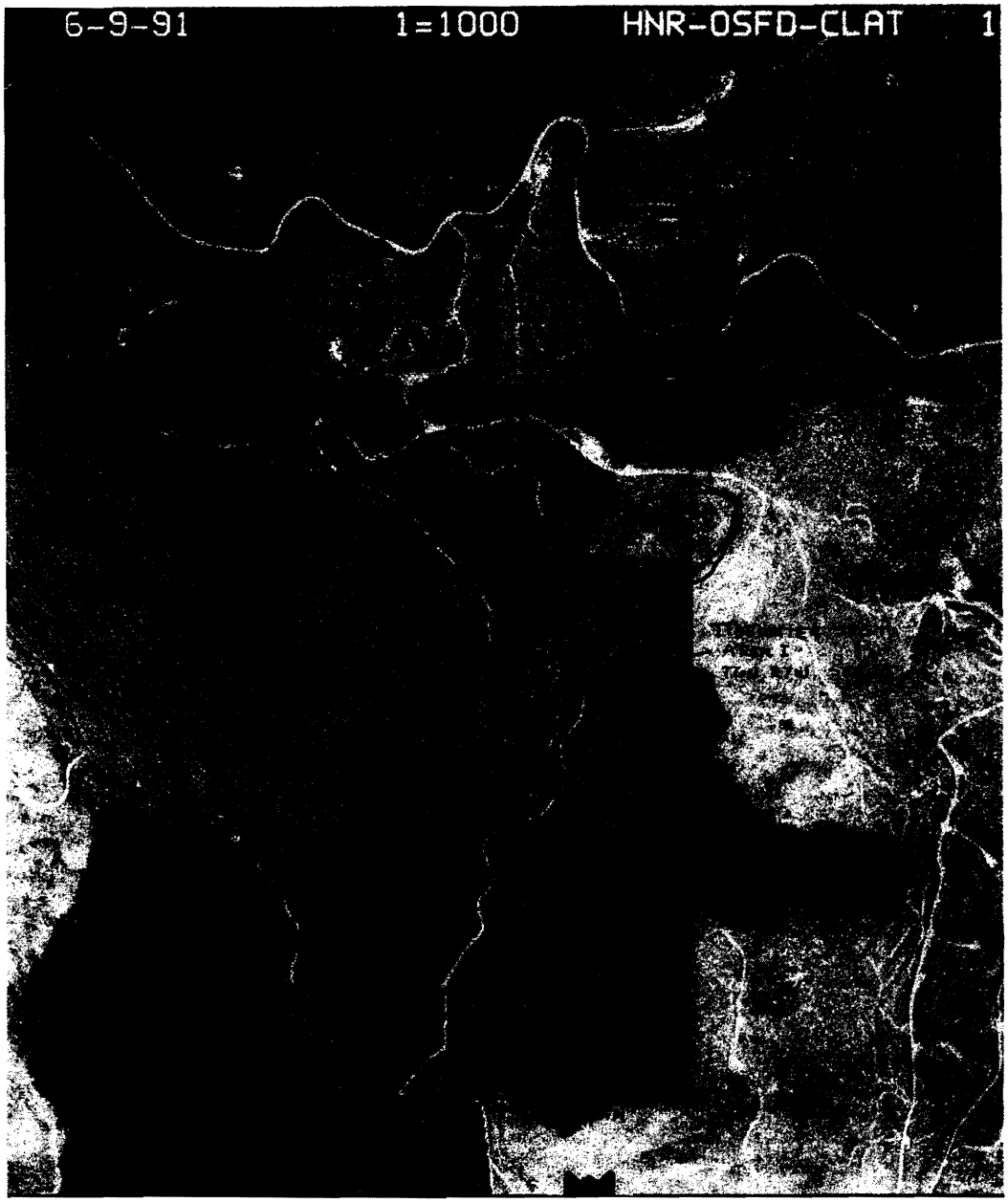


1991 Tidewater earthflow is outlined.

# Appendix B

West Tidewater Earthflow

Soil characteristics of the study area.

Excerpts from the

Soil Survey of Clatsop County, Oregon

Appendix 2
Skipanon Series Soils

## Skipanon Series

The Skipanon series consists of deep, well drained soils in mountainous areas. These soils formed in mixed colluvium. Slopes are 3 to 60 percent. The mean annual precipitation is 70 to 100 inches. The mean annual air temperature is 45 to 51 degrees F. Arial extent is 32,440 acres.

Typical pedon of Skipanon gravelly silt loam, 3 to 30 percent slopes, on a roadcut along spur landing road in the NW1/4NW1/4NE1/4 of sec. 34,T.5N.,R.9 W., Willamette Meridian:

0—2inches to 0; needles, twigs, moss, and woody material.

A-0 to 14 inches; dark brown (7.5YR3/2) gravelly silt loam, dark brown (7.5YR3/3) dry; moderate fine subangular blocky structure and moderate medium granular structure; slightly hard, friable, slightly sticky and slightly plastic; slightly smeary; many very fine roots; many very fine irregular pores; 15 percent gravel and 5 percent cobbles; very strongly acid; clear wavy boundary.

AB-14 to 19 inches; dark brown (7.5YR3/3) gravelly silt loam, brown (7.5YR4/4) dry; moderate medium and fine subangular blocky structure; slightly hard, friable, slightly sticky and slightly plastic; common very fine roots; many very fine tubular pores; 15 percent gravel; very strongly acid; clear wavy boundary.

Bw- 19 to 36 inches; brown (7.5YR4/4) cobbly silt loam, brownish yellow (10YR6/6) dry; moderate medium subangular blocky structure; slightly hard, friable, slightly sticky and slightly plastic; common very fine roots; many very fine tubular pores; 15 percent gravel, 15 percent cobbles, and 5 percent soft fragments; very strongly acid; clear wavy boundary.

C—36 to 53 inches; variegated light yellowish brown anc yellowish brown (10YR6/4, 5/6) silty clay loam, yellow and brownish yellow (10YR7/6, 6/8) dry; massive; sticky and slightly plastic; few very fine roots; common very fine tubular pores; 15 percent soft gravel; extremely acid; gradual wavy boundary.

Cr—53 inches; weathered siltstone.

# Appendix C

## West Tidewater Earthflow

## Atterberg Limits

## Laboratory Data

Sample STA-1

| Blows | Moisture |
|---|---|
| 17 | 56.6 |
| 30 | 46.5 |
| 32 | 56.7 |
| 50 | 36 |

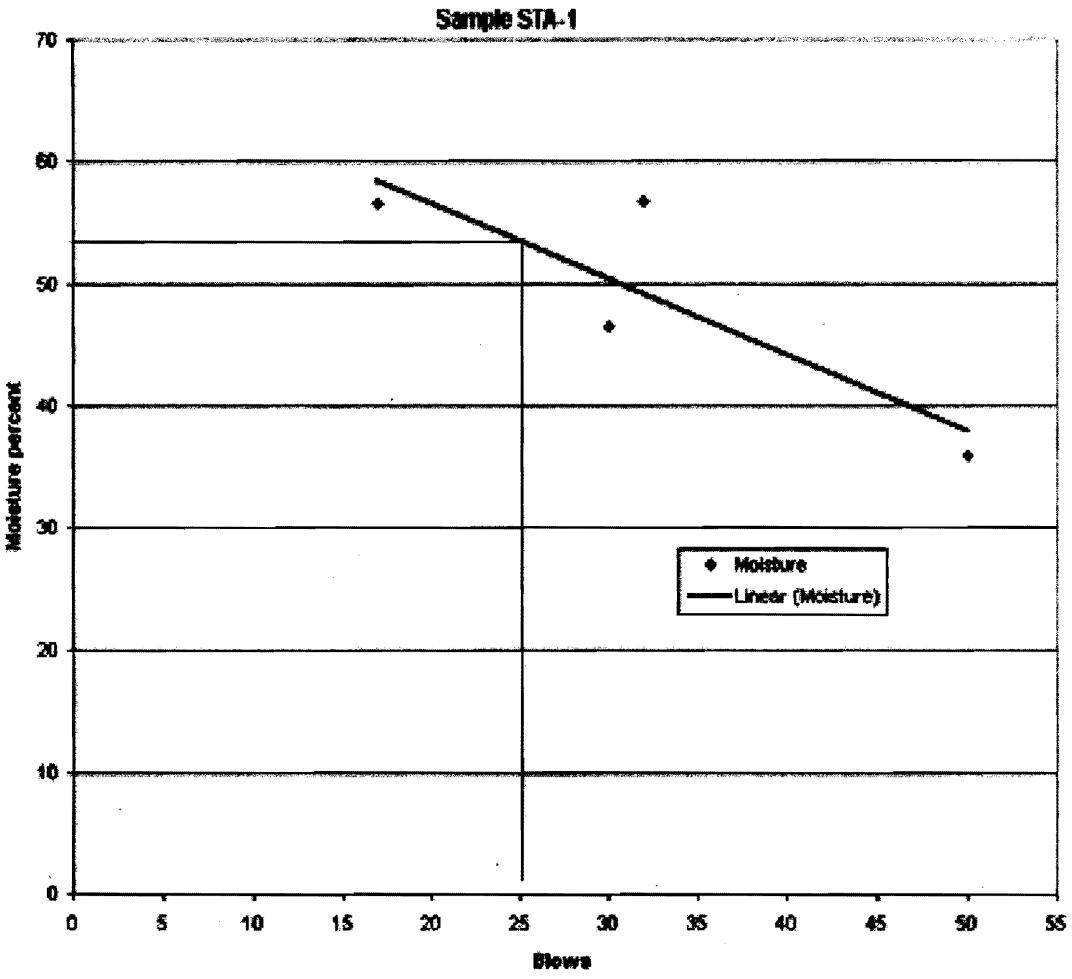


Liquid Limit = 53%

Sample A-3

| Blows | Moist % |
|---|---|
| 15 | 51.2 |
| 26 | 44.2 |
| 28 | 46.5 |
| 32 | 42.4 |
| 50 | 47.8 |

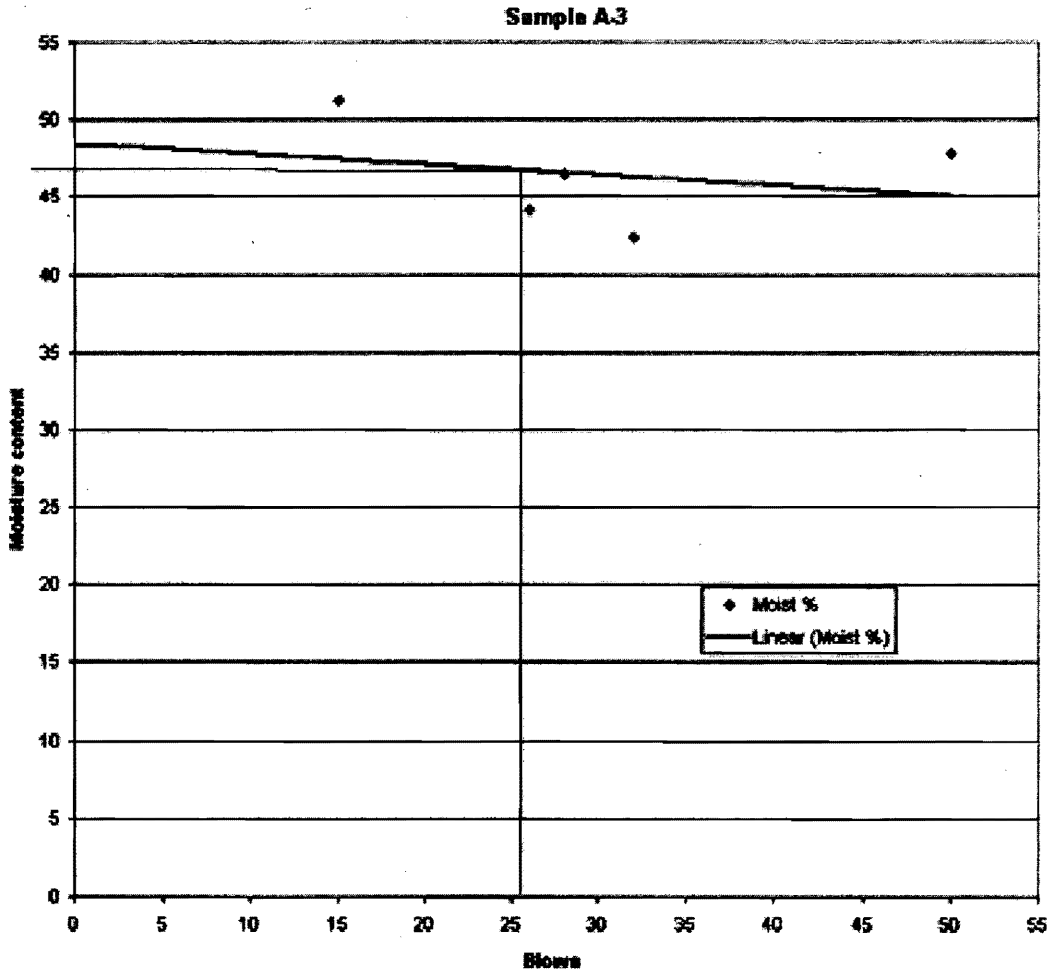


Liquid Limit = 48%

sample A-2

| Blows | Moist % |
|---|---|
| 16 | 94 |
| 21 | 99 |
| 28 | 96 |
| 45 | 91 |

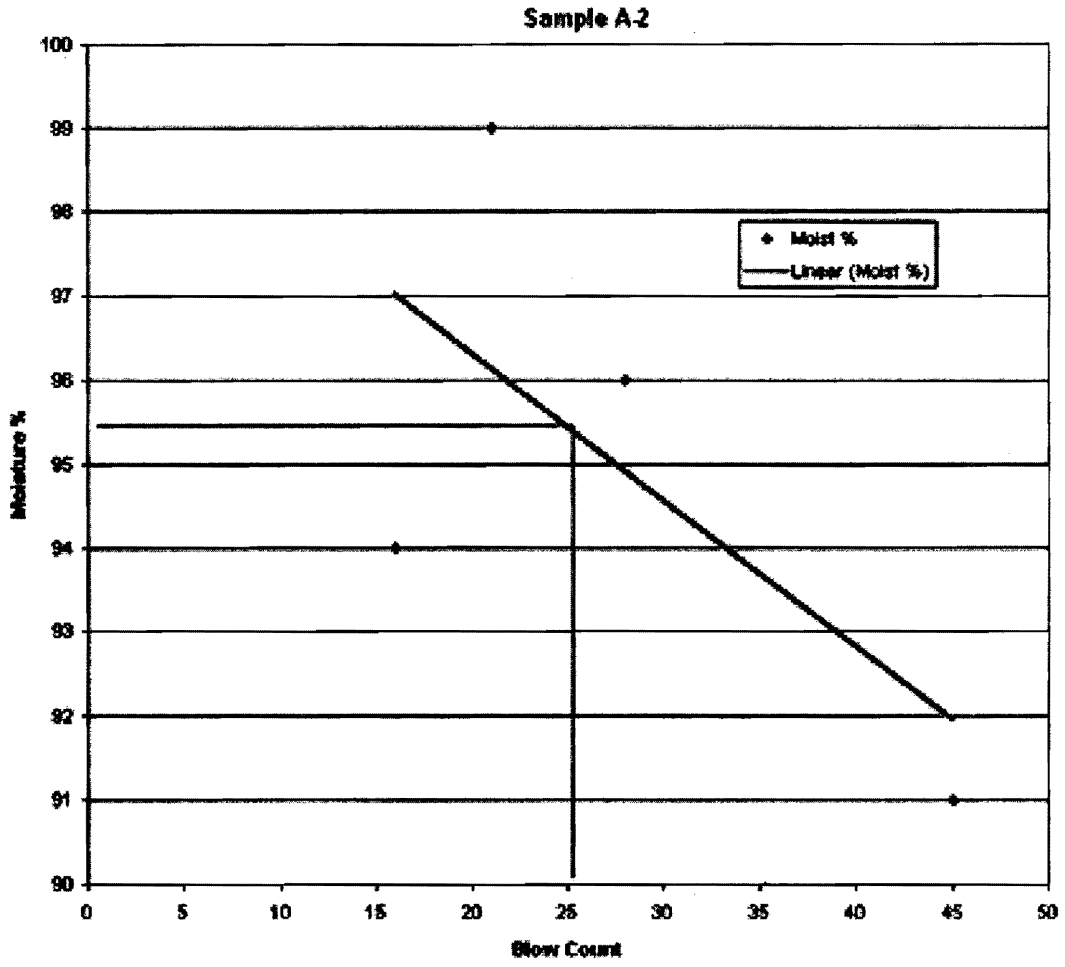


Liquid Limit = 95%

Sample A-8

| Blows | Moisture |
|---|---|
| 10 | 42.3 |
| 11 | 47.2 |
| 21 | 43 |
| 40 | 38.6 |

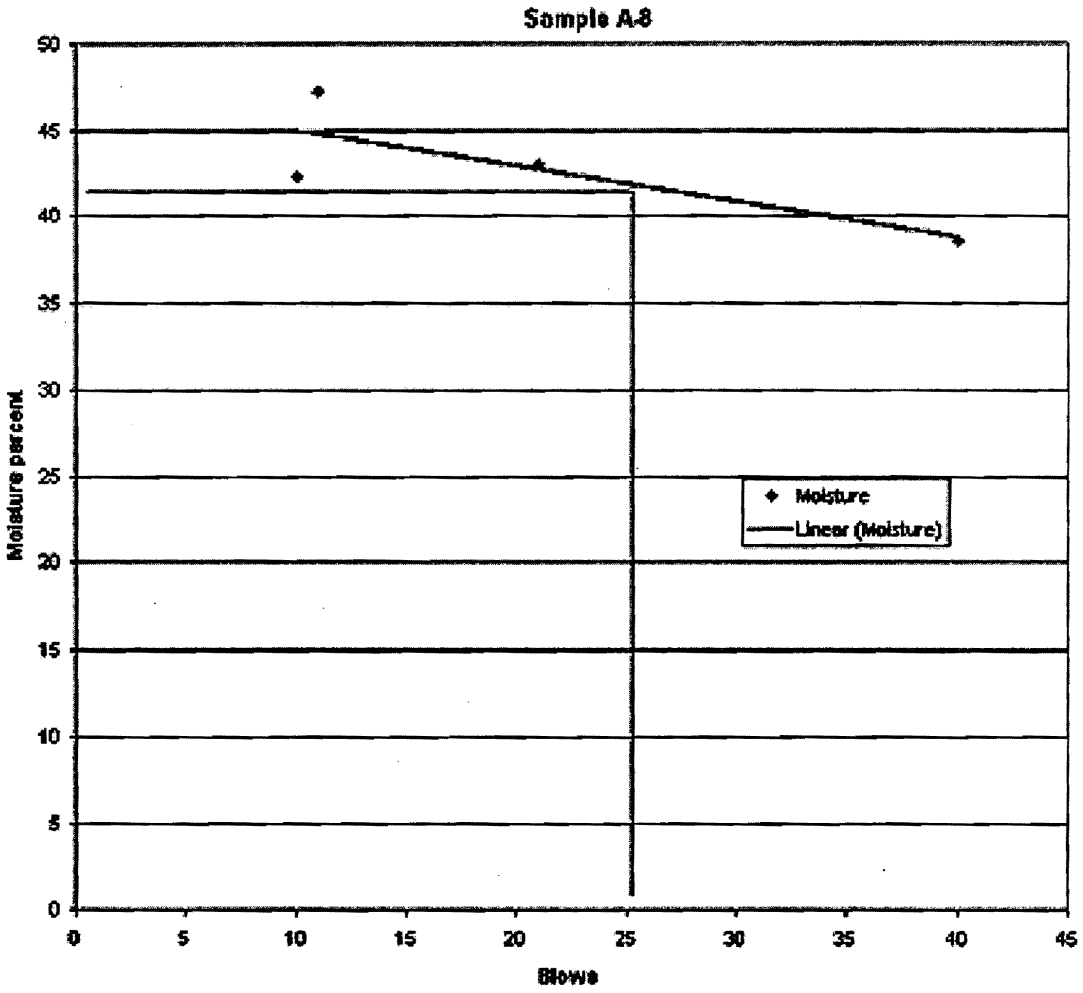


Liquid Limit = 41%

## West Tidewater Earthflow Plastic Limit Data

| Sample A-1 | | |
|---|---|---|
| Trial # | 1 | 2 |
| Dish # | 11 | 18 |
| dish + wet | 8.45 | 10.85 |
| dish + dry | 7.00 | 9.30 |
| wt. dish | 1.90 | 1.90 |
| wt water | 1.45 | 1.55 |
| wt. Soil | 5.10 | 7.40 |
| % water | 41.30 | 20.90 |
| Avg = PL | 24.70 | |

| Sample A-2 | | |
|---|---|---|
| Trial # | 1 | 2 |
| Dish # | 23 | 31 |
| dish + wet | 6.75 | 4.30 |
| dish + dry | 6.10 | 3.90 |
| wt. dish | 1.85 | 1.90 |
| wt water | 0.65 | 0.40 |
| wt. Soil | 4.25 | 2.00 |
| % water | 15.30 | 20.00 |
| Avg = PL | 17.65 | |

| Sample A-3 | | |
|---|---|---|
| Trial # | 1 | 2 |
| Dish # | a3-1 | a3-2 |
| dish + wet | 28.10 | 28.40 |
| dish + dry | 27.55 | 27.75 |
| wt. dish | 25.80 | 26.00 |
| wt water | 0.55 | 0.65 |
| wt. Soil | 1.75 | 1.75 |
| % water | 31.43 | 37.14 |
| Avg = PL | 34.28 | |

| Sample A-5 | | |
|---|---|---|
| Trial # | 1 | 2 |
| Dish # | 12 | 11c |
| dish + wet | 6.30 | 9.70 |
| dish + dry | 5.00 | 7.45 |
| wt. dish | 1.85 | 1.90 |
| wt water | 1.30 | 2.25 |
| wt. Soil | 3.15 | 5.55 |
| % water | 41.30 | 40.50 |
| Avg = PL | 40.9 | |

| Sample A-8 | | |
|---|---|---|
| Trial # | 1 | 2 |
| Dish # | 1 | 12 |
| dish + wet | 8.70 | 10.55 |
| dish + dry | 6.90 | 8.40 |
| wt. dish | 1.90 | 1.85 |
| wt water | 1.80 | 2.15 |
| wt. Soil | 5.00 | 6.55 |
| % water | 36.00 | 32.80 |
| Avg = PL | 34.4 | |

# Appendix D

## West Tidewater Earthflow

## Particle Size & Gradation Analysis

## Sieve and Pipette Data

Sample West Tidewater Earthflow Soil Gradation
STA-1
sand 8/12/97
fraction

| wt passing | weight | weight % | Cum. Wt. | Cum. %. |
|---|---|---|---|---|
| 59.94 | 0.06 | 0.999 | 0.06 | 0.1 |
| 59.74 | 0.2 | 0.996 | 0.26 | 0.43 |
| 59.03 | 0.71 | 0.984 | 0.97 | 1.62 |
| 58.47 | 0.56 | 0.975 | 1.53 | 2.55 |
| 57.92 | 0.55 | 0.965 | 2.08 | 3.47 |
| 57.42 | 0.5 | 0.957 | 2.58 | 4.3 |
| 56.46 | 0.96 | 0.941 | 3.54 | 5.9 |
| 54.28 | 2.18 | 0.905 | 5.71 | 9.53 |

West Tidewater Earthflow Soil
Gradation
Silt-Clay fraction 8/12/97 STA-1

| size mm | draw wt | wt / L | norm wt | wt% | cum wt w/ sand added |
|---|---|---|---|---|---|
| 0.0625 | 0.0124 | 0.496 | 1.21 | 2.02 | 11.55 |
| 0.031 | 0.0093 | 0.372 | 0.91 | 1.51 | 13.06 |
| 0.0156 | 0.0956 | 3.824 | 9.36 | 15.61 | 28.68 |
| 0.0078 | 0.1231 | 4.924 | 12.06 | 20.10 | 48.79 |
| 0.0039 | 0.0704 | 2.816 | 6.89 | 11.49 | 60.28 |
| 0.002 | 0.0579 | 2.316 | 5.67 | 9.45 | 69.74 |
| 0.00098 | 0.0308 | 1.232 | 3.01 | 5.03 | 74.77 |
| 0.00049 | 0.1533 | 6.132 | 15.02 | 25.03 | 99.81 |

West Tidewater Earthflow 8/12/97
Gradation Curve
data from sieve and pipette analysis combined
Sample STA-1 Dark gray mudstone

| size mm | Cum. %. |
|---|---|
| 0.42 | 0.1 |
| 0.25 | 0.43 |
| 0.149 | 1.62 |
| 0.125 | 2.55 |
| 0.106 | 3.47 |
| 0.09 | 4.3 |
| 0.074 | 5.9 |
| 0.063 | 9.53 |
| 0.031 | 13.06 |
| 0.0156 | 28.68 |
| 0.0078 | 48.79 |
| 0.0039 | 60.28 |
| 0.002 | 69.74 |
| 0.00098 | 74.77 |
| 0.00049 | 99.81 |

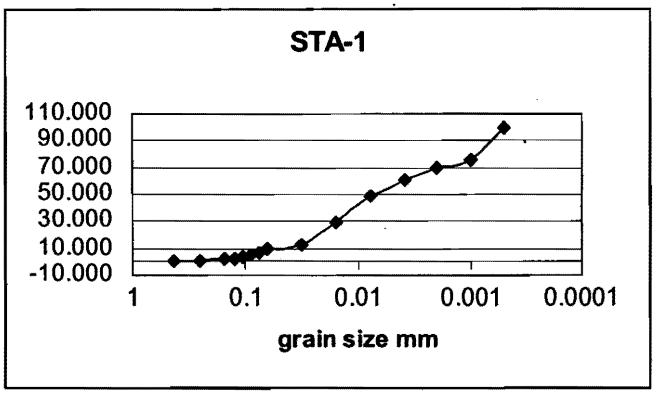

WEST TIDEWATER EARTHFLOW GRADATION CURVE

sample wt = 100gr  Sample A-3  9/20/97

| Mesh size | Size mm | net wt | weight % | cum wt | cum % |
|---|---|---|---|---|---|
| 20 | 0.840 | 0.650 | 0.91 | 0.65 | 0.9 |
| 40 | 0.420 | 1.550 | 2.18 | 2.200 | 3.1 |
| 60 | 0.250 | 5.550 | 7.81 | 7.750 | 10.9 |
| 80 | 0.177 | 3.100 | 4.36 | 10.850 | 15.3 |
| 120 | 0.125 | 3.500 | 4.93 | 14.350 | 20.2 |
| 140 | 0.106 | 3.100 | 4.36 | 17.450 | 24.6 |
| 170 | 0.090 | 2.400 | 3.38 | 19.850 | 27.9 |
| 200 | 0.074 | 3.150 | 4.43 | 23.000 | 32.4 |
| 230 | 0.063 | 2.125 | 2.99 | 25.125 | 35.4 |
| 4.5 phi | 0.044 | 1.340 | 1.89 | 26.465 | 37.2 |
| 5 phi | 0.031 | 6.350 | 8.94 | 32.815 | 46.2 |
| 5.5 phi | 0.022 | 5.195 | 7.31 | 38.010 | 53.5 |
| 6 phi | 0.015 | 7.040 | 9.91 | 45.050 | 63.4 |
| 7 phi | 0.007 | 7.160 | 10.08 | 52.210 | 73.5 |
| 8 phi | 0.004 | 1.740 | 2.45 | 53.950 | 75.9 |
| 9 phi | 0.002 | 5.200 | 7.32 | 59.150 | 83.3 |
| 10 phi | 0.001 | 11.9 | 16.75 | 71.050 | 100.0 |

WEST TIDEWATER EARTHFLOW GRADATION CURVE

sample wt = 100gr Sample A-3 9/20/97

| Size mm | cum % |
|---|---|
| 0.001 | 100.0 |
| 0.002 | 83.3 |
| 0.004 | 75.9 |
| 0.007 | 73.5 |
| 0.015 | 63.4 |
| 0.022 | 53.5 |
| 0.031 | 46.2 |
| 0.044 | 37.2 |
| 0.063 | 35.4 |
| 0.074 | 32.4 |
| 0.090 | 27.9 |
| 0.106 | 24.6 |
| 0.125 | 20.2 |
| 0.177 | 15.3 |
| 0.250 | 10.9 |
| 0.420 | 3.1 |
| 0.840 | 0.9 |

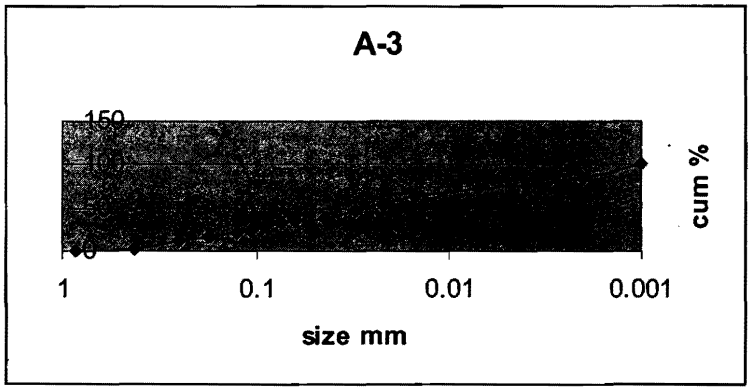

WEST TIDEWATER EARTHFLOW GRADATION CURVE
SILT-CLAY FRACTION Pipette data

Tot wt 25.756 8/12/97 Sample A-5

| Size mm | net wt | wt / L | norm wt | cum % |
|---|---|---|---|---|
| 0.0625 | 0.0209 | 0.836 | 1.672 | 2.787 |
| 0.0310 | 0.0683 | 2.732 | 5.464 | 9.107 |
| 0.0156 | 0.1270 | 5.08 | 10.160 | 16.933 |
| 0.0078 | 0.1254 | 5.016 | 10.032 | 16.720 |
| 0.0039 | 0.0796 | 3.184 | 6.368 | 10.613 |
| 0.0020 | 0.0776 | 3.104 | 6.208 | 10.347 |
| 0.0098 | 0.0345 | 1.38 | 2.760 | 4.600 |
| 0.0049 | 0.1106 | 4.424 | 8.848 | 14.747 |

| MESH | SIZE mm | SAMPLE WEIGHT | WEIGHT PASSING | WEIGHT % | CUM WEIGHT | CUM % |
|---|---|---|---|---|---|---|
| 20.000 | 0.840 | 0.040 | 59.960 | 99.933 | 0.040 | 0.067 |
| 40.000 | 0.420 | 0.280 | 59.720 | 99.533 | 0.320 | 0.533 |
| 60.000 | 0.250 | 0.710 | 59.290 | 98.817 | 1.030 | 1.717 |
| 100.000 | 0.149 | 1.130 | 58.870 | 98.117 | 2.160 | 3.600 |
| 120.000 | 0.125 | 0.650 | 59.350 | 98.917 | 2.810 | 4.683 |
| 150.000 | 0.106 | 0.680 | 59.320 | 98.867 | 3.490 | 5.817 |
| 170.000 | 0.090 | 0.730 | 59.270 | 98.783 | 4.220 | 7.033 |
| 200.000 | 0.074 | 1.290 | 58.710 | 97.850 | 5.510 | 9.183 |
| 230.000 | 0.063 | 2.920 | 57.080 | 95.133 | 8.430 | 14.050 |

Sample A-5

| Size mm | cum % |
|---|---|
| 0.84 | 0.07 |
| 0.42 | 0.53 |
| 0.25 | 1.72 |
| 0.15 | 3.60 |
| 0.13 | 4.68 |
| 0.11 | 5.82 |
| 0.09 | 7.03 |
| 0.07 | 9.18 |
| 0.06 | 11.97 |
| 0.03 | 21.08 |
| 0.02 | 38.01 |
| 0.01 | 54.73 |
| 0.00 | 65.34 |
| 0.00 | 75.69 |
| 0.00 | 80.29 |
| 0.00 | 95.04 |

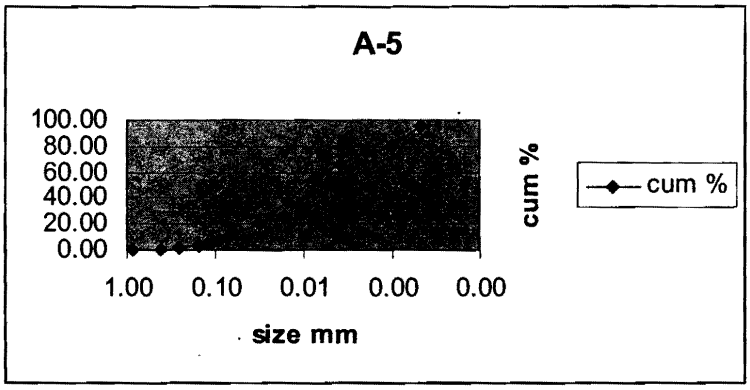

# Appendix E

## West Tidewater Earthflow

## Direct Shear Testing

## Data Tables

Consolidated Drained test trial one 16 kg N force

Direct Shear Testing 8/27/97 max in bold face

sample ST gray mudstone, Shelby tube sample test speed 3

strain rate = 0.063 in. per min.

| Time, min | Load lbs | Strain mm | corrected load lbs | corrected Strain mm | Normal force, newtons | Shear Stress trial 1 kPa |
|---|---|---|---|---|---|---|
| 0 | 0.300 | 0.652 | 0.000 | 0.000 | 0 | 0.000 |
| 0.5 | 4.700 | 1.230 | 4.400 | 0.578 | 19.58 | 6.183 |
| 1 | 8.200 | 1.917 | 7.900 | 1.265 | 35.155 | 11.100 |
| 1.5 | 11.200 | 2.640 | 10.900 | 1.988 | 48.505 | 15.316 |
| 2 | 13.700 | 3.385 | 13.400 | 2.733 | 59.63 | 18.829 |
| 2.5 | 15.400 | 4.144 | 15.100 | 3.492 | 67.195 | 21.217 |
| 3 | 17.300 | 4.925 | 17.000 | 4.273 | 75.65 | 23.887 |
| 3.5 | 17.600 | 5.696 | 17.300 | 5.044 | 76.985 | 24.308 |
| 4 | 18.100 | 6.476 | 17.800 | 5.824 | 79.21 | 25.011 |
| 4.5 | **18.500** | **7.246** | **18.200** | **6.594** | **80.99** | **25.573** |
| 5 | **18.500** | **8.015** | **18.200** | **7.363** | 80.99 | **25.573** |
| 5.5 | 18.100 | 8.780 | 17.800 | 8.128 | 79.21 | 25.011 |
| 6 | 17.400 | 9.676 | 17.100 | 9.024 | 76.095 | 24.027 |

Consolidated Drained test trial two 16 kg N force

Direct Shear Testing 8/27/97 max in bold face

sample ST gray mudstone, Shelby tube sample Reversed

| Time, min | Load lbs | Strain mm | corrected load lbs | corrected Strain mm | Normal force, newtons | Shear Stress trial 1 kPa |
|---|---|---|---|---|---|---|
| 0 | 0.500 | 0.442 | 0.000 | 0.000 | 0.000 | 0.000 |
| 0.5 | 9.000 | 1.200 | 8.500 | 0.758 | 37.825 | 11.943 |
| 1 | 12.800 | 1.965 | 12.300 | 1.523 | 54.735 | 17.283 |
| 1.5 | 14.300 | 2.745 | 13.800 | 2.303 | 61.410 | 19.391 |
| 2 | 15.200 | 3.455 | 14.700 | 3.013 | 65.415 | 20.655 |
| 2.5 | 15.300 | 4.278 | 14.800 | 3.836 | 65.860 | 20.796 |
| 3 | 15.500 | 5.015 | 15.000 | 4.573 | 66.750 | 21.077 |
| 3.5 | 15.700 | 5.859 | 15.200 | 5.417 | 67.640 | 21.358 |
| 4 | **15.800** | **6.551** | **15.300** | **6.109** | **68.085** | **21.498** |
| 4.5 | 15.400 | 7.393 | 14.900 | 6.951 | 66.305 | 20.936 |
| 5 | 15.400 | 8.155 | 14.900 | 7.713 | 66.305 | 20.936 |
| 5.5 | 14.600 | 8.955 | 14.100 | 8.513 | 62.745 | 19.812 |
| 6 | 14.400 | 9.776 | 13.900 | 9.334 | 61.855 | 19.531 |

Consolidated Drained test trial three 16 kg N force
Direct Shear Testing 8/27/97 max in bold face
sample ST gray mudstone, Shelby tube sample Reversed

| Time, min | Load lbs | Strain mm | corrected load lbs | corrected Strain mm | Normal force, newtons | Shear Stress trial 1 kPa |
|---|---|---|---|---|---|---|
| 0 | 2.300 | 0.994 | 0.000 | 0.000 | 0.000 | 0.000 |
| 0.5 | 3.300 | 1.655 | 1.000 | 0.661 | 4.450 | 1.405 |
| 1 | 7.800 | 2.421 | 5.500 | 1.427 | 24.475 | 7.728 |
| 1.5 | 10.200 | 3.161 | 7.900 | 2.167 | 35.155 | 11.100 |
| 2 | 11.900 | 4.025 | 9.600 | 3.031 | 42.720 | 13.489 |
| 2.5 | 13.100 | 4.706 | 10.800 | 3.712 | 48.060 | 15.175 |
| 3 | 14.100 | 5.484 | 11.800 | 4.490 | 52.510 | 16.580 |
| 3.5 | 14.700 | 6.216 | 12.400 | 5.222 | 55.180 | 17.423 |
| 4 | 14.700 | 7.058 | 12.400 | 6.064 | 55.180 | 17.423 |
| 4.5 | 15.000 | 7.821 | 12.700 | 6.827 | 56.515 | 17.845 |
| 5 | **15.300** | **8.643** | **13.000** | **7.649** | **57.850** | **18.266** |
| 5.5 | 15.300 | 9.401 | 13.000 | 8.407 | 57.850 | 18.266 |
| 6 | 15.300 | 10.216 | 13.000 | 9.222 | 57.850 | 18.266 |
| 6.5 | 14.800 | 11.068 | 12.500 | 10.074 | 55.625 | 17.564 |
| 7 | 14.700 | 11.875 | 12.400 | 10.881 | 55.180 | 17.423 |

Consolidated Drained test trial four 16 kg N force
Direct Shear Testing 8/27/97 max in bold face
sample ST gray mudstone, Shelby tube sample Reversed

| Time, min | Load lbs | Strain mm | corrected load lbs | corrected Strain mm | Normal force, newtons | Shear Stress trial 1 kPa |
|---|---|---|---|---|---|---|
| 0 | 0.400 | -0.053 | 0.000 | 0.000 | 0.000 | 0.000 |
| 0.5 | 9.400 | 0.556 | 9.000 | 0.609 | 40.050 | 12.646 |
| 1 | 13.300 | 1.274 | 12.900 | 1.327 | 57.405 | 18.126 |
| 1.5 | 14.400 | 1.985 | 14.000 | 2.038 | 62.300 | 19.672 |
| 2 | 14.600 | 2.727 | 14.200 | 2.780 | 63.190 | 19.953 |
| 2.5 | 14.900 | 3.488 | 14.500 | 3.541 | 64.525 | 20.374 |
| 3 | 15.300 | 4.204 | 14.900 | 4.257 | 66.305 | 20.936 |
| 3.5 | 15.400 | 4.921 | 15.000 | 4.974 | 66.750 | 21.077 |
| 4 | **15.500** | **5.686** | **15.100** | **5.739** | **67.195** | **21.217** |
| 4.5 | 15.200 | 6.476 | 14.800 | 6.529 | 65.860 | 20.796 |
| 5 | 15.100 | 7.156 | 14.700 | 7.209 | 65.415 | 20.655 |
| 5.5 | 15.000 | 7.919 | 14.600 | 7.972 | 64.970 | 20.515 |
| 6 | 15.100 | 8.683 | 14.700 | 8.736 | 65.415 | 20.655 |
| 6.5 | 15.200 | 9.450 | 14.800 | 9.503 | 65.860 | 20.796 |

Consolidated Drained
test trial five 16 kg N force
Direct Shear Testing 8/27/97 max in bold face
sample ST gray mudstone, Shelby tube sample Reversed

| Time, min | Load lbs | Strain mm | corrected load lbs | corrected Strain mm | Normal force, newtons | Shear Stress trial 1 kPa |
|---|---|---|---|---|---|---|
| 0 | 0.400 | 0.903 | 0.000 | 0.000 | 0.000 | 0.000 |
| 0.5 | 8.500 | 1.672 | 8.100 | 0.769 | 36.045 | 11.381 |
| 1 | 11.300 | 2.337 | 10.900 | 1.434 | 48.505 | 15.316 |
| 1.5 | 13.000 | 3.125 | 12.600 | 2.222 | 56.070 | 17.704 |
| 2 | 13.400 | 3.954 | 13.000 | 3.051 | 57.850 | 18.266 |
| 2.5 | 14.100 | 4.716 | 13.700 | 3.813 | 60.965 | 19.250 |
| 3 | 14.400 | 5.565 | 14.000 | 4.662 | 62.300 | 19.672 |
| 3.5 | 14.500 | 6.234 | 14.100 | 5.331 | 62.745 | 19.812 |
| 4 | 14.700 | 7.052 | 14.300 | 6.149 | 63.635 | 20.093 |
| 4.5 | 14.300 | 7.835 | 13.900 | 6.932 | 61.855 | 19.531 |
| 5 | 14.500 | 8.596 | 14.100 | 7.693 | 62.745 | 19.812 |
| 5.5 | **14.600** | **9.410** | **14.200** | **8.507** | **63.190** | **19.953** |
| 6 | 14.300 | 10.216 | 13.900 | 9.313 | 61.855 | 19.531 |
| 6.5 | 14.000 | 11.018 | 13.600 | 10.115 | 60.520 | 19.110 |
| 7 | 14.000 | 11.857 | 13.600 | 10.954 | 60.520 | 19.110 |

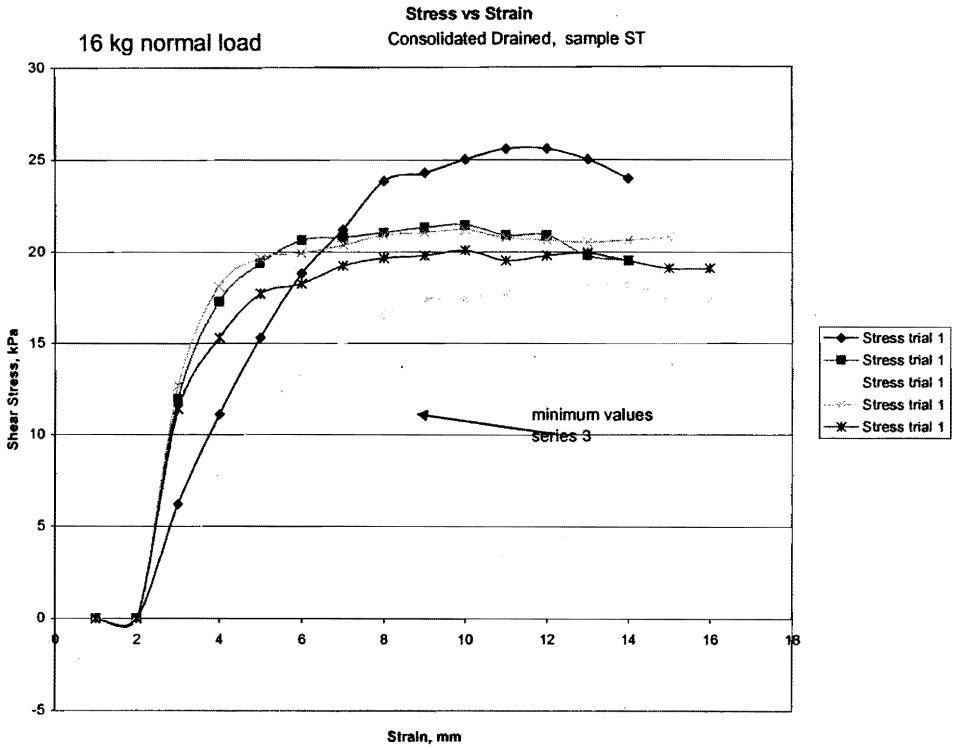
Stress vs Strain
16 kg normal load
Consolidated Drained, sample ST
30
25
20
15
10
5
0
-5
0
2
4
6
8
10
12
14
16
18
Shear Stress, kPa
Strain, mm
minimum values
series 3
Stress trial 1
Stress trial 1
Stress trial 1
Stress trial 1
Stress trial 1

# West Tidewater Earthflow Direct Shear Test Results

Strain Controlled STA-1

Consolidated Drained method

| Trial Number | Normal Stress, kPa | Shear Stress, kPa |
|---|---|---|
| 1, 16 kg | 49.561 | 17.477 |
| 2, 32 kg | 99.122 | 37.068 |
| 3, 64 kg | 148.683 | 47.999 |

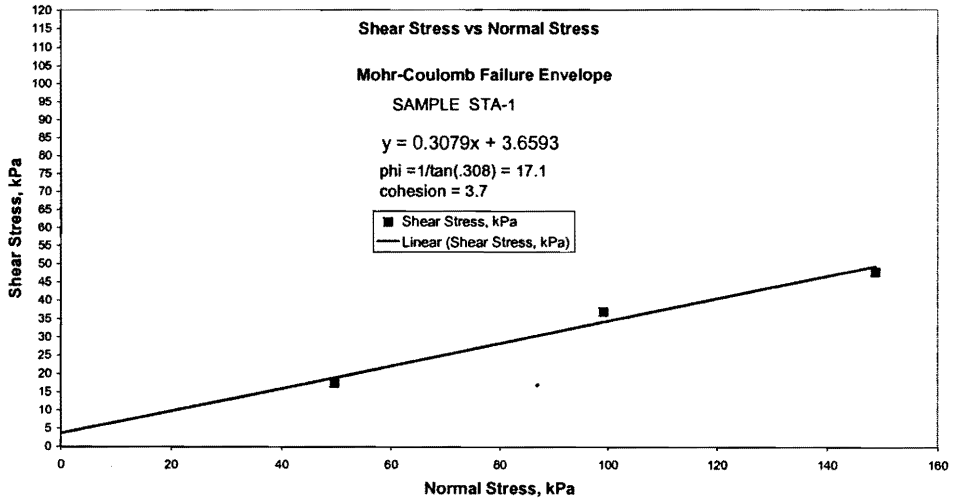
Shear Stress vs Normal Stress
Mohr-Coulomb Failure Envelope
SAMPLE STA-1
y = 0.3079x + 3.6593
phi =1/tan(.308) = 17.1
cohesion = 3.7
Shear Stress, kPa
Linear (Shear Stress, kPa)
Shear Stress, kPa
Normal Stress, kPa
0
5
10
15
20
25
30
35
40
45
50
55
60
65
70
75
80
85
90
95
100
105
110
115
120
0
20
40
60
80
100
120
140
160

West Tidewater Earthflow 8/27/96

Direct Shear test Consolidated Drained Normal load = 16kg

Trial one A-3 Strain Controlled test speed 3

| Time, min | Load lbs | Strain mm | corrected load lbs | corrected Strain mm | Normal force, newtons | Shear Stress trial 1 kPa |
|---|---|---|---|---|---|---|
| 0.000 | 0.000 | 0.812 | 0.000 | 0.000 | 0.000 | 0.000 |
| 0.500 | 0.000 | 0.812 | 0.000 | 0.000 | 0.000 | 0.000 |
| 1.000 | 4.300 | 1.096 | 4.300 | 0.284 | 19.135 | 6.042 |
| 1.500 | 6.800 | 1.570 | 6.800 | 0.758 | 30.260 | 9.555 |
| 2.000 | 8.600 | 2.048 | 8.600 | 1.236 | 38.270 | 12.084 |
| 2.500 | 9.900 | 2.510 | 9.900 | 1.698 | 44.055 | 13.911 |
| 3.000 | 10.900 | 2.997 | 10.900 | 2.185 | 48.505 | 15.316 |
| 3.500 | 10.500 | 3.377 | 10.500 | 2.565 | 46.725 | 14.754 |
| 4.000 | 12.200 | 3.866 | 12.200 | 3.054 | 54.290 | 17.142 |
| 4.500 | 13.000 | 4.342 | 13.000 | 3.530 | 57.850 | 18.266 |
| 5.000 | 13.500 | 4.848 | 13.500 | 4.036 | 60.075 | 18.969 |
| 5.500 | 13.800 | 5.311 | 13.800 | 4.499 | 61.410 | 19.391 |
| 6.000 | 14.300 | 5.806 | 14.300 | 4.994 | 63.635 | 20.093 |
| 6.500 | 14.600 | 6.280 | 14.600 | 5.468 | 64.970 | 20.515 |
| 7.000 | 14.900 | 6.789 | 14.900 | 5.977 | 66.305 | 20.936 |
| 8.000 | 15.400 | 7.289 | 15.400 | 6.477 | 68.530 | 21.639 |
| 8.500 | 15.600 | 8.075 | 15.600 | 7.263 | 69.420 | 21.920 |
| 9.000 | 16.100 | 8.796 | 16.100 | 7.984 | 71.645 | 22.622 |
| 9.500 | 16.200 | 9.656 | 16.200 | 8.844 | 72.090 | 22.763 |
| 10.000 | 16.300 | 10.315 | 16.300 | 9.503 | 72.535 | 22.903 |
| 10.500 | 16.200 | 11.086 | 16.200 | 10.274 | 72.090 | 22.763 |
| 11.000 | 16.300 | 11.774 | 16.300 | 10.962 | 72.535 | 22.903 |
| 11.500 | 16.300 | 12.445 | 16.300 | 11.633 | 72.535 | 22.903 |
| 12.000 | **16.700** | **13.250** | **16.700** | **12.438** | **74.315** | **23.465** |
| 12.500 | 16.400 | 13.989 | 16.400 | 13.177 | 72.980 | 23.044 |
| 13.000 | 16.300 | 14.577 | 16.300 | 13.765 | 72.535 | 22.903 |

West Tidewater Earthflow 8/27/96

Consolidated

Direct Shear test Drained Normal load = 32 kg

Trial two A-3 Strain Controlled test speed 3

| Time, min | Load lbs | Strain mm | corrected load lbs | corrected Strain mm | Normal force, newtons | Shear Stress trial 1 kPa |
|---|---|---|---|---|---|---|
| 0.000 | 1.000 | 0.796 | 0.000 | 0.000 | 0.000 | 0.000 |
| 0.500 | 15.900 | 1.110 | 14.900 | 0.314 | 66.305 | 20.936 |
| 1.000 | 20.900 | 1.547 | 19.900 | 0.751 | 88.555 | 27.962 |
| 1.500 | 25.000 | 1.994 | 24.000 | 1.198 | 106.800 | 33.723 |
| 2.000 | 27.700 | 2.443 | 26.700 | 1.647 | 118.815 | 37.517 |
| 2.500 | 29.200 | 2.885 | 28.200 | 2.089 | 125.490 | 39.624 |
| 3.000 | 30.000 | 3.355 | 29.000 | 2.559 | 129.050 | 40.748 |
| 3.500 | 30.400 | 3.807 | 29.400 | 3.011 | 130.830 | 41.310 |
| 4.000 | 30.500 | 4.270 | 29.500 | 3.474 | 131.275 | 41.451 |
| 4.500 | 30.700 | 4.696 | 29.700 | 3.900 | 132.165 | 41.732 |
| 5.000 | 30.800 | 5.170 | 29.800 | 4.374 | 132.610 | 41.872 |
| **5.500** | **30.900** | **5.690** | **29.900** | **4.894** | **133.055** | **42.013** |
| 6.000 | 30.700 | 6.077 | 29.700 | 5.281 | 132.165 | 41.732 |
| 6.500 | 30.700 | 6.549 | 29.700 | 5.753 | 132.165 | 41.732 |
| 7.000 | 30.400 | 6.993 | 29.400 | 6.197 | 130.830 | 41.310 |
| 8.000 | 30.300 | 7.430 | 29.300 | 6.634 | 130.385 | 41.170 |
| 8.500 | 30.200 | 7.908 | 29.200 | 7.112 | 129.940 | 41.029 |

West Tidewater Earthflow 8/27/96

Consolidated

Direct Shear test Drained Normal load = 48 kg

Trial three A-3 Strain Controlled test speed 3

| Time, min | Load lbs | Strain mm | corrected load lbs | corrected Strain mm | Normal force, newtons | Shear Stress trial 1 kPa |
|---|---|---|---|---|---|---|
| 0.000 | 1.200 | 0.673 | 0.000 | 0.000 | 0.000 | 0.000 |
| 0.500 | 20.200 | 0.906 | 19.000 | 0.233 | 84.550 | 26.697 |
| 1.000 | 33.900 | 1.536 | 32.700 | 0.863 | 145.515 | 45.947 |
| 1.500 | 38.200 | 2.323 | 37.000 | 1.650 | 164.650 | 51.989 |
| 2.000 | 39.800 | 3.107 | 38.600 | 2.434 | 171.770 | 54.237 |
| 2.500 | 40.600 | 3.916 | 39.400 | 3.243 | 175.330 | 55.362 |
| 3.000 | 40.700 | 4.666 | 39.500 | 3.993 | 175.775 | 55.502 |
| 3.500 | 41.000 | 5.475 | 39.800 | 4.802 | 177.110 | 55.924 |
| 4.000 | 40.800 | 6.233 | 39.600 | 5.560 | 176.220 | 55.643 |
| 4.500 | **41.100** | **6.976** | **39.900** | **6.303** | **177.555** | **56.064** |
| 5.000 | 40.800 | 7.801 | 39.600 | 7.128 | 176.220 | 55.643 |
| 5.500 | 41.000 | 8.584 | 39.800 | 7.911 | 177.110 | 55.924 |
| 6.000 | 41.000 | 9.332 | 39.800 | 8.659 | 177.110 | 55.924 |

**West Tidewater Earthflow** **Shear Stress vs Strain**
Sample A-3 Consolidated Drained test

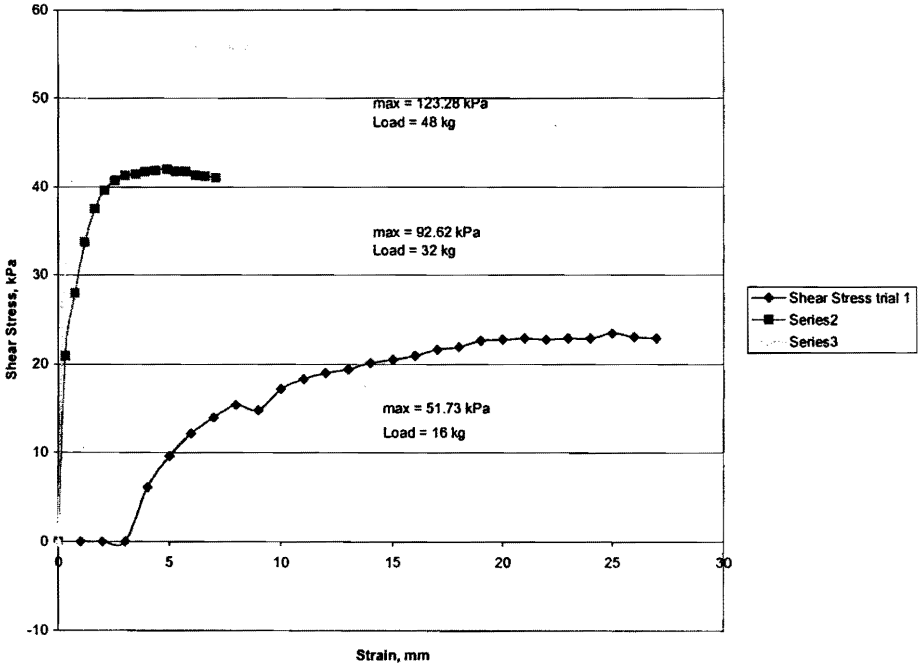

# West Tidewater Earthflow Direct Shear Test Results

Direct Shear test
Strain Controlled

Consolidated Drained
test speed = 3

Sample
A-3

| Trial number | Normal Stress | Shear Stress, kPa |
|---|---|---|
| 1, 16 kg | 49.561 | 23.465 |
| 2, 32 kg | 99.122 | 42.013 |
| 3, 48 kg | 148.683 | 56.064 |

West Tidewater Earthflow
Sample A-3

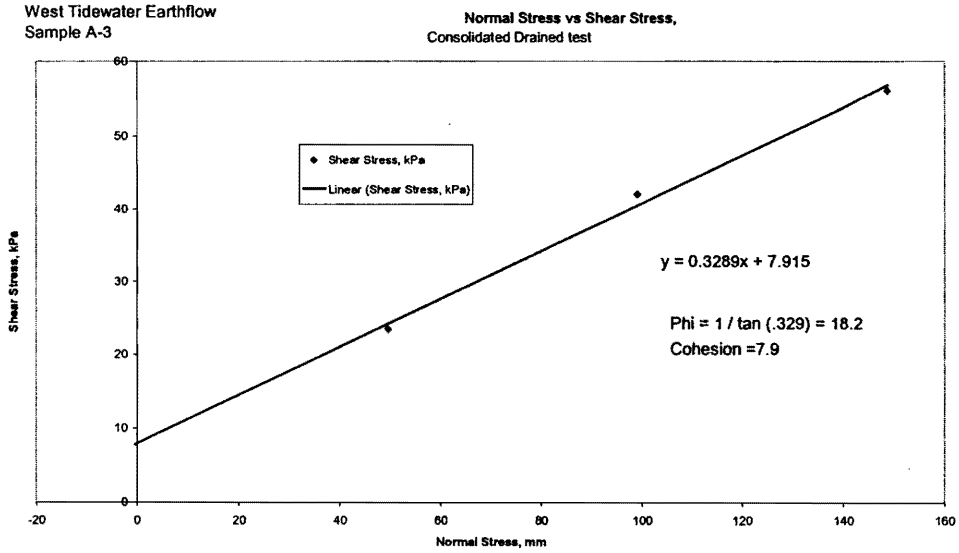

Consolidated Drained test trial one 16 kg N load
Direct Shear Testing 8/27/97 max in bold face
sample A-5 yellow-gray colluvium test speed 3

| Time, min | Load lbs | Strain mm | corrected load lbs | corrected Strain mm | Normal force, newtons | Shear Stress trial 1 kPa |
|---|---|---|---|---|---|---|
| 0.000 | 1.800 | 0.756 | 0.000 | 0.000 | 0.000 | 0.000 |
| 0.500 | 10.200 | 1.390 | 8.400 | 0.634 | 37.380 | 11.803 |
| 1.000 | 13.200 | 2.194 | 11.400 | 1.438 | 50.730 | 16.018 |
| 1.500 | 14.900 | 2.886 | 13.100 | 2.130 | 58.295 | 18.407 |
| 2.000 | 15.900 | 3.674 | 14.100 | 2.918 | 62.745 | 19.812 |
| 2.500 | 16.900 | 4.424 | 15.100 | 3.668 | 67.195 | 21.217 |
| 3.000 | 17.500 | 5.234 | 15.700 | 4.478 | 69.865 | 22.060 |
| 3.500 | 17.500 | 5.998 | 15.700 | 5.242 | 69.865 | 22.060 |
| 4.000 | 17.600 | 6.755 | 15.800 | 5.999 | 70.310 | 22.201 |
| 4.500 | 18.600 | 7.544 | 16.800 | 6.788 | 74.760 | 23.606 |
| 5.000 | 18.800 | 8.331 | 17.000 | 7.575 | 75.650 | 23.887 |
| 6.000 | **18.900** | **9.052** | **17.100** | **8.296** | **76.095** | **24.027** |
| 6.500 | 18.300 | 9.842 | 16.500 | 9.086 | 73.425 | 23.184 |
| 7.000 | 18.500 | 10.664 | 16.700 | 9.908 | 74.315 | 23.465 |
| 7.500 | 18.800 | 11.450 | 17.000 | 10.694 | 75.650 | 23.887 |
| 8.000 | 18.800 | 12.206 | 17.000 | 11.450 | 75.650 | 23.887 |

Consolidated Drained test — trial one — 32 kg N force

Direct Shear Testing — 9/25/97 — max in bold face

sample A-5 — Yellow-gray colluvium — test speed 3

| Time, min | Load lbs | Strain mm | corrected load lbs | corrected Strain mm | Normal force, newtons | Shear Stress trial 1 kPa |
|---|---|---|---|---|---|---|
| 0 | 2.300 | 1.086 | 0.000 | 0.000 | 0.000 | 0.000 |
| 0.5 | 10.500 | 1.679 | 8.200 | 0.593 | 36.490 | 11.522 |
| 1 | 14.400 | 2.470 | 12.100 | 1.384 | 53.845 | 17.002 |
| 1.5 | 17.200 | 3.175 | 14.900 | 2.089 | 66.305 | 20.936 |
| 2 | 18.800 | 3.977 | 16.500 | 2.891 | 73.425 | 23.184 |
| 2.5 | 20.600 | 4.724 | 18.300 | 3.638 | 81.435 | 25.714 |
| 3 | 21.700 | 5.485 | 19.400 | 4.399 | 86.330 | 27.259 |
| 3.5 | 22.600 | 6.224 | 20.300 | 5.138 | 90.335 | 28.524 |
| 4 | 23.200 | 7.009 | 20.900 | 5.923 | 93.005 | 29.367 |
| 4.5 | 23.500 | 7.777 | 21.200 | 6.691 | 94.340 | 29.788 |
| 5 | 24.000 | 8.556 | 21.700 | 7.470 | 96.565 | 30.491 |
| 5.5 | 24.100 | 9.345 | 21.800 | 8.259 | 97.010 | 30.632 |
| 6 | **24.400** | **10.097** | **22.100** | **9.011** | **98.345** | **31.053** |
| 6.5 | 24.100 | 10.906 | 21.800 | 9.820 | 97.010 | 30.632 |
| 7 | 24.300 | 11.655 | 22.000 | 10.569 | 97.900 | 30.913 |
| 7.5 | 23.600 | 12.395 | 21.300 | 11.309 | 94.785 | 29.929 |

## Consolidated Drained test

trial two 32 kg N force

Direct Shear Testing 9/25/97

max in bold face

sample A-5 Yellow-gray colluvium test speed 3

strain rate = 217 cm per day

| Time, min | Load lbs | Strain mm | corrected load lbs | corrected Strain mm | Normal force, newtons | Shear Stress trial 1 kPa |
|---|---|---|---|---|---|---|
| 0.0 | 4.100 | 1.733 | 0.000 | 0.000 | 0.000 | 0.000 |
| 0.5 | 15.000 | 2.322 | 10.900 | 0.589 | 48.505 | 15.316 |
| 1.0 | 17.900 | 3.062 | 13.800 | 1.329 | 61.410 | 19.391 |
| 1.5 | 20.000 | 3.847 | 15.900 | 2.114 | 70.755 | 22.341 |
| 2.0 | 21.000 | 4.607 | 16.900 | 2.874 | 75.205 | 23.746 |
| 2.5 | 22.000 | 5.377 | 17.900 | 3.644 | 79.655 | 25.152 |
| 3.0 | 22.400 | 6.171 | 18.300 | 4.438 | 81.435 | 25.714 |
| 3.5 | 22.700 | 6.957 | 18.600 | 5.224 | 82.770 | 26.135 |
| 4.0 | 22.900 | 7.719 | 18.800 | 5.986 | 83.660 | 26.416 |
| 4.5 | 23.800 | 8.519 | 19.700 | 6.786 | 87.665 | 27.681 |
| 5.0 | **23.800** | **9.302** | **19.700** | **7.569** | **87.665** | **27.681** |
| 5.5 | 23.700 | 10.106 | 19.600 | 8.373 | 87.220 | 27.540 |
| 6.0 | 23.400 | 10.866 | 19.300 | 9.133 | 85.885 | 27.119 |

## Consolidated Drained test

trial three 48 kg N force

Direct Shear Testing 9/25/97

max in bold face

Yellow-gray

sample A-5 colluvium

test speed 3

strain rate = 217 cm per day

| Time, min | Load lbs | Strain mm | corrected load lbs | corrected Strain mm | Normal force, newtons | Shear Stress trial 1 kPa |
|---|---|---|---|---|---|---|
| 0 | 3.900 | 0.970 | 0.000 | 0.000 | 0.000 | 0.000 |
| 0.5 | 12.900 | 1.665 | 9.000 | 0.695 | 40.050 | 12.646 |
| 1 | 15.100 | 2.407 | 11.200 | 1.437 | 49.840 | 15.737 |
| 1.5 | 16.500 | 3.167 | 12.600 | 2.197 | 56.070 | 17.704 |
| 2 | 17.900 | 3.911 | 14.000 | 2.941 | 62.300 | 19.672 |
| 2.5 | 19.100 | 4.638 | 15.200 | 3.668 | 67.640 | 21.358 |
| 3 | 20.200 | 5.437 | 16.300 | 4.467 | 72.535 | 22.903 |
| 3.5 | 20.900 | 6.197 | 17.000 | 5.227 | 75.650 | 23.887 |
| 4 | 21.200 | 6.957 | 17.300 | 5.987 | 76.985 | 24.308 |
| 4.5 | 21.500 | 7.757 | 17.600 | 6.787 | 78.320 | 24.730 |
| 5 | 22.100 | 8.484 | 18.200 | 7.514 | 80.990 | 25.573 |
| 5.5 | 22.400 | 9.229 | 18.500 | 8.259 | 82.325 | 25.995 |
| 6 | 22.900 | 10.066 | 19.000 | 9.096 | 84.550 | 26.697 |
| 6.5 | **22.900** | **10.803** | **19.000** | **9.833** | **84.550** | **26.697** |
| 7 | 22.700 | 11.622 | 18.800 | 10.652 | 83.660 | 26.416 |
| 7.5 | 22.600 | 12.394 | 18.700 | 11.424 | 83.215 | 26.276 |

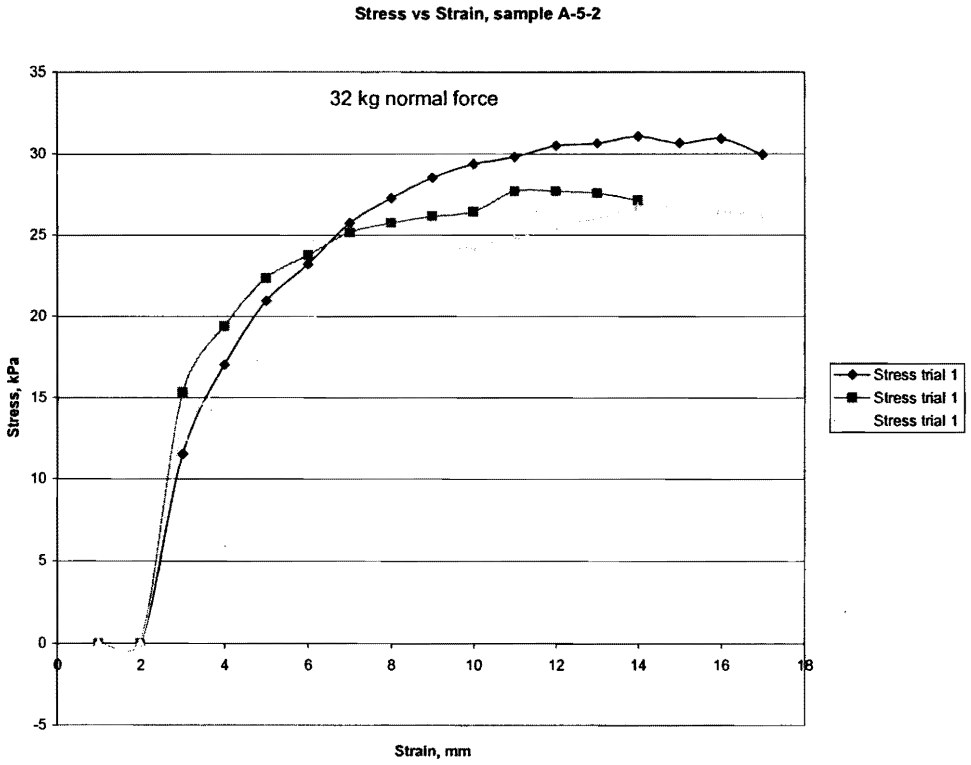
Stress vs Strain, sample A-5-2
32 kg normal force
Stress, kPa
Strain, mm
Stress trial 1
Stress trial 1
Stress trial 1
35
30
25
20
15
10
5
0
-5
0
2
4
6
8
10
12
14
16
18

## Consolidated Drained test

Direct Shear Testing 9/25/97 trial one 48 kg N force

Yellow-gray

sample A-5 colluvium test speed 3

strain rate = 0.063 mm per min. max in bold face

| Time, min | Load lbs | Strain mm | corrected load lbs | corrected Strain mm | Normal force, newtons | Shear Stress trial 1 kPa |
|---|---|---|---|---|---|---|
| 0 | 5.500 | 0.838 | 0.000 | 0.000 | 0.000 | 0.000 |
| 0.5 | 16.900 | 1.541 | 11.400 | 0.703 | 50.730 | 16.018 |
| 1 | 23.900 | 2.211 | 18.400 | 1.373 | 81.880 | 25.854 |
| 1.5 | 27.700 | 2.967 | 22.200 | 2.129 | 98.790 | 31.194 |
| 2 | 30.900 | 3.733 | 25.400 | 2.895 | 113.030 | 35.690 |
| 2.5 | 33.200 | 4.506 | 27.700 | 3.668 | 123.265 | 38.922 |
| 3 | 34.500 | 5.267 | 29.000 | 4.429 | 129.050 | 40.748 |
| 3.5 | 35.200 | 6.085 | 29.700 | 5.247 | 132.165 | 41.732 |
| 4 | **35.600** | **6.850** | **30.100** | **6.012** | **133.945** | **42.294** |
| 4.5 | 35.300 | 7.616 | 29.800 | 6.778 | 132.610 | 41.872 |
| 5 | 35.000 | 8.441 | 29.500 | 7.603 | 131.275 | 41.451 |

## Consolidated Drained test

trial two 48 kg N force

Direct Shear Testing 9/25/97

max in bold face

Yellow-gray

sample A-5 colluvium

test speed 3

strain rate = 0.063 mm per min.

| Time, min | Load lbs | Strain mm | corrected load lbs | corrected Strain mm | Normal force, newtons | Shear Stress trial 1 kPa |
|---|---|---|---|---|---|---|
| 0 | 4.000 | 0.858 | 0.000 | 0.000 | 0.000 | 0.000 |
| 0.5 | 20.400 | 1.389 | 16.400 | 0.531 | 72.980 | 23.044 |
| 1 | 24.900 | 2.192 | 20.900 | 1.334 | 93.005 | 29.367 |
| 1.5 | 27.200 | 2.956 | 23.200 | 2.098 | 103.240 | 32.599 |
| 2 | 29.200 | 3.723 | 25.200 | 2.865 | 112.140 | 35.409 |
| 2.5 | 30.200 | 4.462 | 26.200 | 3.604 | 116.590 | 36.814 |
| 3 | 32.000 | 5.243 | 28.000 | 4.385 | 124.600 | 39.343 |
| 3.5 | 32.800 | 5.995 | 28.800 | 5.137 | 128.160 | 40.467 |
| 4 | 33.100 | 6.792 | 29.100 | 5.934 | 129.495 | 40.889 |
| 4.5 | **33.300** | **7.557** | **29.300** | **6.699** | **130.385** | **41.170** |
| 5 | 33.000 | 8.336 | 29.000 | 7.478 | 129.050 | 40.748 |
| 5.5 | 33.100 | 9.111 | 29.100 | 8.253 | 129.495 | 40.889 |

Direct Shear
Testing 9/25/97 max in bold face
sample A-5 Yellow-gray colluvium test speed 3
strain rate = 0.063 mm per min.

| Time, min | Load lbs | Strain mm | corrected load lbs | corrected Strain mm | Normal force, newtons | Shear Stress trial 1 kPa |
|---|---|---|---|---|---|---|
| 0 | 3.900 | 0.429 | 0.000 | 0.000 | 0.000 | 0.000 |
| 0.5 | 19.500 | 1.017 | 15.600 | 0.588 | 69.420 | 21.920 |
| 1 | 22.700 | 1.806 | 18.800 | 1.377 | 83.660 | 26.416 |
| 1.5 | 25.200 | 2.584 | 21.300 | 2.155 | 94.785 | 29.929 |
| 2 | 27.000 | 3.362 | 23.100 | 2.933 | 102.795 | 32.458 |
| 2.5 | 28.100 | 4.110 | 24.200 | 3.681 | 107.690 | 34.004 |
| 3 | 29.100 | 4.905 | 25.200 | 4.476 | 112.140 | 35.409 |
| 3.5 | 30.200 | 5.664 | 26.300 | 5.235 | 117.035 | 36.955 |
| 4 | 30.400 | 6.436 | 26.500 | 6.007 | 117.925 | 37.236 |
| 4.5 | 31.200 | 7.185 | 27.300 | 6.756 | 121.485 | 38.360 |
| 5 | 31.700 | 7.975 | 27.800 | 7.546 | 123.710 | 39.062 |
| 5.5 | 32.200 | 8.744 | 28.300 | 8.315 | 125.935 | 39.765 |
| 6 | 32.400 | 9.546 | 28.500 | 9.117 | 126.825 | 40.046 |
| 6.5 | **32.500** | **10.296** | **28.600** | **9.867** | **127.270** | **40.186** |
| 7 | 32.200 | 11.125 | 28.300 | 10.696 | 125.935 | 39.765 |

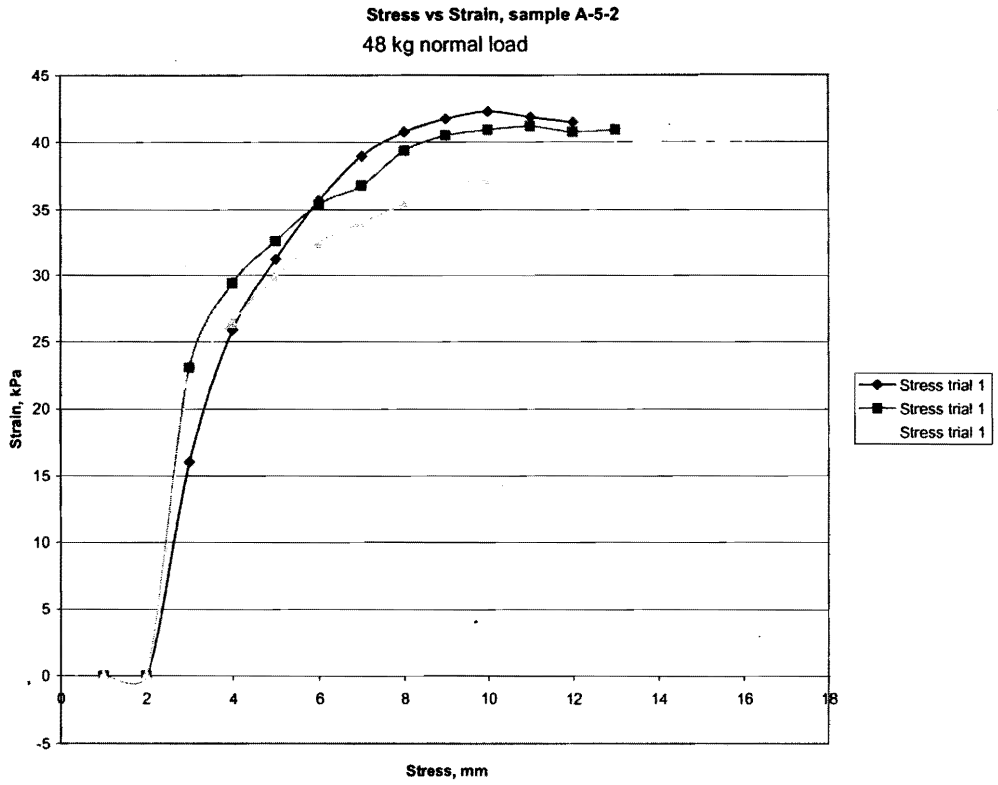
Stress vs Strain, sample A-5-2
48 kg normal load
Strain, kPa
Stress, mm
45
40
35
30
25
20
15
10
5
0
-5
0
2
4
6
8
10
12
14
16
18
Stress trial 1
Stress trial 1
Stress trial 1

# West Tidewater Earthflow Direct Shear Test Results

Sample A-5-2

Consolidated Drained method Strain Controlled

| Trial Nurnber | Normal Stress, kPa | Shear Stress, kPa |
|---|---|---|
| 1, 16 kg | 49.561 | 16.908 |
| 2, 32 kg | 99.122 | 28.477 |
| 3, 64 kg | 148.683 | 41.217 |

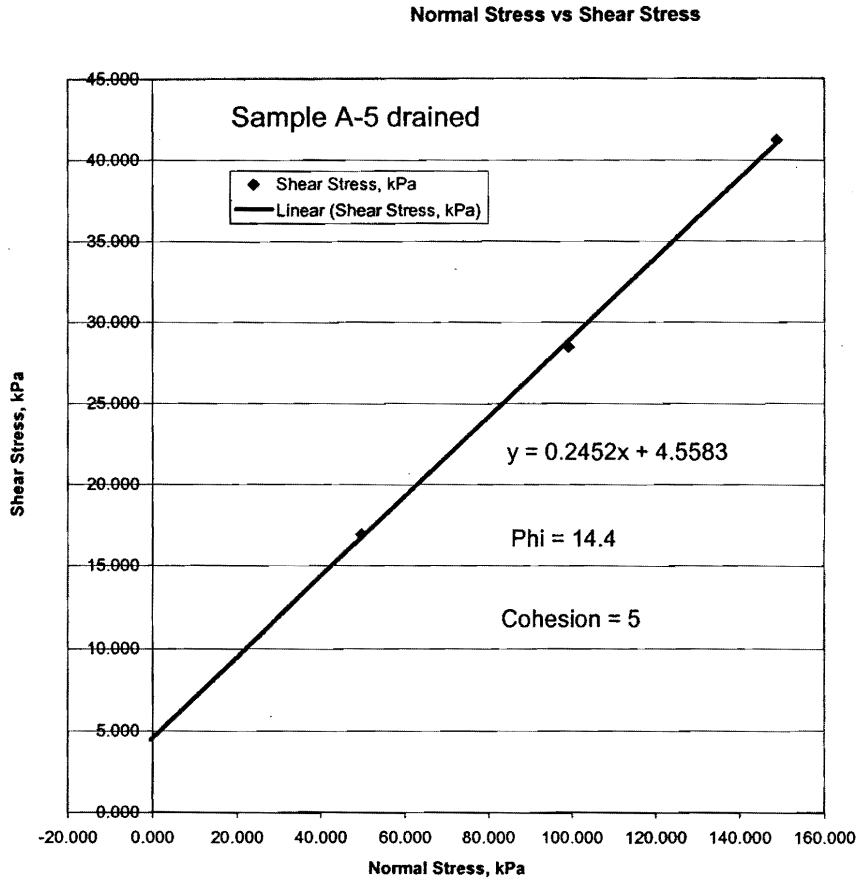
Normal Stress vs Shear Stress
Sample A-5 drained
Shear Stress, kPa
Linear (Shear Stress, kPa)
y = 0.2452x + 4.5583
Phi = 14.4
Cohesion = 5
Shear Stress, kPa
Normal Stress, kPa
45.000
40.000
35.000
30.000
25.000
20.000
15.000
10.000
5.000
0.000
-20.000
0.000
20.000
40.000
60.000
80.000
100.000
120.000
140.000
160.000

Consolidated Undrained test trial one 16 kg N load
Direct Shear Testing 8/27/97 max in bold face
yellow-gray
sample A-5 colluvium 16 kg test speed 3

| Time, min | Load lbs | Strain mm | corrected load lbs | corrected Strain mm | Normal force, newtons | Shear Stress trial 1 kPa |
|---|---|---|---|---|---|---|
| 0.000 | 1.800 | 0.756 | 0.000 | 0.000 | 0.000 | 0.000 |
| 0.500 | 10.200 | 1.390 | 8.400 | 0.634 | 37.380 | 11.803 |
| 1.000 | 13.200 | 2.194 | 11.400 | 1.438 | 50.730 | 16.018 |
| 1.500 | 14.900 | 2.886 | 13.100 | 2.130 | 58.295 | 18.407 |
| 2.000 | 15.900 | 3.674 | 14.100 | 2.918 | 62.745 | 19.812 |
| 2.500 | 16.900 | 4.424 | 15.100 | 3.668 | 67.195 | 21.217 |
| 3.000 | 17.500 | 5.234 | 15.700 | 4.478 | 69.865 | 22.060 |
| 3.500 | 17.500 | 5.998 | 15.700 | 5.242 | 69.865 | 22.060 |
| 4.000 | 17.600 | 6.755 | 15.800 | 5.999 | 70.310 | 22.201 |
| 4.500 | 18.600 | 7.544 | 16.800 | 6.788 | 74.760 | 23.606 |
| 5.000 | 18.800 | 8.331 | 17.000 | 7.575 | 75.650 | 23.887 |
| 6.000 | **18.900** | **9.052** | **17.100** | **8.296** | **76.095** | **24.027** |
| 6.500 | 18.300 | 9.842 | 16.500 | 9.086 | 73.425 | 23.184 |
| 7.000 | 18.500 | 10.664 | 16.700 | 9.908 | 74.315 | 23.465 |
| 7.500 | 18.800 | 11.450 | 17.000 | 10.694 | 75.650 | 23.887 |
| 8.000 | 18.800 | 12.206 | 17.000 | 11.450 | 75.650 | 23.887 |

Consolidated Undrained test trial one 32 kg N load
Direct Shear Testing 8/27/97 max in bold face
yellow-gray
sample A-5 colluvium test speed 3

| Time, min | Load lbs | Strain mm | corrected load lbs | corrected Strain mm | Normal force, newtons | Shear Stress trial 1 kPa |
|---|---|---|---|---|---|---|
| 0.000 | 3.100 | 0.784 | 0.000 | 0.000 | 0.000 | 0.000 |
| 0.500 | 12.600 | 1.292 | 9.500 | 0.508 | 42.275 | 13.349 |
| 1.000 | 16.300 | 2.049 | 13.200 | 1.265 | 58.740 | 18.548 |
| 1.500 | 18.400 | 2.835 | 15.300 | 2.051 | 68.085 | 21.498 |
| 2.000 | 19.600 | 3.565 | 16.500 | 2.781 | 73.425 | 23.184 |
| 2.500 | 20.900 | 4.345 | 17.800 | 3.561 | 79.210 | 25.011 |

| | | | | | | |
|---|---|---|---|---|---|---|
| 3.000 | 22.000 | 5.079 | 18.900 | 4.295 | 84.105 | 26.557 |
| 3.500 | 22.900 | 5.835 | 19.800 | 5.051 | 88.110 | 27.821 |
| 4.000 | 23.600 | 6.621 | 20.500 | 5.837 | 91.225 | 28.805 |
| 4.500 | 24.400 | 7.413 | 21.300 | 6.629 | 94.785 | 29.929 |
| 5.000 | 25.600 | 8.176 | 22.500 | 7.392 | 100.125 | 31.615 |
| 6.000 | 26.400 | 8.944 | 23.300 | 8.160 | 103.685 | 32.739 |
| 6.500 | 27.800 | 9.760 | 24.700 | 8.976 | 109.915 | 34.706 |
| 7.000 | 28.800 | 10.527 | 25.700 | 9.743 | 114.365 | 36.111 |
| 7.500 | 29.200 | 11.355 | 26.100 | 10.571 | 116.145 | 36.674 |
| 8.000 | 29.900 | 12.110 | 26.800 | 11.326 | 119.260 | 37.657 |
| 8.500 | 30.600 | 12.890 | 27.500 | 12.106 | 122.375 | 38.641 |
| 9.000 | 30.900 | 13.730 | 27.800 | 12.946 | 123.710 | 39.062 |
| 9.500 | **31.600** | **14.560** | **28.500** | **13.776** | **126.825** | **40.046** |
| 10.000 | 31.100 | 15.430 | 28.000 | 14.646 | 124.600 | 39.343 |
| 10.500 | 30.900 | 16.326 | 27.800 | 15.542 | 123.710 | 39.062 |
| 11.000 | 31.100 | 17.378 | 28.000 | 16.594 | 124.600 | 39.343 |

Consolidated Undrained test trial one 48 kg N load

Direct Shear Testing 8/27/97 max in bold face

yellow-gray

sample A-5 colluvium test speed 3

| Time, min | Load lbs | Strain mm | corrected load lbs | corrected Strain mm | Normal force, newtons | Shear Stress trial 1 kPa |
|---|---|---|---|---|---|---|
| 0.000 | 3.100 | 0.707 | 0.000 | 0.000 | 0.000 | 0.000 |
| 0.500 | 19.500 | 1.316 | 16.400 | 0.609 | 72.980 | 23.044 |
| 1.000 | 24.000 | 2.103 | 20.900 | 1.396 | 93.005 | 29.367 |
| 1.500 | 26.400 | 2.835 | 23.300 | 2.128 | 103.685 | 32.739 |
| 2.000 | 27.700 | 3.640 | 24.600 | 2.933 | 109.470 | 34.566 |
| 2.500 | 29.700 | 4.387 | 26.600 | 3.680 | 118.370 | 37.376 |
| 3.000 | 31.200 | 5.168 | 28.100 | 4.461 | 125.045 | 39.484 |
| 3.500 | 31.900 | 5.943 | 28.800 | 5.236 | 128.160 | 40.467 |
| 4.000 | 32.400 | 6.703 | 29.300 | 5.996 | 130.385 | 41.170 |
| 4.500 | 32.700 | 7.452 | 29.600 | 6.745 | 131.720 | 41.591 |
| 5.000 | 33.700 | 8.243 | 30.600 | 7.536 | 136.170 | 42.997 |
| 6.000 | 34.500 | 9.001 | 31.400 | 8.294 | 139.730 | 44.121 |
| 6.500 | 35.700 | 9.832 | 32.600 | 9.125 | 145.070 | 45.807 |
| 7.000 | 35.800 | 10.586 | 32.700 | 9.879 | 145.515 | 45.947 |
| 7.500 | **36.100** | **11.323** | **33.000** | **10.616** | **146.850** | **46.369** |
| 8.000 | 35.700 | 12.083 | 32.600 | 11.376 | 145.070 | 45.807 |
| 8.500 | 36.000 | 12.901 | 32.900 | 12.194 | 146.405 | 46.228 |
| 9.000 | 35.400 | 13.743 | 32.300 | 13.036 | 143.735 | 45.385 |
| 9.500 | 34.700 | 14.622 | 31.600 | 13.915 | 140.620 | 44.402 |

West Tidewater Earthflow
Consolidated Undrained Test
Sample A-5

Direct Shear Test
Results
Strain Controlled

| | Normal Stress, kPa | Shear Stress, kPa |
|---|---|---|
| 1, 16 kg | 49.561 | 15.649 |
| 2, 32 kg | 99.122 | 40.046 |
| 3, 48 kg | 148.683 | 46.369 |

**Shear Stress vs Normal Stress, sample A-5**

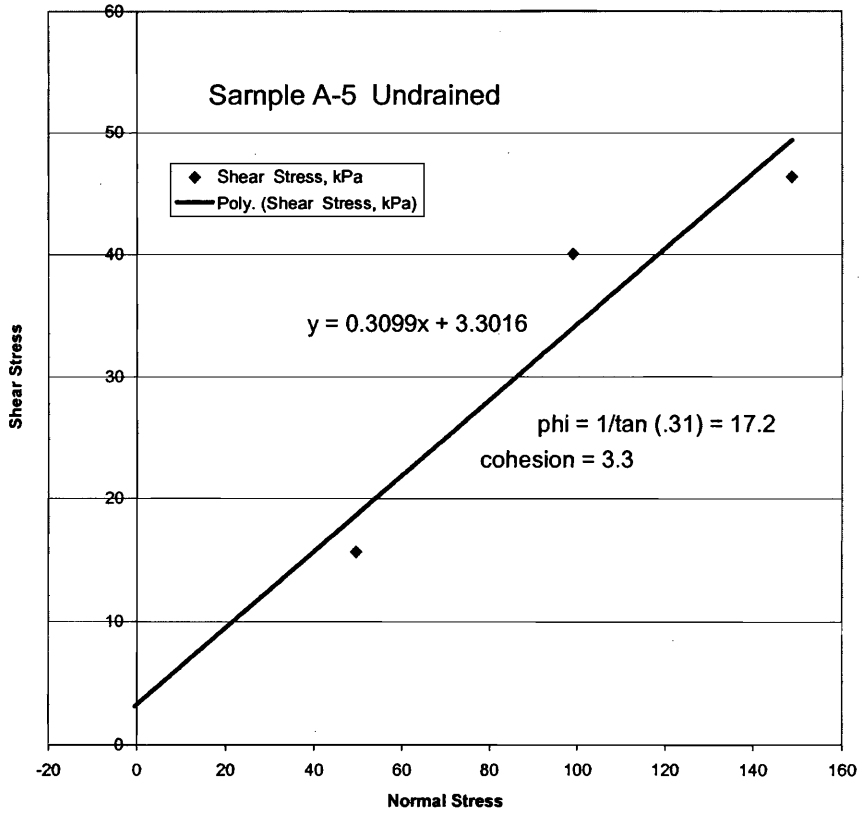

# Appendix F

## West Tidewater Earthflow

## X-ray Diffraction Analysis

## Clay Mineralogy

September 17, 1997

Report on the Clay Mineralogy of Samples A1 and A5

Prepared by Sean D. Wilson, Portland State University Dept. of Geology

## INTRODUCTION AND METHODS

The fine grained fraction of samples A1 and A5 had been obtained by the wet sieve method and were kept in a hydrated state before preparation on clay tiles. The clay-size fraction (<2μ) for each sample was separated from the silt fraction by centrifuging the samples in containers filled with deionized water.

Oriented clay samples were prepared by delivering the <2μ clay slurries to ceramic tiles. The ceramic tiles were placed over a fritted disc filter hooked up to a vacuum. The vacuum system removed the water from the sample by drawing it through a porous ceramic tile. The clay minerals were oriented on the tile with the (001) face parallel to the tile surface (Moore and Reynolds, 1989).

Three ceramic tiles were prepared for each sample so that the clay fraction of each sample was separated into three subsamples consisting of: 1) an untreated subsample; 2) a potassium saturated subsample; and 3) a magnesium saturated subsample with glycerol treatment. For the potassium-saturated subsamples, drops of 1N potassium chloride were placed on the tile and after 20 minutes the potassium

chloride was sucked through the sample on the vacuum. This step was repeated twice. The magnesium treated subsamples were treated in the same manner but used a solution of 0.1 M magnesium chloride. The magnesium saturated samples were treated with glycerol by coating the clay tile and letting it air dry. A total of six tiles were prepared for analysis.

The untreated samples were run through the X-ray first, followed by the magnesium-saturated, and the potassium saturated samples. Each sample was run on a Norelco X-ray diffractometer at a scan speed of 1° per 30 seconds. The goniometer had a 0.2 receiving slit and used a copper tube. After the first run of the potassium-saturated samples, they were heated in a furnace for 1 hour at 500° C and were re-run in the X-ray diffractometer.

The diffractograms from all the samples were analyzed for peak location, intensity, shape, and width. The clay mineralogy was determined from this data and a qualitative analysis of the clay minerals was done by using the peak height normalization technique of untreated samples' (001) peak.

## RESULTS

By observing the X-ray diffraction patterns and using the table from Chen (1977), the clay fractions of sample A1 and A5 were determined (Table F1).

Table F1.

| Clay Fraction | Sample A1 (%) | Sample A-5 (%) |
|---|---|---|
| Smectite | 87 | 80 |
| Illite | 7 | 15 |
| Kaolinite | 6 | 5 |

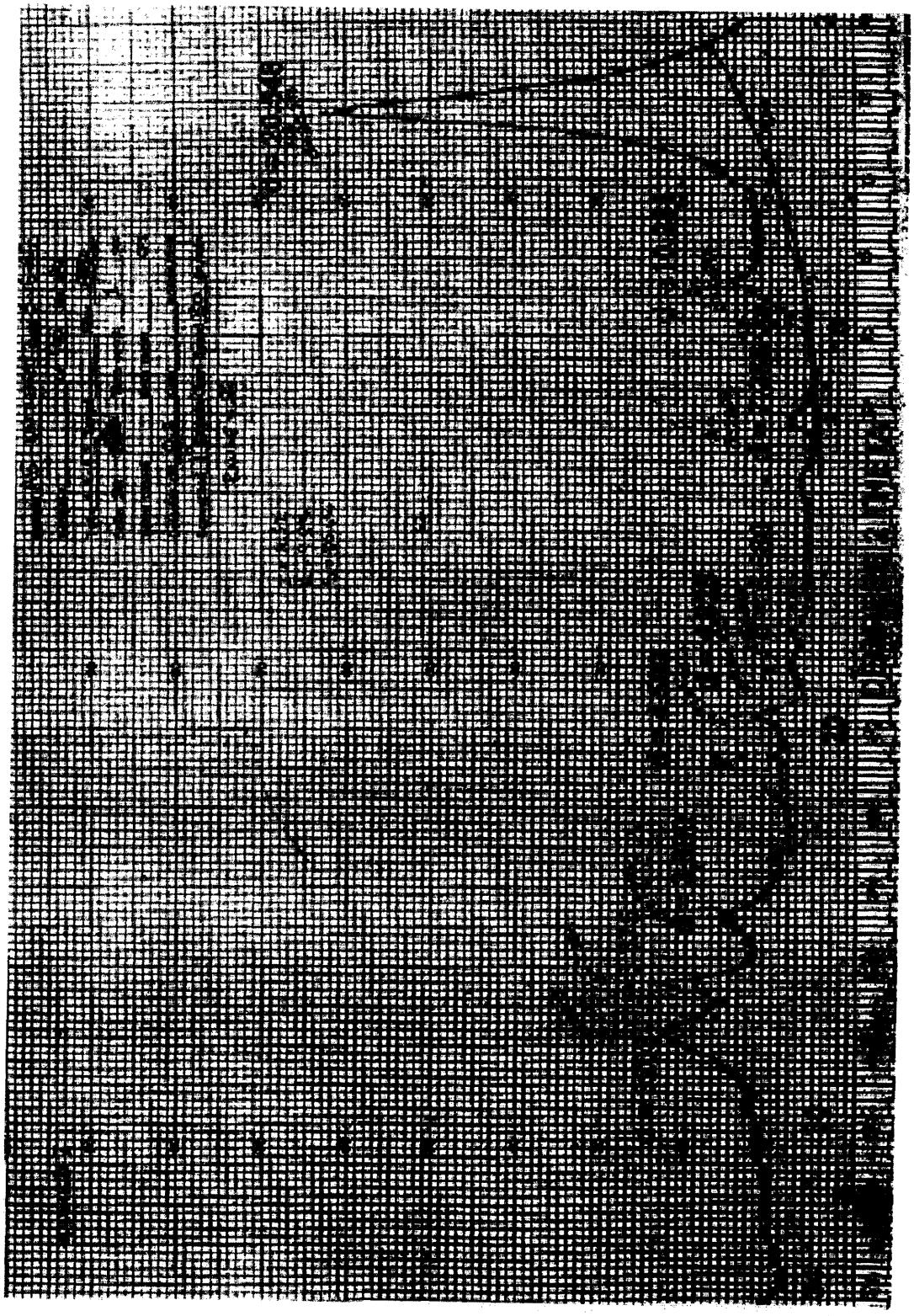

Figure F1. Sample A5 untreated.

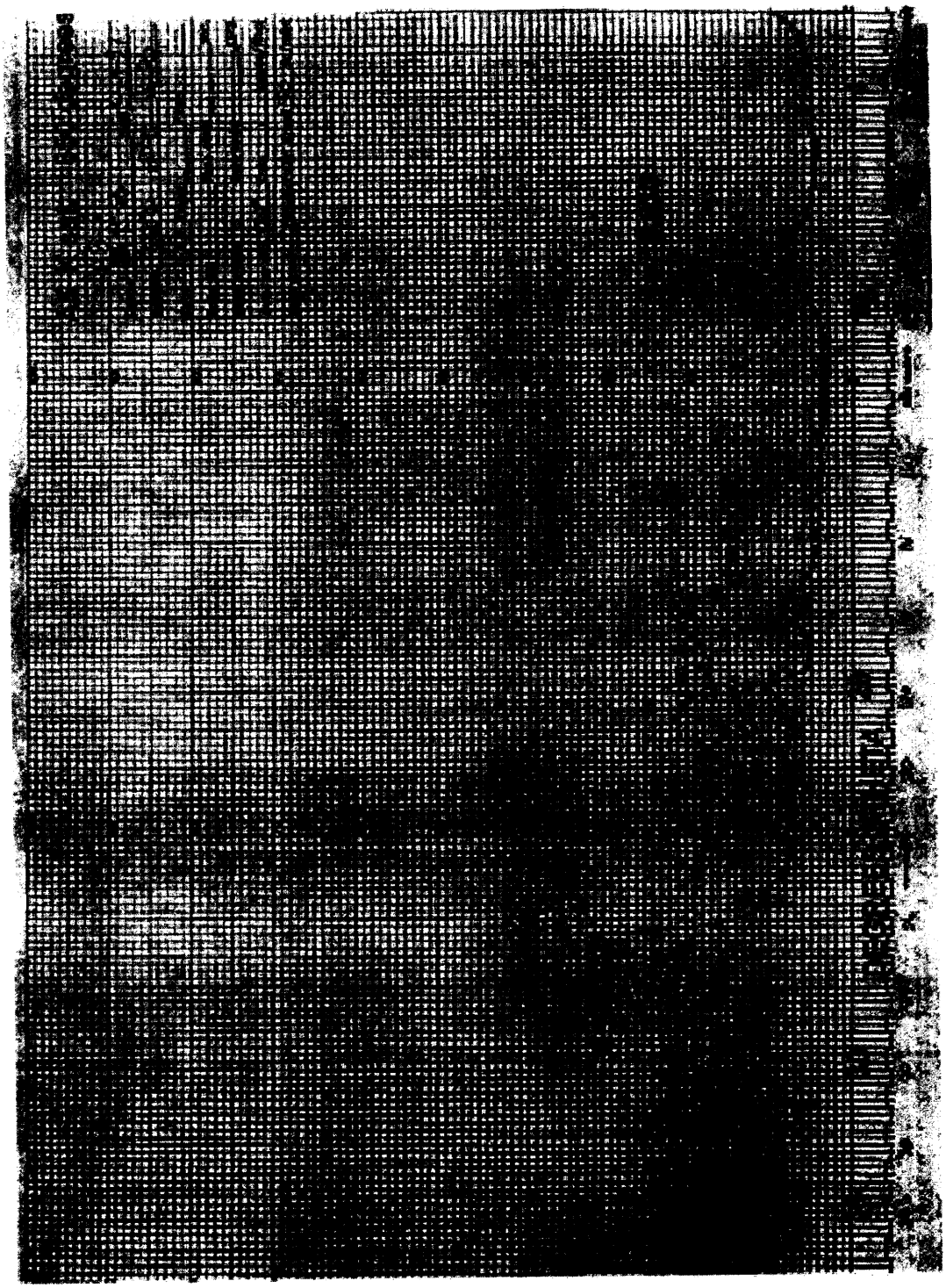

Figure F2. Sample A5 heat treated 650°

Figure F3. Sample A5 Mg + glycol saturated.

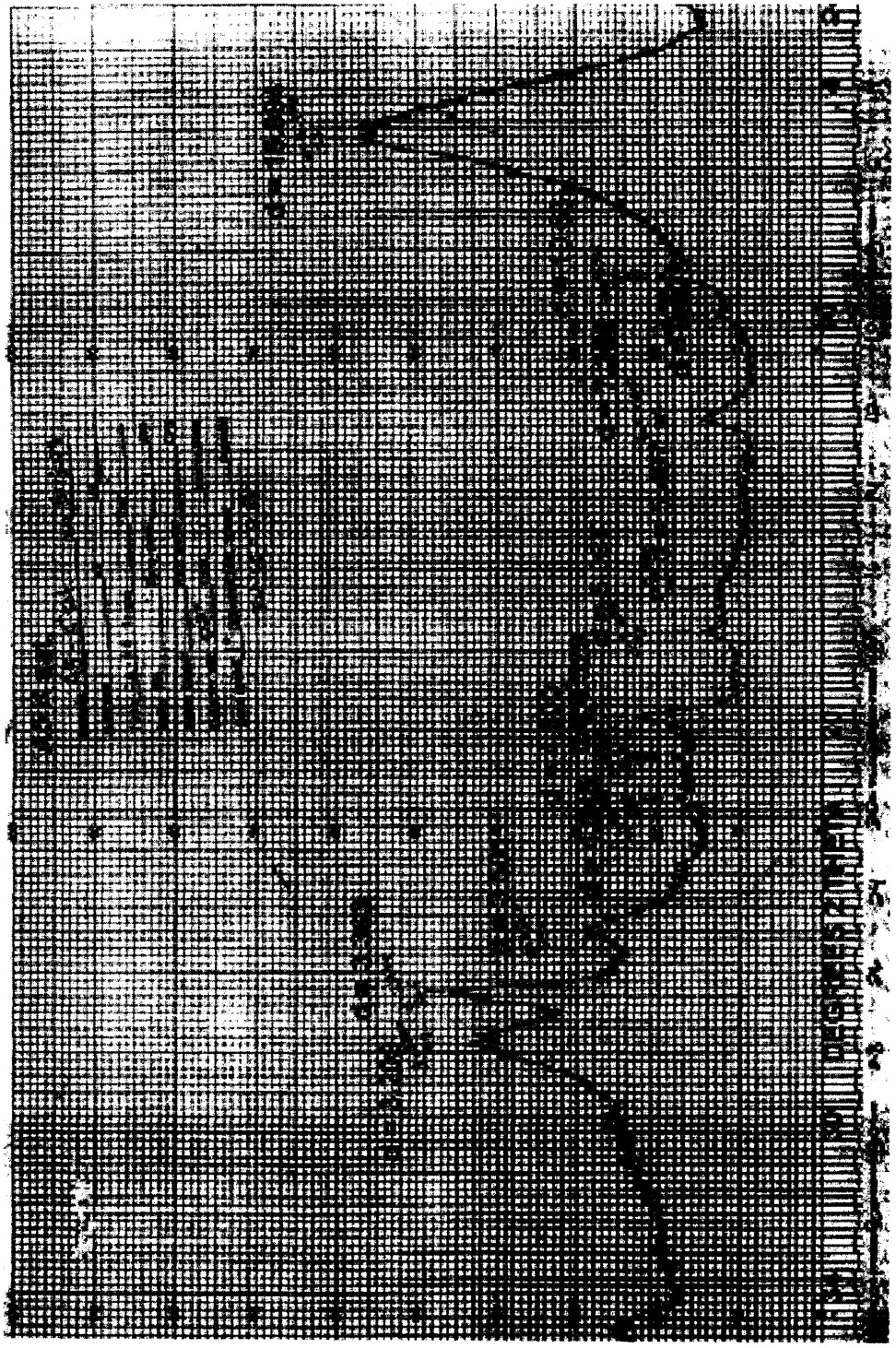

Figure F4. Sample A5 K saturated

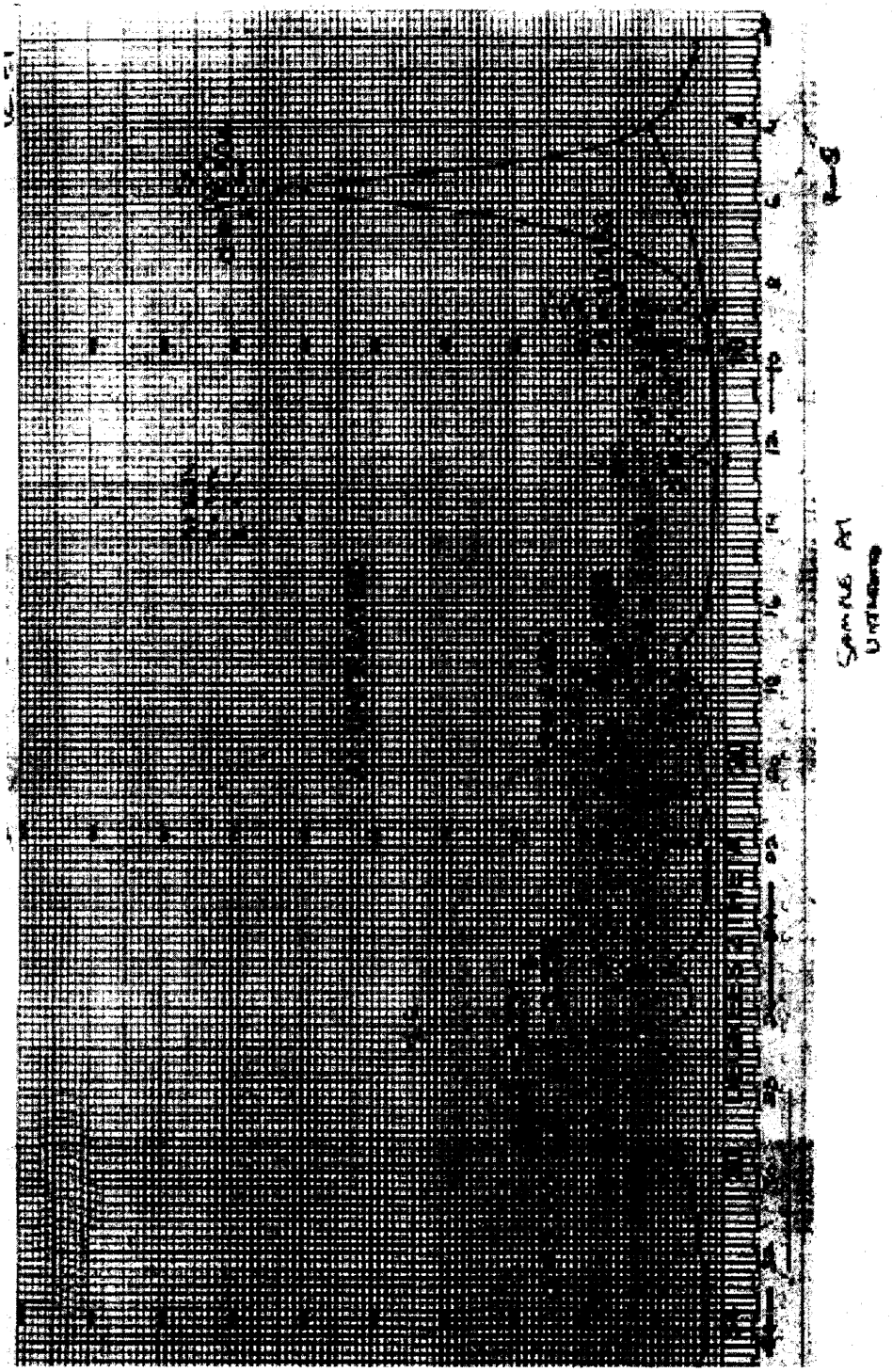

Figure F5. Sample A1 untreated.

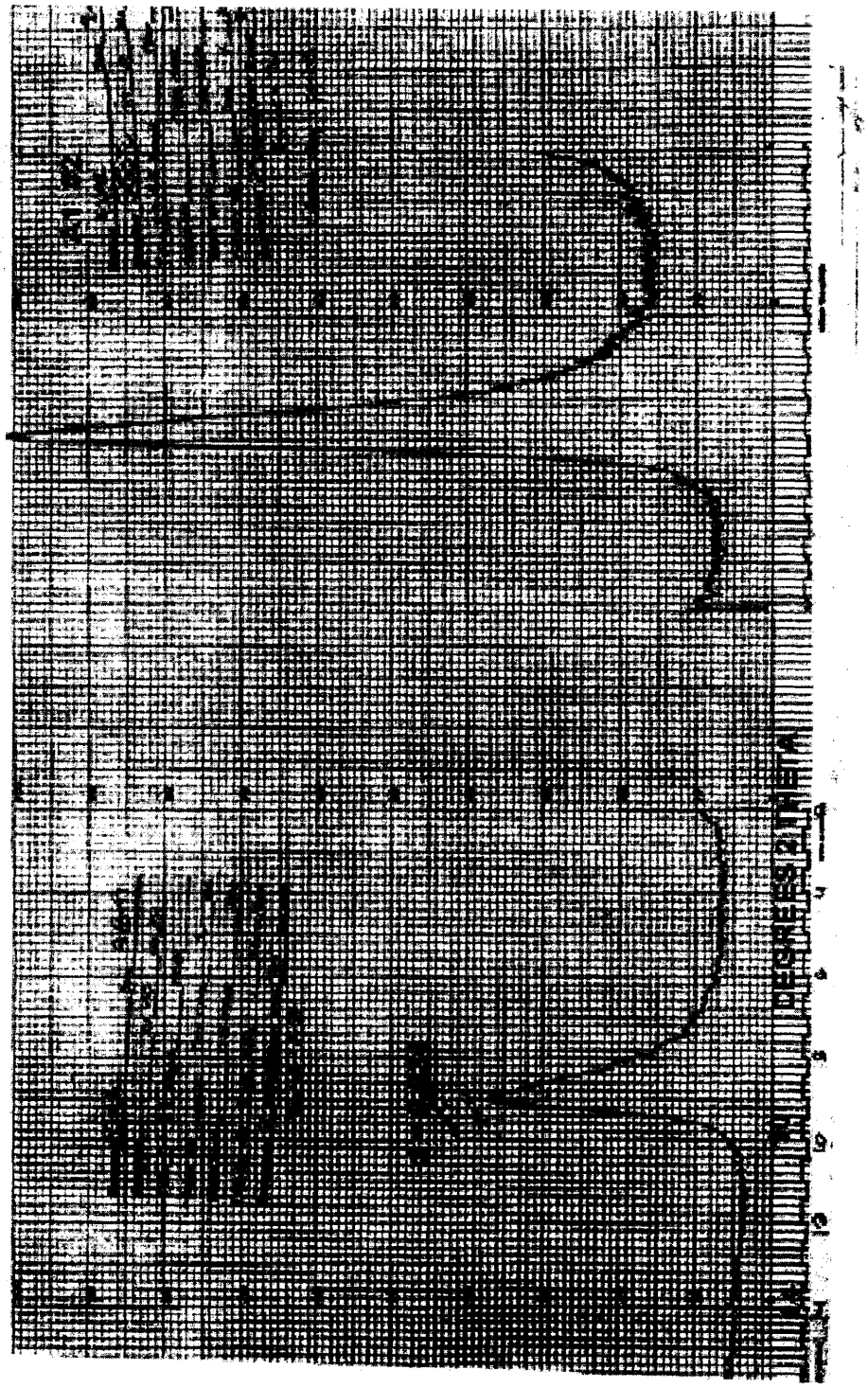

Sample F6. Sample A1 heat treated

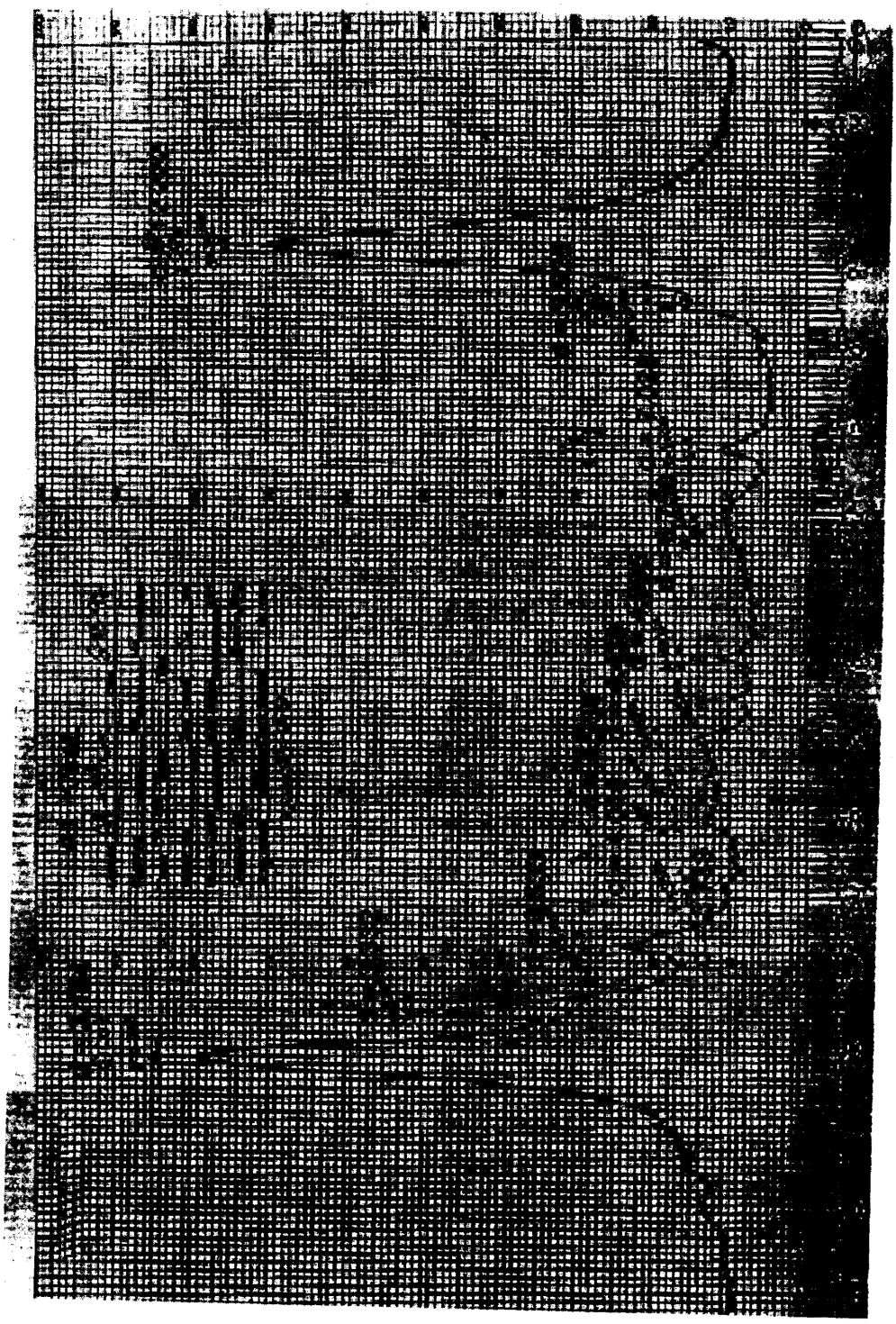

Figure F7. Sample A5 Al-K saturated.

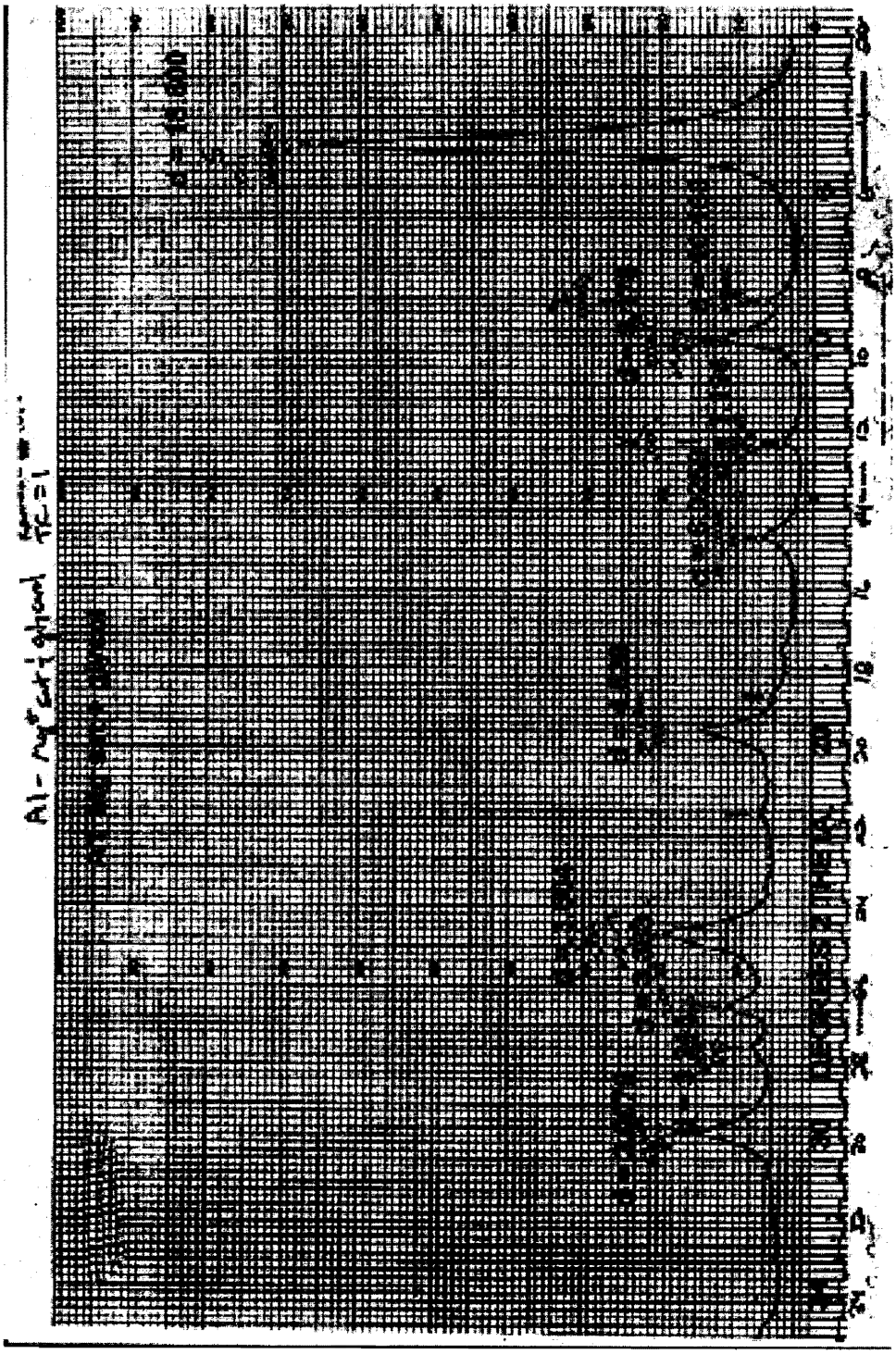

Figure F8. Sample A1 Mg + glycol saturated.

# Appendix G

West Tidewater Earthflow

Radiocarbon Dating

Buried Trees

BETA

BETA ANALYTIC INC.

DR. M.A. TAMERS and MR. D.G. HOOD

UNIVERSITY BRANCH
4985 S.W. 74 COURT
MIAMI, FLORIDA, USA 33155
PH: 305/667-5167 FAX: 305/663-0964
E-MAIL: beta@radiocarbon.com

# REPORT OF RADIOCARBON DATING ANALYSES

Dr. Scott Burns

Portland State University

July 20, 1999

August 6, 1999

| Sample Data | Measured C14 Age | C13/C12 Ratio | Conventional C14 Age (*) |
|---|---|---|---|
| Beta-132479 | 700 +/- 50 BP | -25.0* o/oo | 700 +/- 50* BP |

SAMPLE #: 98-5C-3
ANALYSIS: radiometric-standard
MATERIAL/PRETREATMENT:(wood): acid/alkali/acid

NOTE: It is important to read the calendar calibration information and to use the calendar calibrated results (reported separately) when interpreting these results in AD/BC terms.

**Dates are reported as RCYBP (radiocarbon years before present, "present" = 1950A.D.). By international convention, the modern reference standard was 95% of the C14 content of the National Bureau of Standards' Oxalic Acid & calculated using the Libby C14 half life (5568 years). Quoted errors represent 1 standard deviation statistics (68% probability) & are based on combined measurements of the sample, background, and modern reference standards.**

**Measured C13/C12 ratios were calculated relative to the PDB-1 international standard and the RCYBP ages were normalized to -25 per mil. If the ratio and age are accompanied by an (*), then the C13/C12 value was estimated, based on values typical of the material type. The quoted results are NOT calibrated to calendar years. Calibration to calendar years should be calculated using the Conventional C14 age.**